The Brazilian Equatorial Margin from Rift to Drift: Faulting, Deposition, and Deformation in the Offshore Barreirinhas Basin

---

A Dissertation

Presented to

the Faculty of the Department of Earth and Atmospheric Sciences

University of Houston

In Partial Fulfillment

of the Requirements for the Degree

Doctor of Philosophy

By

Ana Krueger

December 2012

The Brazilian Equatorial Margin from Rift to Drift: Faulting, Deposition, and Deformation in the Offshore Barreirinhas Basin

_____

Ana Krueger

APPROVED:

_____

Dr. Michael Murphy, Advisor

_____

Dr. Kevin Burke

_____

Dr. Jonathan Snow

_____

Dr. Oscar Gilbert

_____

Dr. Mark A. Smith, Dean College of Natural Sciences and Mathematics

This Dissertation is dedicated to my husband Alex and my daughters Antonia and Isabel.

ACKNOWLEDGEMENTS

WesternGeco kindly provided permission to publish the four seismic lines depicted here. Much of the mapping and structural restoration was done through the auspices of Devon Energy, and we especially acknowledge permission to use the interpreted seismic grids that are the basis of the isochron maps. Structural restorations were performed using Lithotect software. Special thanks to Michael Hankins (HRT America, formerly of Devon), and to Pedro Zalan, Ivo Trosdtorf, and Jorge Picanzo Figueiredo (Petrobras) for discussions of the local geology. Thanks to Dale Bird (Bird Geophysical), for the South Atlantic flow lines and discussions on the regional geology. Nancy Engelhardt-Moore of Devon Energy provided key information on the implications of the paleontological data to both age-dating and sedimentation rates. Also, special thanks to Laura Unverzagt (University of Houston), and Jorge Mendoza and Abraham Gonzales (Devon) for help with Arc-GIS.

The Brazilian Equatorial Margin from Rift to Drift: Faulting, Deposition, and Deformation in the Offshore Barreirinhas Basin

An Abstract of a Dissertation

Presented to

the Faculty of the Department of Earth and Atmospheric Sciences

University of Houston

In Partial Fulfillment

of the Requirements for the Degree

Doctor of Philosophy

By

Ana Krueger

December 2012

ABSTRACT

The Equatorial South Atlantic contains elements of an oblique-rifted margin and a sheared margin. The Barreirinhas Basin is a basin on the Brazilian coast located north of the shoreward limit of the Romanche Fracture Zone and south of the shoreward limit of the Saint Paul's Fracture Zone. The main characteristic of the Barreirinhas Basin is an abrupt transition zone between oceanic and continental crust as a result of being located on a transform margin with, consequently, a very narrow and steep continental slope. This study focuses on the rift to drift evolution of the Barreirinhas Basin and the Barreirinhas Basin deep-water fold-belt, and is the first detailed published local study of the tectonic evolution of the Brazilian Equatorial margin. Complementary structural work over most of the Brazilian Equatorial margin provided a framework in which to place the tectonic history of the Barreirinhas Basin.

Regional seismic reflection profiles across the Barreirinhas Basin on the Brazilian Equatorial margin reveal two major deep-water fold and thrust belts linked landward to extensional fault systems. Thrust faults are interpreted to be products of shortening caused by gravity-driven extension on the continental margin that involve rocks at both the shelf and the slope. Two main deformation events during the Cretaceous (99.6 to 83.5 Ma) and the Cenozoic (65.5 to 0 Ma) were distinguished. The Cretaceous deformation affected only a one kilometer thick section but the Cenozoic structural episodes involved a thicker (over 4 km) sedimentary sequence of Turonian to Miocene age, and cross-cut the pre-existing Cretaceous deformed sequence. Normal faults connect to the thrust faults at depth, forming two discrete bowl-shaped fault systems, linked at depth at different

stratigraphic levels. Plots of displacement versus time show normal and thrust fault movements at the same time intervals, indicating close linkage between extension on the continental shelf and shortening on the slope.

Deformation has increased dramatically during the past ten million years, with movement on all earlier and some newly formed faults. The increased deformation coincided with regional paleogeographic changes in northern South America in the Late Miocene that led to an increase in the sediment supply to the Barreirinhas Basin.

TABLE OF CONTENTS

TABLE OF FIGURES

CHAPTER 2: THE BRAZILIAN EQUATORIAL MARGIN: FROM RIFT TO DRIFT

CHAPTER 3: DEPOSITION AND DEFORMATION IN DEEP-WATER SEDIMENTS OF THE OFFSHORE BARREIRINHAS BASIN

CHAPTER 1: INTRODUCTION

1.1 OVERVIEW AND RESEARCH FOCUS

Our research focus on the rift to drift evolution of the Barreirinhas Basin and the Barreirinhas Basin deep-water foldbelt. The Barreirinhas Basin is one of a set of basins on the Equatorial Brazilian margin and it is located north of the onland projection of the Romanche Fracture Zone and south of the onland projection of the Saint Paul Fracture Zone (Fig. 1).

The Brazilian Equatorial margin is an oblique-divergent passive margin. Other examples of oblique rifts include the Gulf of California, the Gulf of Aden, and the Dead Sea among others (Bird, 2001). Oblique rifts have a strong strike-slip component during the early rift stages. Oblique rifts start as a complex pattern of pull-apart basins along strike-slip fault systems that eventually coalesce into through going systems. Extension continues up to the point of continental break-up and formation of oceanic crust.

The main characteristic of the Barreirinhas Basin is an abrupt transition zone between oceanic and continental crust as a result of being located on an oblique margin (Fig. 2-1) with, consequently, a very narrow and steep continental slope. The post-rift sedimentary sequence of the Barreirinhas Basin is dominated by a series of thrusts and folds in deep water that form the Barreirinhas Basin deep-water foldbelt linked to a series of normal faults on the continental shelf.

1.2 ORGANIZATION OF DISSERTATION

The dissertation is divided into three chapters. Chapters 2 and 3 represent the main body of the research. Because no comprehensive work has been published on the tectonic evolution of the Brazilian Equatorial margin, some introductory work extending over most of the Brazilian Equatorial margin was necessary in order to establish the tectonic history of the Barreirinhas Basin. Chapter 2 therefore is focused on the whole margin and chapter 3 is focused on the Barreirinhas Basin. Each of the two chapters makes up a manuscript that will be submitted to a peer-reviewed journal for publication.

Chapter 2 focuses on the rifting of the Brazilian Equatorial margin an oblique rifted margin. Chapter 2 describes the Brazilian Equatorial margin as a margin segmented by major oceanic transform zones and concentrates on the geometry of the basement faults of the margin near the continental oceanic transition zone. The limit between continental crust and the oceanic transitional zone (COTZ) has been mapped using potential field data that has been compared with the seismic information. The difference in the basement fault geometries of the different segments of the margin and its implications for the tectonic evolution of the margin and the oblique spreading of the Equatorial Atlantic and how spreading direction angles change from oblique at the COTZ on the continental margin to orthogonal on the mid-oceanic ridge are also addressed.

Chapter 3 focuses on the Barreirinhas Basin, one of the larger basins of the Brazilian Equatorial margin and describes the geometries of the Barreirinhas foldbelt, a

four kilometer thick unit of highly deformed post-rift sediments, with updip normal faults linked to downdip thrust faults. The chapter addresses the linkage of normal and thrust faults in a quantitative way and discusses the forming mechanisms for the system.

CHAPTER 2: THE BRAZILIAN EQUATORIAL MARGIN: FROM RIFT TO DRIFT

ABSTRACT

Interpretation of seismic reflection profiles (500,000 km of 2D lines) describes a transform margin geometry in the Ceará Basin that transitions to oblique in the Barreirinhas and Pará-Maranhão Basins to almost orthogonal north of the Foz do Amazonas. Analysis of satellite-derived gravity and magnetics are used here to describe a history of oblique continental rifting and oblique sea-floor spreading in the Equatorial Atlantic.

The objectives of this work are to: 1) map the basement structures from the continental shelf to the abyssal plains, 2) map the continental oceanic transition zone (COTZ), 3) describe the structures formed in the continental oceanic transition zone (COTZ) of the margin, and 4) discuss implications of the basement structures for the tectonic evolution of this transform margin. The geometries associated with oblique-rifting are described and the possibility of oblique sea-floor spreading is discussed in the study area. Detailed mapping of the basement using 500,000 km of 2D seismic lines on a 16 km by 8 km grid from the continental shelf to the oceanic basin was used to characterize the structural aspects of the continental-oceanic transition zone.

2.1 INTRODUCTION

The Brazilian Equatorial continental margin in northeastern South America and the eastern part of the Equatorial South Atlantic Ocean has a continental shelf that is characterized as very broad in the north and very narrow in the south. The main physiographic features of the margin are the Amazon Delta, the Chain, Romanche, Saint Paul, and 4^{o}N Fracture Zones, and the Ceará Rise which is the counterpart of the West African Sierra Leone Rise. The main sedimentary basins along the coast are, from north to south, the Foz do Amazonas, Pará-Maranhão, Barreirinhas, Piauí-Ceará, and Potiguar Basins (Fig. 2-1). Our study area extends from the Foz do Amazonas to the Piauí-Ceará Basin.

Rifting within Northeast Brazil and the Guinean coast of Africa started with the reactivation of old Pan-African faults as strike-slip mega-shear zones (Darros de Matos, 1999, Greenroyd et al., 2008, Antobreh et al., 2009). The rifting that gave rise to the Brazilian Equatorial margin was oblique to the large-scale direction of separation of the continents. The term oblique rifted margin was used by Yang and Escalona (2011) to describe the Equatorial South Atlantic.

Oblique rifts are rifts in which the continent ocean transition zone (COTZ) is not normal to the direction of spreading and to the oceanic fracture zones. Oblique rifts differ from orthogonal-rifts where the COTZ is normal to the direction of spreading and to the trend of fracture zones. Oblique-divergent plate boundaries are a much less well

understood type of plate boundary than classic rifts with orthogonally divergent plate boundaries (Umhoefer et al., 2002). Other examples of oblique-rifted margins include the Gulf of California (Lizarralde et al., 2007, Umhoefer et al., 2011), the Gulf of Aden (d'Acremont et al., 2006, Fournier et al., 2007, Autin et al., 2010, Daoud et al., 2011), the East coast of Madagascar, and the Dead Sea (Cochran, et al., 1983, Bird, 2001).

Oblique rifts have a strong strike-slip component expressed primarily during the early rift stages. Oblique rifts start as a complex pattern of pull-apart basins along strike-slip fault systems that eventually coalesce into through going systems (Umhoefer et al., 2002). In the Brazilian Equatorial margin rifting started as a set of strike-slip basins and as oceanic crust formed the basins coalesced (Darros de Matos, 1999).

Extension continues up to the point of continental break-up and formation of oceanic crust; oblique rifting is likely followed by oblique sea-floor spreading. According to Greenroyd et al. (2008), based on sea-floor spreading anomalies (Mueller et al., 2008) the last point of break-up was the continental margin of French Guiana and its conjugate Liberian margin in Late Aptian time at 113 Ma. It is likely that oceanic crust started forming prior to the first marine incursion, documented by Trosdtorf et al. (2007) at 102 Ma (Fig. 2-2).

Oblique sea-floor spreading has been well-documented in the modern Arctic Ocean basin. Oblique sea-floor spreading has been associated with slow spreading centers and areas characterized by an absence of oceanic crust (Dick et al., 2003). Those

authors have speculated that as sea-floor spreading evolves the spreading centers change gradually to develop normal orientations to the fracture zones.

The relationship between obliquity, spreading rate, mantle composition, and dynamics has led to recognition of a new class of plate boundaries (Snow et al., 2001), termed amagmatic spreading ridges (Dick et al., 2003). The primary mode of accretion along the magma-poor segments appears to be the emplacement of mantle peridotite directly onto the rift valley floor along the axis of rifting and parallel to the ridge trend, with subsequent fault capture and block rotation to form the rift valley walls (Dick et al., 2003). The fundamental difference between magma-rich and magma-poor accretionary plate boundaries is that in magma-rich plate boundaries lithospheric failure starts from the top of the lithosphere and in magma-poor plate boundaries lithospheric failure starts from the bottom of the lithosphere (Dick et al., 2003). The Brazilian Equatorial margin was a magma-poor continental margin, during early stages of rifting.

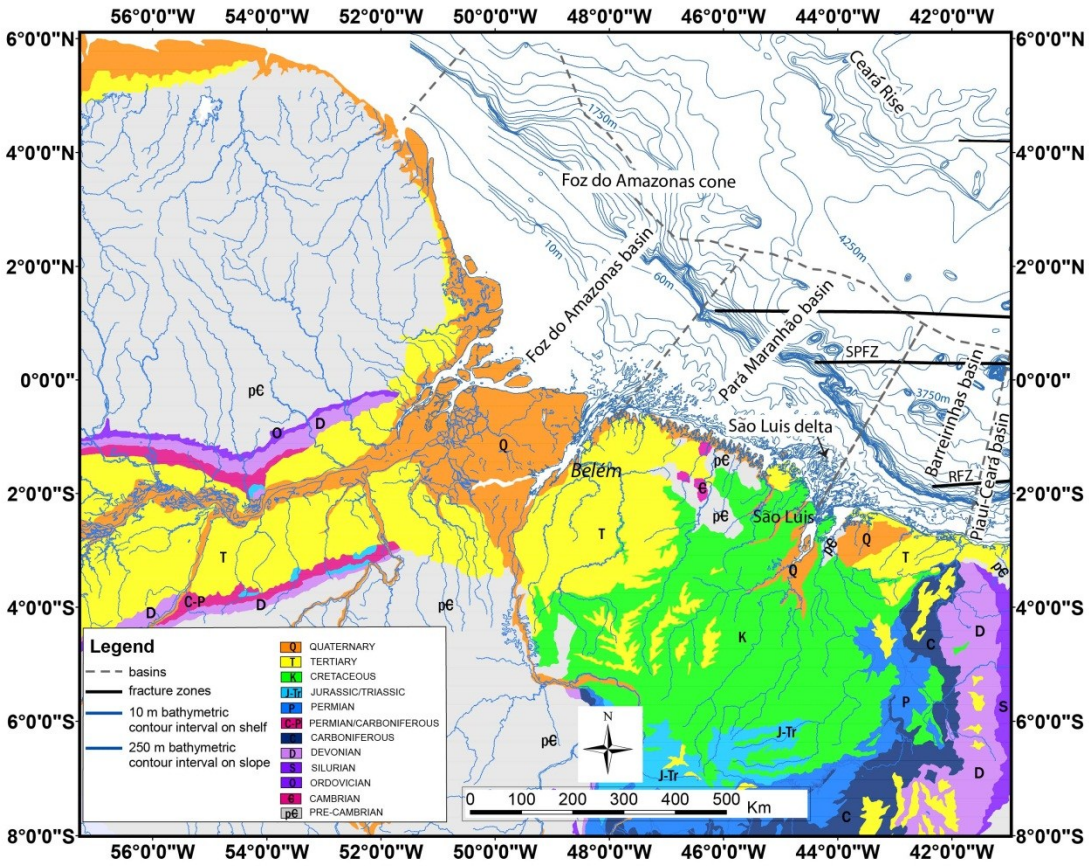

Figure 2-1. Location map showing onshore surface geology, offshore bathymetry, main physiographic features, and offshore basin outlines. Surface geology is based on the Geologic Map of South America (Schobbenhaus and Bellizia, 2001) (www.cprm.gov.br). Bathymetric data are derived from the ETOPO 1 grid (Amante and Eakins, 2009). Offshore basin outlines are from Agência Nacional de Petróleo (www.anp.gov.br).

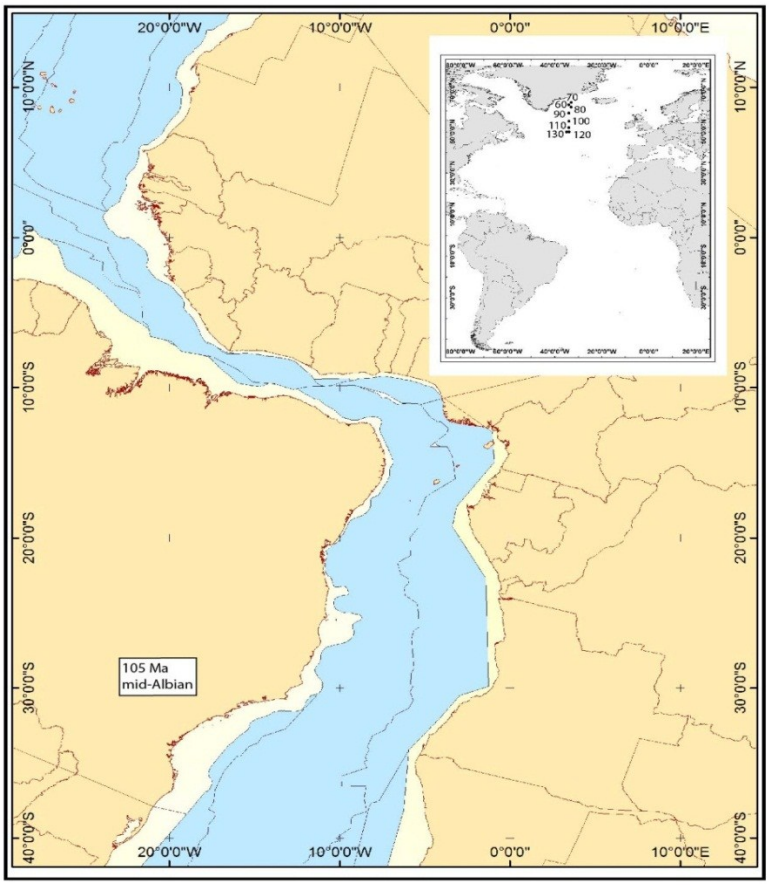

Figure 2-2. South Atlantic in mid-Albian (~105 Ma). Calculated using Paleogis software and the University of Texas Institute for Geophysics (UTIG) plates model. Showing continents in beige, continental shelves in yellow and, ocean floor in blue. Inset shows poles of rotation for South Atlantic for times between ~130 and 70Ma. Continental break-up of eastern and western Gondwana was associated with oblique rifting in the south (Falklands Plateau and South African margin) and in the north (Equatorial Atlantic). Continental break-up was orthogonal in the central South Atlantic where mantle plumes were present.

2.2 DATA AND METHODOLOGY

2.2.1 Seismic Data

Several 2D surveys of different vintages were used to map approximately 500,000 km of 2D seismic data, with an average grid spacing of 8 km over the Brazilian Equatorial margin from north of the Foz do Amazonas to the Ceará Basin (Fig. 2-1). Two seismic horizons were mapped; the sea-floor (Fig. 2-3) and the basement horizons (Fig. 2-4). The mapping was based on seismic character.

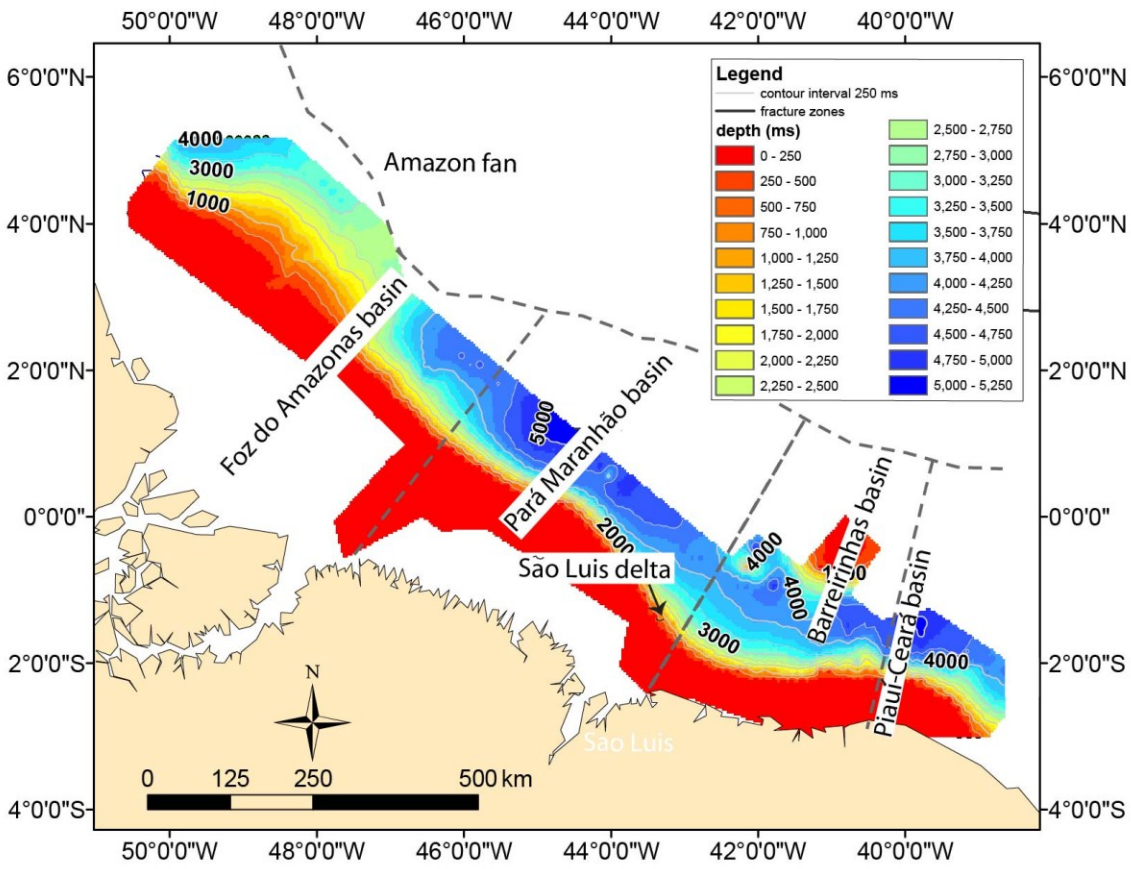

Figure 2-3. Bathymetry of the Brazilian Equatorial margin, mapped on the water bottom signal of ~ 500,000 km of 2D seismic reflection profiles. Offshore basin outlines are from Agência Nacional de Petróleo (www.anp.gov.br).

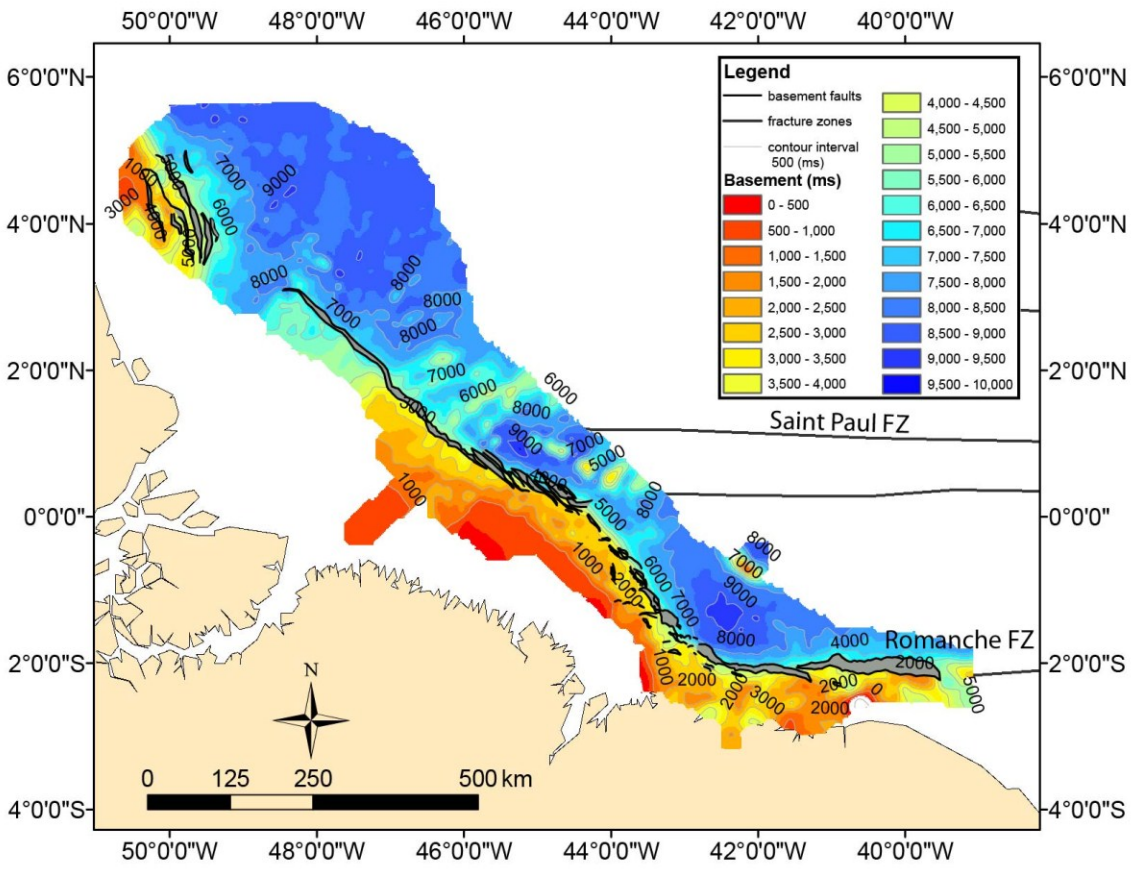

Figure 2-4. Depth to basement in the study area. Basement faults and fracture zones mapped are part of this study. The basement faults mapped are preferentially located around the COTZ and the most seaward fault mapped marks the contact with oceanic crust in the hanging wall. Faults shown are in the basement which is now overlain by 1 to 5 seconds of sediments. Basement faults under the Amazon Delta are not mapped as they are deeper than the seismic record.

2.2.2 GRAVITY DATA

Gravity is a very important tool for interpreting basins. It maps subtle changes in the Earth's gravitational field caused by variations in the density of the underlying rocks, and it provides valuable information on basement topography and the nature of the deeper parts of the crust and mantle beneath the basins. Important intra-basin elements often have an associated gravity signature indicating that each element is related to a deep basement structure.

In order to interpret the geological source of a gravity anomaly, the data must be calibrated. Gravity images show density contrasts within the crust, but the source of the contrast is not unique. As a regional tool gravity yields information both on the density of bodies within the crust and on differences in mantle depth and composition.

2.2.2.1 Free-air Gravity Anomalies

The free-air gravity anomalies dataset (Fig. 2-5) used was the new global satellite Free-Air data obtained from the SATELLITE GEODESY gravity data (Version 18.1: released April 2009). Composed of free-air anomalies derived from radar altimetry measurements of ocean surface, the free-air anomaly grid has a grid cell size of 1-arc minute, equivalent to about 2km (Sandwell and Smith, 2009).

The gradient of the free-air gravity delineates the boundary of the gravity anomalies by amplifying the high frequency component of the spectrum. Noise is also

enhanced in this process. We calculated the gradient of the free-air anomaly (Fig. 2-6) using the dip function algorithm on Geoframe (Schlumberger software), and using the free-air gravity grid (Fig. 2-5). Because it delineates the shapes of the gravity sources, the gradient of the free-air gravity is an efficient tool to map the main tectonic features in the area (Fig. 2-6).

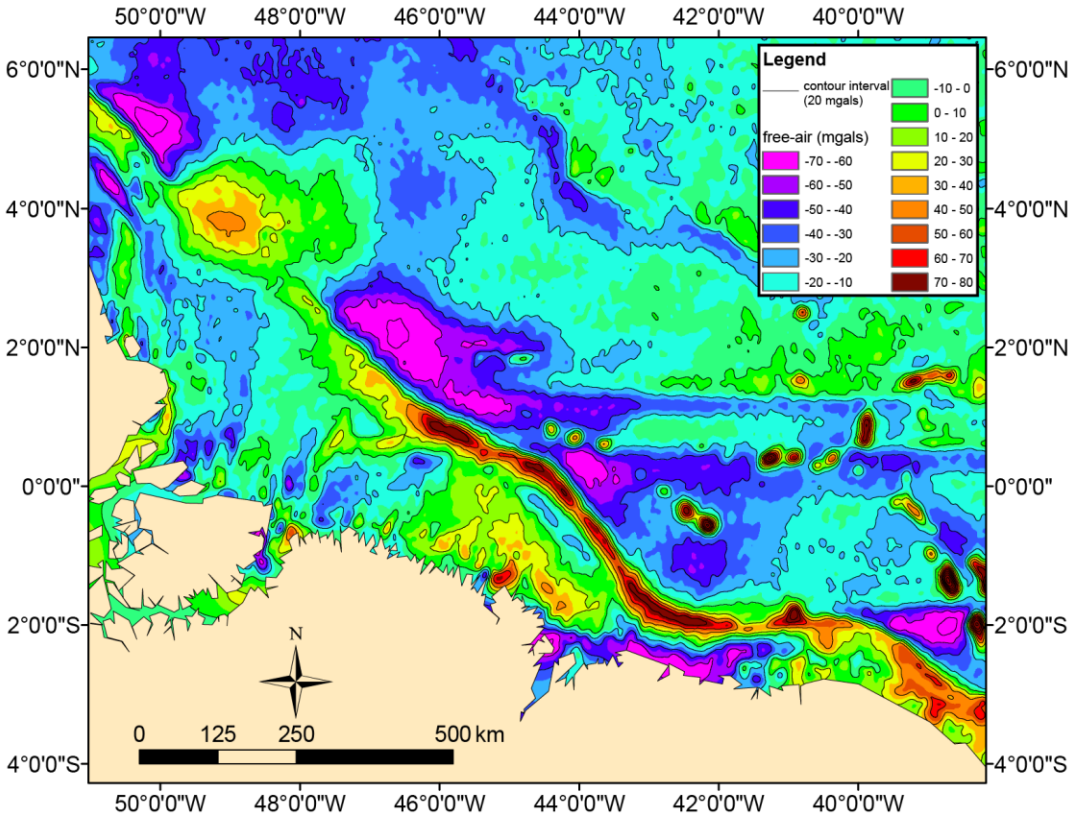

Figure 2-5. Free-air gravity anomaly map (mgals). Free-air gravity anomaly map was used to map the main bathymetric features of the study area. Fracture zones correspond to negative anomalies (-70 to -40 mgals). Free-air gravity anomalies have positive high amplitudes on the edge of the continental margin (20 to 80 mgals) and negative high amplitudes on the oceanic crust (-20 to -70 mgals). The slope is narrow (15 to 35 km wide), with the exception of the area under the Amazon Delta and corresponds to low amplitude positive and negative gravity anomalies (+20 to -20 mgals).

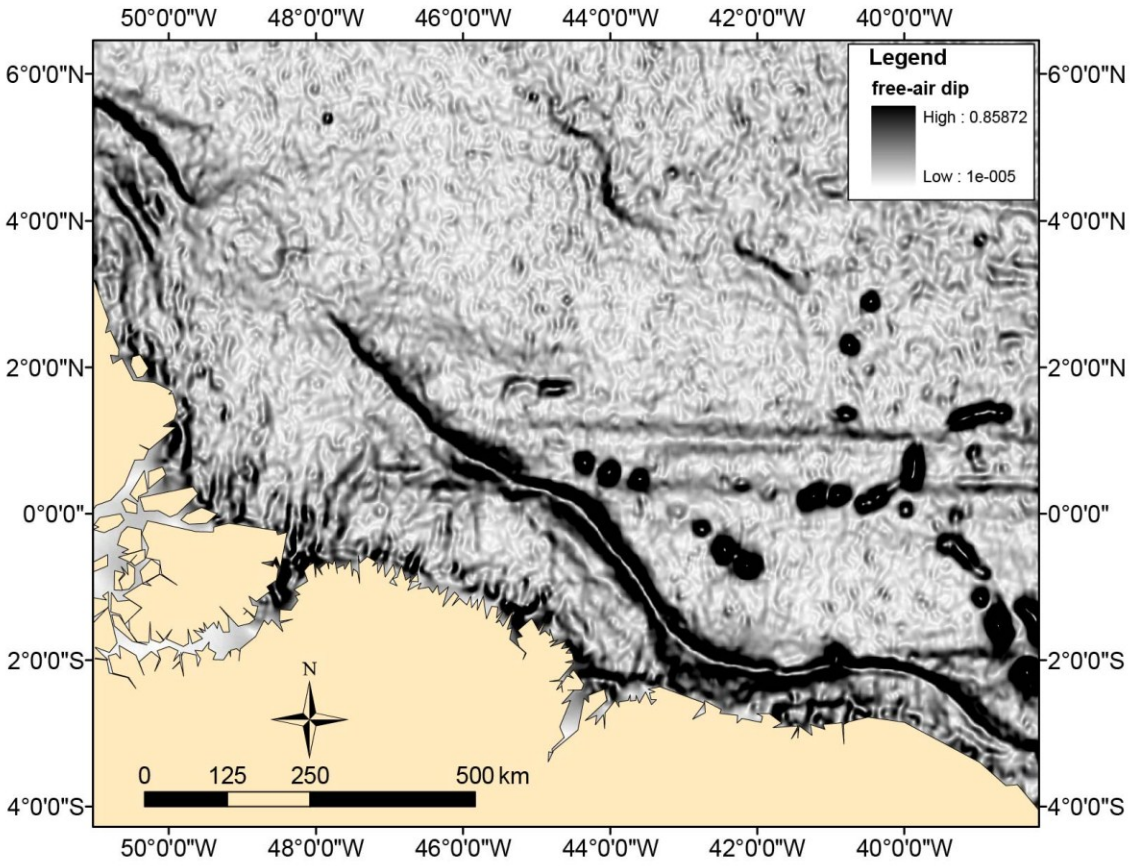

Figure 2-6. Gradient of free-air gravity map, shows many tectonic features including the continental margin, Ceará Rise, fracture zones, and seamounts.

2.2.2.2 Bouguer Gravity Anomalies

Free-air gravity data is reduced to Bouguer gravity by the calculation and removal of the effects topography (rock/water or rock/air interface) on the gravity anomaly. The Bouguer anomaly grid (Fig. 2-7) was calculated by subtracting the Bouguer correction from the free-air anomaly grid from Sandwell and Smith (2009).

$F_{bouguer}=F_{air}- \Delta G$

ΔG = Bouguer correction

The Bouguer correction ΔG was calculated using the slab equation, in which we have used densities of 2.65 for the crust and 1.03 for the water:

$\Delta G = 0.04185 \Delta\rho H$,

H= bathymetry

$\Delta\rho$= density contrast

$\Delta\rho = \rho$ crust – ρ water,

ρ crust = density of the crust=2.65

ρ water= density of the water=1.03

The ocean floor interpreted on the seismic grid was gridded and depth converted using a velocity of 1500 m/s for the water and extended into the oceanic basins using the

Etopo1 grid (Amante and Eakins, 2009). The result is the grid on figure 2-4. The ETOPO1 is a 1 arc-minute, equivalent to about 2km, global bathymetric grid.

Bouguer gravity anomalies (Fig. 2-7) are associated to changes in density and therefore are used to understand the crustal nature of the basement. The gradient of the Bouguer gravity (Fig. 2-8) enhances near surface contrasts in density by amplifying the high frequency component of the spectrum. Noise is also enhanced in this process.

We calculated the gradient of the Bouguer anomaly using the dip function algorithm on Geoframe (Schlumberger software), and calculated a Bouguer gravity gradient grid (Fig. 2-8). Because it enhances the difference in density contrast, the gradient of the Bouguer gravity is an efficient tool to map the contact between oceanic crust and transitional crust.

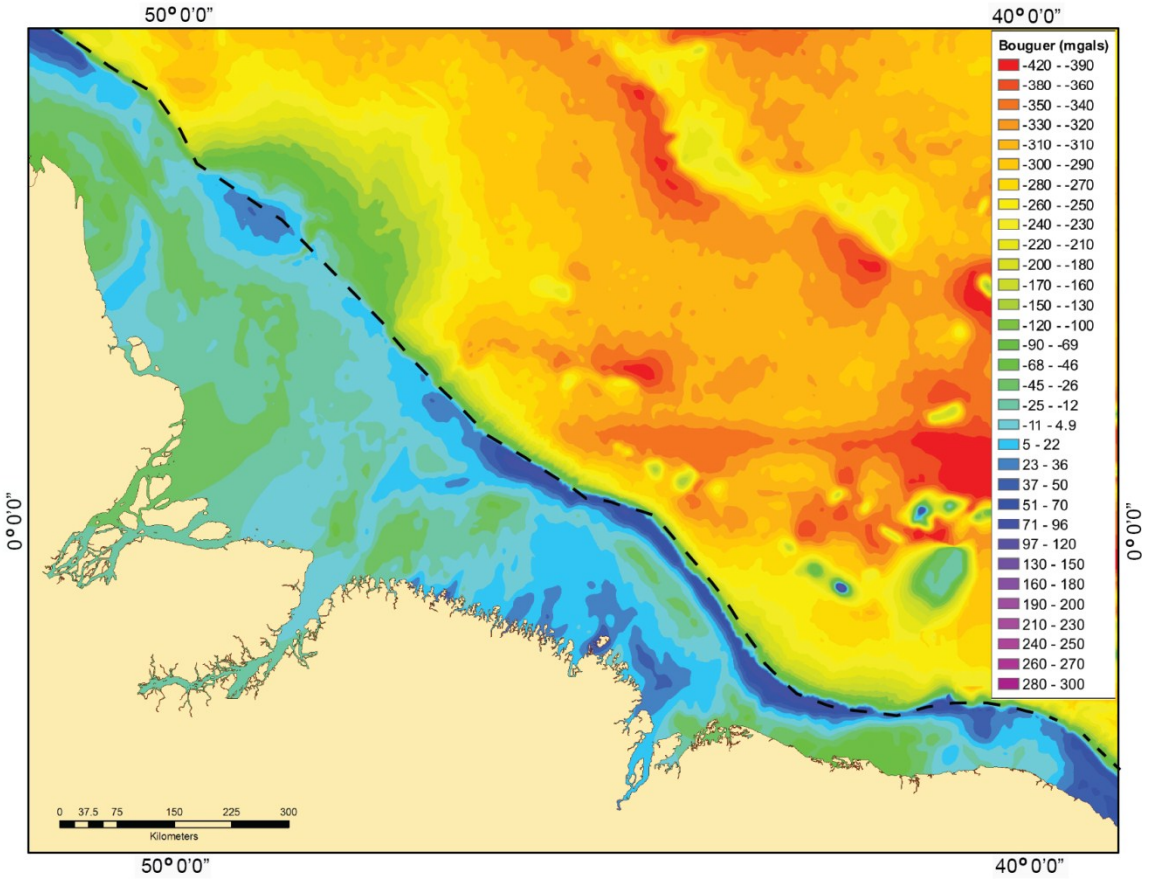

Figure 2-7. Bouguer gravity anomaly map of the Brazilian Equatorial margin. The Bouguer correction was calculated using a water bottom map generated by a merger of two grids. A depth-converted water-bottom grid based on the seismic interpretation on the shelf and slope, infilled in the area without seismic coverage with an Etopo1 grid (Amante and Eakins, 2009). The Bouguer correction was applied to the free-air anomaly map (Fig. 2-5) to calculate the Bouguer gravity anomaly map.

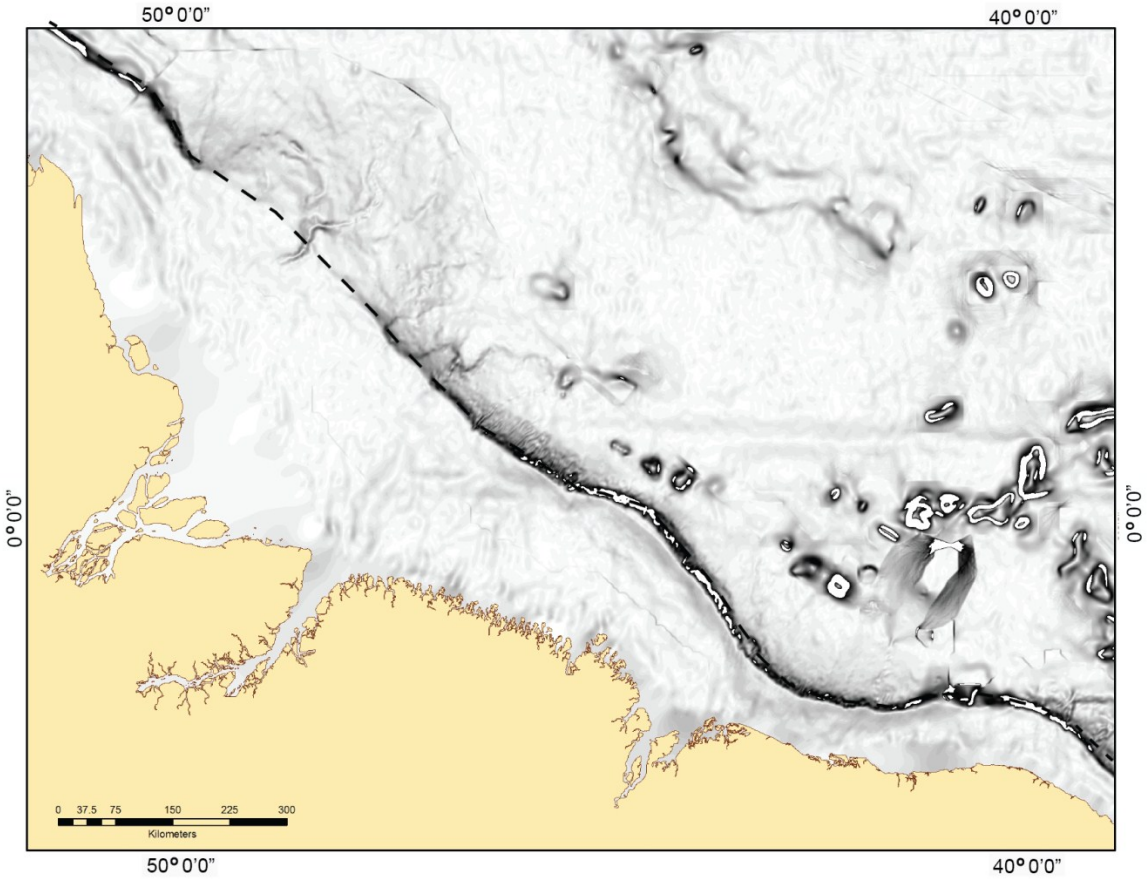

Figure 2-8. Gradient of the Bouguer anomaly map. Continental-oceanic transition zone is shown in a dashed line.

2.2.3 Magnetic Data

We have used the global Earth Magnetic Anomaly Grid (EMAG2), a total magnetic intensity grid at an altitude of 4 km above mean sea-level of 2-arc minute resolution (approximately 4 km) (Maus et al., 2009). The data (Total Magnetic Intensity) anomalies were used in the form published by Maus et al. (2009), with no corrections applied (Fig. 2-9). The TMI is the measurement of total magnetic field at a location with the International Geomagnetic Reference Field (IGRF) removed. Magnetic data measure variations in the Earth's magnetic field caused by variations in the magnetic susceptibility of the underlying rocks. It provides information on the structure and composition of magnetic basement and intra-sedimentary magnetic units, if present. Most bodies within the basement have a distinct magnetic signature characterized by the magnitude, heterogeneity, and fabric of the magnetic signal.

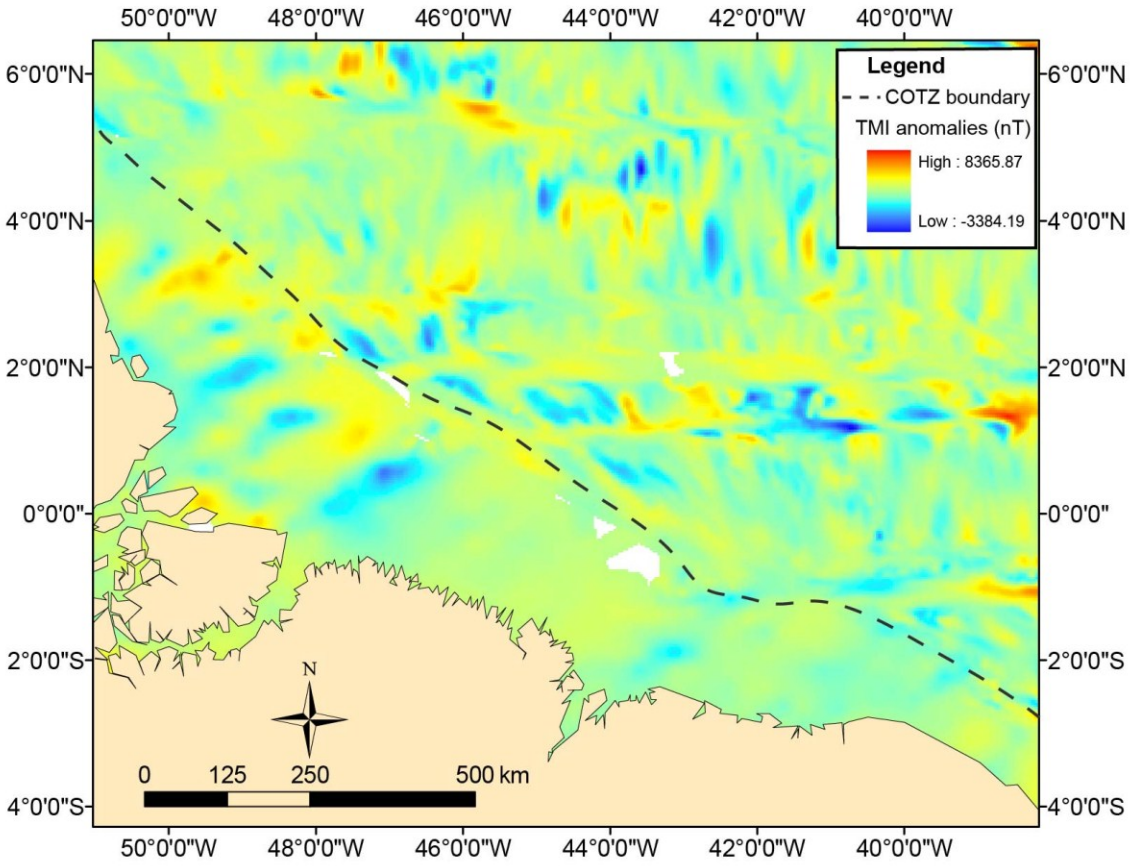

Figure 2-9. Total magnetic intensity anomaly map of the Equatorial margin of Brazil data from the global magnetic anomaly grid (Maus et al., 2009). The continent-ocean transition zone separates NE-trending Proterozoic (Birimian, ~2.1Ga) magnetic anomalies from N-S-trending anomalies of the Cretaceous ocean floor rocks. The boundary is shown as a dashed line and corresponds approximately to the COTZ boundary, but is not as sharply defined as on the first derivative of the Bouguer anomaly map (Fig. 2-8).

2.3 SEISMIC DATA INTERPRETATION

Two seismic horizons were mapped in the area to describe the geometries of the continental margin and the COTZ; the water bottom and the basement. Mapping of the water bottom horizon describes a very broad continental shelf in the north of the study area (over 300 km) in the Foz do Amazonas (Fig. 2-1). Here interpreted to be a result of the extreme progradation that took place in the Late Miocene on the Brazilian Equatorial margin (Morais Neto et al., 2006 and 2009, Figueiredo et al., 2009). In the south, away from the sediment sources, the continental margin is narrower (less than 100 km) in the Ceará Basin (Fig. 2-1).

The interpreted basement horizon in the continental shelf corresponds to a combination of the crystalline basement and the top of the pre-rift mega-sequence, where present. The pre-rift mega-sequence was described by Trosdtorf et al. (2007) and is not discussed in this work. Basinward in the continental slope and in the ocean basin it corresponds to the top of transitional and oceanic crust as defined seismically, discussed in chapter 3 (Figs. 3-7 to 3-10). The basement structural map (Fig. 2-4) is less than 3000 ms deep under the continental shelf and is more than 6000 ms deep on the toe of slope. This abrupt transition occurs in an extent of less than 20 km, and is here interpreted to be the Continent Ocean Transition Zone (COTZ). The basement faults mapped are mostly located around this boundary. Basement faults under the Amazon Delta could not be mapped on the seismic as they are deeper than the seismic record.

2.4 POTENTIAL FIELD DATA INTERPRETATION

Marine gravity anomalies derived from radar altimetry measurements.of ocean surface slope (Sandwell and Smith, 2009) are the primary data for investigating global tectonics and continental margin structure. The free-air gravity anomaly map (Fig.2-5) was used to map the main tectonic features of the study area. Free-air gravity anomalies have positive high amplitudes on the edge of the continental margin (20 to 80 mgals) and negative high amplitudes in the abyssal plains (-20 to -70 mgals) (Fig. 2-5).

The Continental Oceanic Transition Zone (COTZ) is interpreted based in the free-air gravity anomalies as a transition zone between the positive anomalies in the margin to the negative anomalies in the ocean basins. It is a narrow zone (15 to 35 km wide), with the exception of the area under the Amazon Delta. The Amazon Delta sits on the continental slope. Gravity anomalies in the area, firstly described by Cochran (1973), have low positive and negative amplitudes (+20 to -20 mgals) and large wavelength (Fig. 2-5). Fracture zones correspond to negative anomalies (-70 to -40 mgals) and stop abruptly east of the positive amplitude free-air anomalies in the continental slope. Seamounts correspond to positive free-air anomalies. The geometries of the observed bathymetric features are enhanced using the gradient of free-air anomalies gravity map (Fig. 2-6).

Bouguer gravity anomalies are negative on the ocean basins and positive on the continental margin (Fig. 2-7). The Bouguer correction creates a boundary of high positive

amplitudes at the continental slope traditionally interpreted as the continental/oceanic boundary. The high amplitude boundary is enhanced by the gradient of the Bouguer anomalies (Fig. 2-7) and can be followed under the Amazon Delta. Because it enhances the difference in density contrast, the gradient of the Bouguer gravity is an efficient tool to map the contact between oceanic crust and transitional crust.

Two main directional trends are observed in the total magnetic intensity anomaly map (Fig. 2-9); a NE-SW trend in the continental margin here interpreted to be caused by Proterozoic (Birimian, ~2.1Ga) rocks, and a N-S-trend in the ocean basin, here interpreted to be Cretaceous ocean floor rocks. The nature of the ocean floor rocks cannot be evaluated with magnetic data alone (Sibuet et al., 2007). Sibuet et al. (2007) demonstrated that serpentinization of exhumed mantle rocks can cause magnetic anomalies similar to oceanic crust and therefore can be used to date the age of the ocean floor, but not to distinguish crustal nature. The continent-ocean boundary, interpreted using the gradient of Bouguer anomalies, is shown as a dashed line at the top of the total magnetic anomalies map (Fig. 2-9). It shows a very good fit, as the boundary between the N-S and NE-SW anomalies corresponds approximately to the COTZ boundary interpreted using the gradient of the Bouguer anomaly map (Fig. 2-8).

2.5 MAPPING OF THE OCEAN CONTINENT TRANSITION ZONE (COTZ)

We use the continent ocean transition zone (COTZ) defininition from Direen et al. (2012); i.e. a region of highly attenuated continental crust on the continental margin that lies between the outboard edge of unequivocal continental crust, and the inboard edge of unequivocal oceanic crust. The COTZ includes both sedimentary and magmatic components in proportions that vary both along and across the margin, and may include areas of failed sea-floor spreading (Direen et al., 2012). Note that this definition is similar, but not identical, to the term ocean–continent transition (OCT) as used by Manatschal (2004) and Reston (2007) for the transition from the distal continental margin to the first oceanic crust. We use the term continent–ocean boundary (COB) for the inboard edge of unequivocal oceanic crust (Direen et al., 2012).

We interpreted the continent ocean transition zone (COTZ) using the basement map (Fig. 2-4) in combination with the first derivative of the Bouguer gravity anomalies (Fig. 2-8) and the world magnetic (total magnetic intensity) map (Fig. 2-9). The continent ocean transition zone (COTZ) geophysical characteristic is a high continuous gravity gradient anomaly (Fig. 2-8) that parallels the shelf and separates a pattern of NE-SW magnetic anomalies generated by continental crust from N-S sea-floor spreading magnetic anomalies (Fig. 2-9).

In the basement structural map (Fig. 2-4) the transition from continental crust to oceanic crust corresponds to a change from basement depths of less than 3000 ms on the

continental shelf to depths of more than 6000 ms on the toe of slope in less than 20 km. This area is interpreted to be the COTZ. Basement is overlain by 1 to 5 seconds of sediments. The basement faults mapped are mostly located within the COTZ and the most seaward faults mapped mark the contact with oceanic crust in the hanging wall. Basement faults under the Amazon Delta could not be mapped as they are deeper than the seismic record. Under the Amazon Delta the location of the COTZ is based only on potential field data. In our interpretation the Amazon Delta covers the COTZ and progrades onto the oceanic crust.

2.6 BASEMENT GEOMETRY AND MARGIN SEGMENTATION

Four main segments based on fault geometry are described in the study area: 1) Piauí-Ceará, 2) Barreirinhas, 3) Pará-Maranhão-Foz do Amazonas, and 4) Amapá.

2.6.1 Piauí-Ceará Margin

The continental margin is narrow, only 90 kilometers in the segment of the Northeast Brazilian margin occupied by the Piauí-Ceará Basin (Fig. 2-10). The continental margin on the Piauí-Ceará segment is composed of a series of large, mostly over 200 km long E-W faults that trace to the Romanche Fracture Zone on the oceanic crust (Fig. 2-10). Basement faults are represented on the rose diagram (Fig. 2-10).

In this area the transition between continental and oceanic crust is extremely sharp. The transition from the continental crust to the abyssal basin oceanic crust involves two main low angle (~15 degrees ±5) and large displacement (> 5 km) E-W-trending fault zones. The rose diagram on figure 2-10 indicates the prevalence of E-W-trending faults in the Piauí-Ceará Basin. The cross section in figure 2-10 represents the geometry of the COTZ in the Piauí-Ceará Basin. Represented in the cross-section is a low angle (~15 ^{o}) and large displacement (4 seconds) basement fault that separates continental crust from the continental oceanic transition zone (COTZ). Sedimentary rocks are represented in yellow, basement rocks are represented in brown, and water is represented in blue in the cross section.

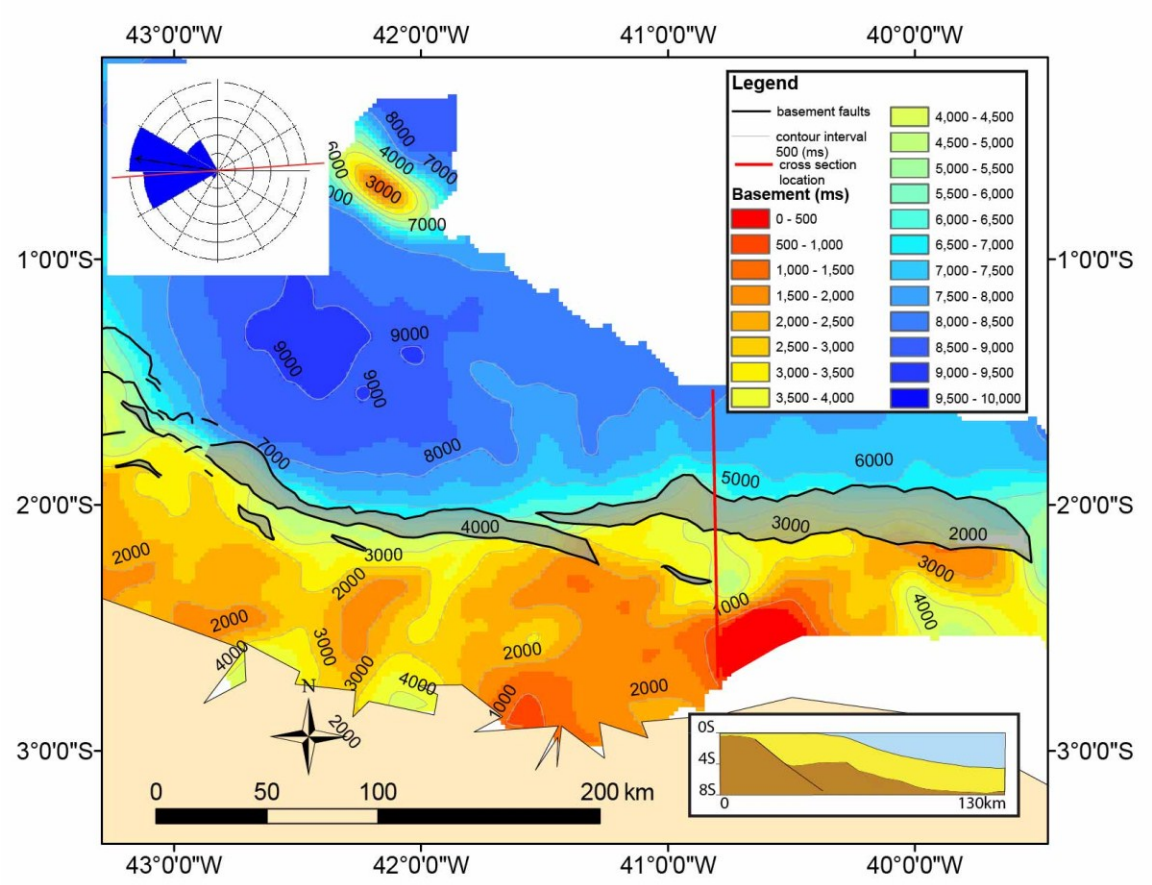

Figure 2-10. Basement map of the Piauí-Ceará Basin. Two E-W trending fault zones, each above 100 km long at ~2 ° S, extend from 39 °40'W to 42°30'W. The gray areas represent fault heaves. Insets: 1) Rose diagram normalized to fault lengths, represents prevalent strike direction of basement faults in the map. Mean direction calculated was 278°. Red line in the rose diagram represents the main spreading direction at 105 Ma, measured on the Romanche Fracture Zone and calculated on the flow lines on Figure 2.15. 2) Cross section, vertical scale in seconds and horizontal scale in kilometers, sedimentary rocks are represented in yellow, basement rocks in brown, and water in blue.

2.6.2 Barreirinhas Margin

The Barreirinhas continental margin is narrow (160 kilometers), and the transition between continental and oceanic crust is sharp (~20 kilometers) (Fig. 2-11). Barreirinhas Basin basement faults trend close to E-W in the southern part of the basin, adjacent to the Piauí-Ceará Basin and trend NW-SE in rest of the basin. The contact between NW-SE and E-W-trending faults forms a basement low with the shape of half a rhombohedron. The rose diagram on figure 2-11 represents the most prevalent strike direction for the faults in the area.

The south Barreirinhas basement faults belong to the same fault set as those on the Piauí-Ceará Basin described in the previous section, and therefore are plotted in the rose diagram on figure 2-10. Basement faults in the rest of the basin belong to a NW-SE fault system, plotted on the rose diagram on figure 2-11, a very similar trend extends north and covers most of the neighboring Pará-Maranhão Basin, described on the next section and plotted on the rose diagram on figure 2-12. Here we refer to the Barreirinhas Basin basement faults as the NW-SE trend in figure 2-11. Basement faults in the Barreirinhas Basin have lengths from 5 to 50 km, low angle (~15 ^{o}), and large displacement (3 seconds) (Fig. 2-11).

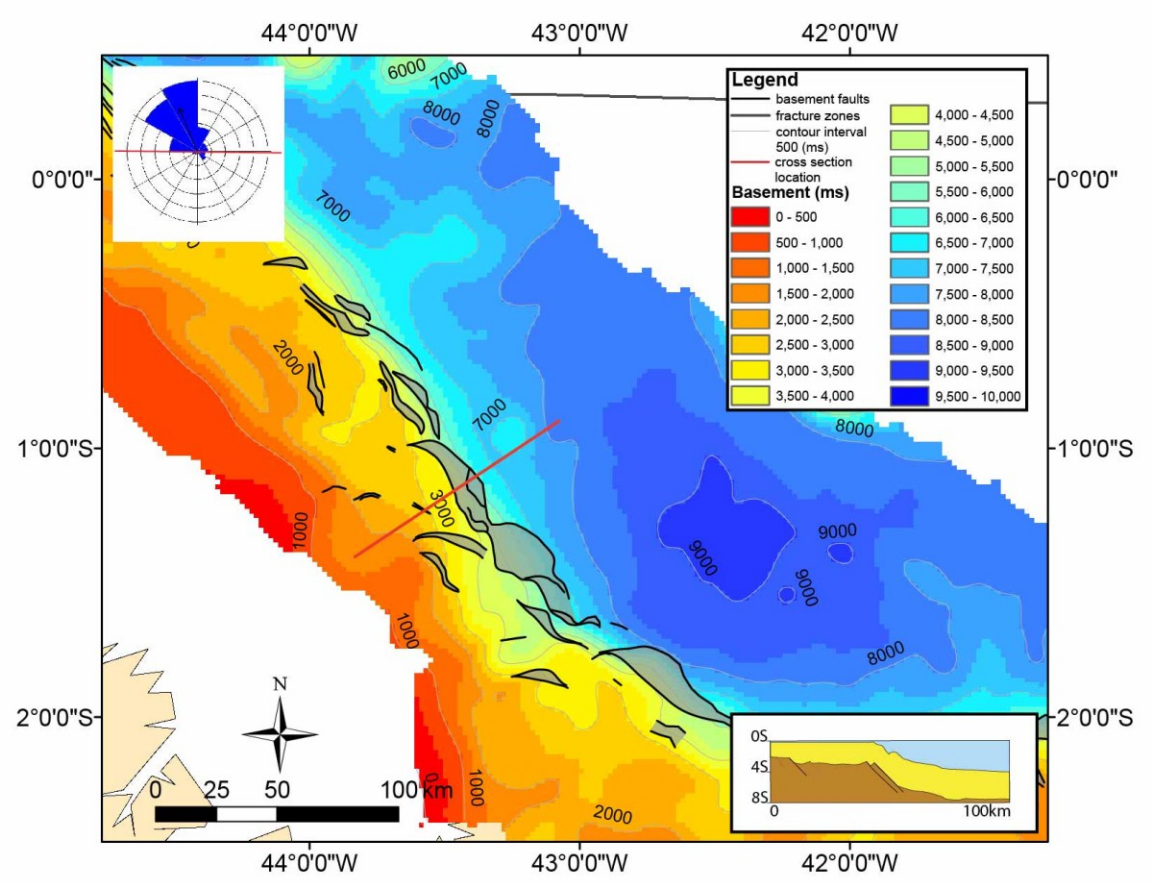

Figure 2-11. Basement map of the Barreirinhas Basin. Basement faults have lengths from 5 to 50 km and a NW-SE trend. The gray areas represent fault heaves. Insets: 1) Rose diagram for basement faults, normalized to fault lengths. Mean direction calculated was 337°. Red line in the rose diagram represents the main spreading direction at 105 Ma, measured on the Saint Paul Fracture Zone and calculated on the flow lines on Figure 2.15. 2) Cross section, vertical scale in seconds and horizontal scale in kilometers, sedimentary rocks are yellow, basement rocks are brown, and water is blue.

2.6.3 Pará-Maranhão to Foz do Amazonas Margin

The continental margin is wider (~220 kilometers) in the Pará-Maranhão Basin. The Pará-Maranhão Basin is more heavily faulted than the Piauí-Ceará Basin; faults are smaller, and have smaller displacements, but similar dip angles (15^{o} to 20^{o}) (Fig. 2-12). Basement faults have lengths of 5 to 50 km, and NW-SE direction (see rose diagram insert to Fig. 2-12).

The transition from the continental margin to the abyssal basin (COTZ) is more gradual, being accommodated by many fault sets. The COTZ in this margin segment correspond to a series of normal fault zones. Two fault zones are represented in the cross section, (Fig. 2-12) the total displacement accommodated by the sum of both faults is 4 seconds in 20 kilometers, the same as observed in the other segments of the margin. The difference is that in this area it is distributed in a larger number of smaller fault zones.

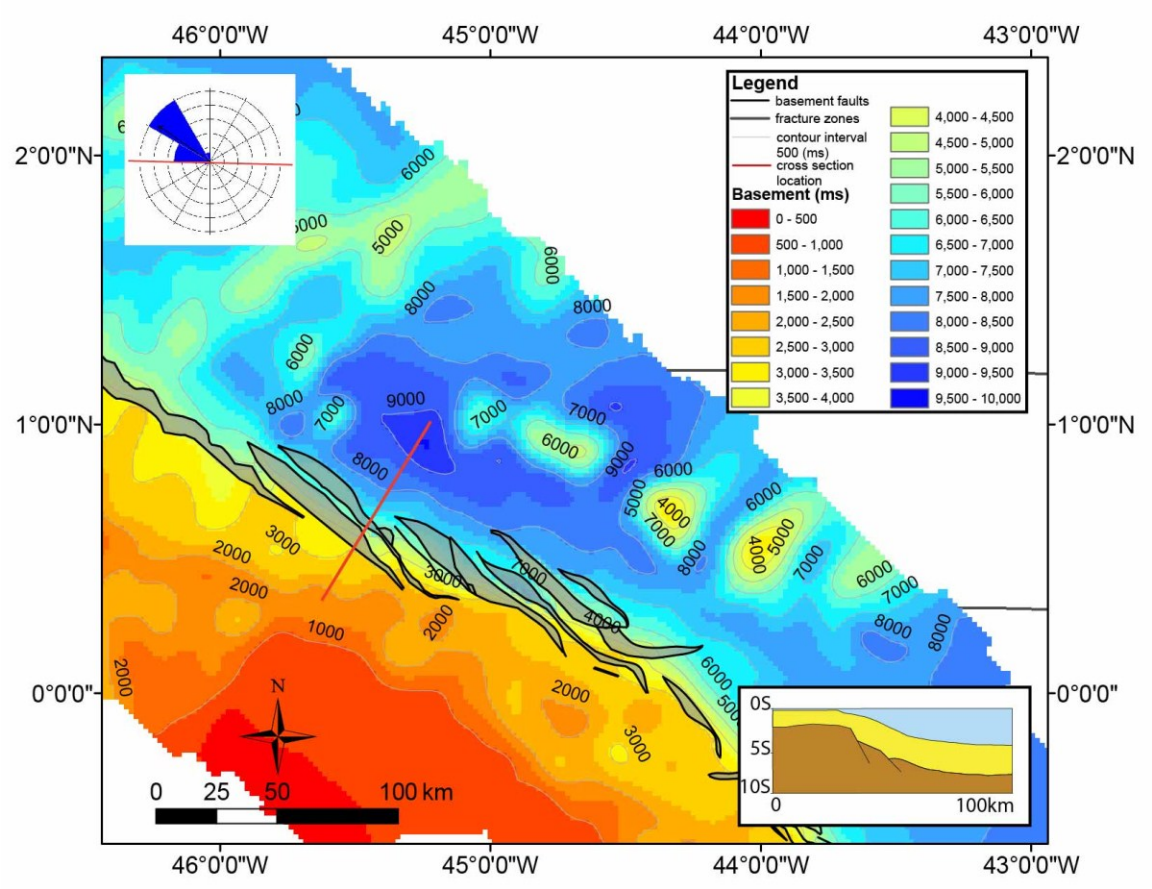

Figure 2-12. Basement map of the Pará-Maranhão Basin. Basement faults have lengths of 5 to 50 km and NW-SE direction. The gray areas represent fault heaves. Insets: 1) Rose diagram for basement faults normalized to fault lengths. Mean direction calculated was 304 °. Red line in the rose diagram represents the main spreading direction at 105 Ma, measured on the Saint Paul Fracture Zone and calculated on the flow lines on Figure 2.15. 2) Cross section, vertical scale in seconds and horizontal scale in kilometers, sedimentary rocks are yellow, basement rocks are brown, and water is blue.

2.6.4 Amapá Margin

The Amapá continental margin is very wide, 330 kilometers. Basement faults have lengths of 40 to 180 km and trend NW-SE, as can be seen on the basement map (Fig. 2-13). The COTZ is characterized by faults with approximately 15^{o} dip angles and 1 second displacements. The continental crust basement is 2 seconds (twt) deep and transitions to 7 seconds (twt) deep, where composed of oceanic crust. The transition occurs in 90 kilometers in the strike direction, making it the broadest COTZ on the Brazilian Equatorial margin. The COTZ in the margin corresponds to a series of normal fault zones. Three fault zones are represented in the cross section (inset Fig. 2-13) ; the total displacement accommodated by the sum of both faults is six seconds in 100 kilometers, which results in a less steep basement slope than the observed in the other segments of the margin. Fault dip angles are similar 15^{o} to 20^{o}, but have a smaller displacement (Fig. 2-13).

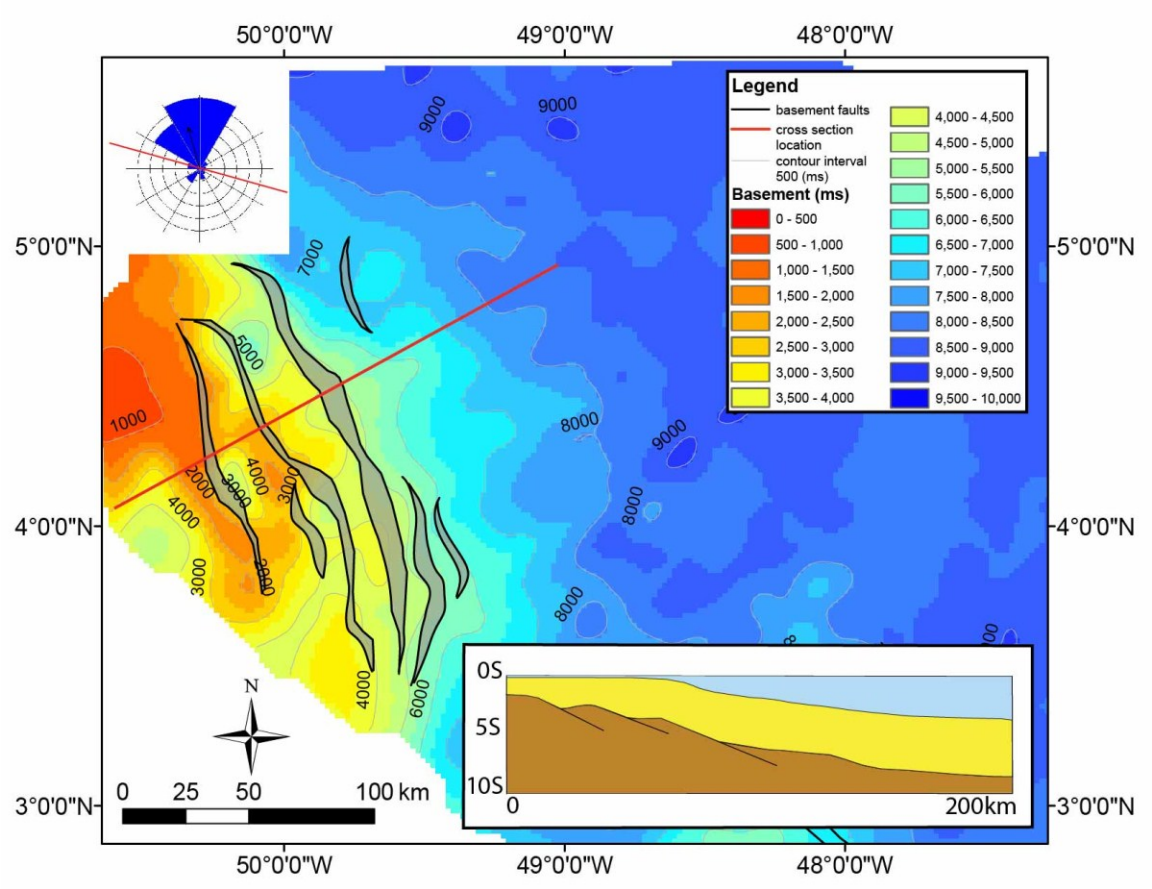

Figure 2-13. Basement map of the Amapá margin. Basement faults have lengths of 40 to 180 km and NW-SE direction. The gray areas represent fault heaves. Insets: 1) Rose diagram for basement faults has been normalized to fault lengths. Mean direction calculated is 345°. Red line in the rose diagram represents the main spreading direction at 105 Ma, calculated on the flow lines on Figure 2.15. 2) Cross section, vertical scale in seconds and horizontal scale in kilometers, sedimentary rocks are yellow, basement rocks are brown, and water is blue.

2.7 DISCUSSION

2.7.1 Segmentation of the Brazilian Continental Margin.

The geometry of the continental oceanic transition zone (COTZ) gets locked at the time of intrusive contact that is the emplacement of the oceanic crust. Prior to the emplacement of oceanic crust, the rift faults are formed and grow, but fault movement ceases as soon as oceanic crust is emplaced. Therefore the COTZ geometry gives a snapshot in time for the geometry of the fault system at the time of the rifting. In the Brazilian Equatorial margin that is very significant as most of basement faults are limited to the COTZ (Fig. 3-7) as a result of being located along a transform margin to oblique-rifted margin. (Fig. 3-1).

Rift geometries are more complex than described by the classic models (McKenzie, 1978 and Wernicke, 1985). Rifting can involve different processes of extension operating simultaneously in different segments of the margin and can involve multiple phases of subsidence, uplift, and volcanism (Autin et al., 2010). Several mechanisms exist that are thought to facilitate rifting, here discussed in the context of the Brazilian Equatorial margin;

1. Inherited weak zones originate from the amalgamation of distinct tectonic plates that are reactivated by the rift process (Ziegler and Cloetingh, 2004). This causes stress to focus in weaker points, first causing break-up to

propagate in a certain direction, as was the case for the opening of the South Atlantic (Torsvik et al., 2009).

2. Melt generation and magma transport weaken the lithosphere both by efficient heating, and by mechanical strength reduction (Buck, 2007). It is caused by mantle plumes which play an important role in triggering continental break-up on magma-rich margins (Ziegler and Cloetingh, 2004). It is mostly absent in magma-poor margins, as in the case of the Equatorial Atlantic.
3. Most recently Brune et al. (2012), focusing on magma-poor rift settings, showed that oblique extension significantly facilitates the rift process, because oblique deformation requires less force in order to reach the plastic yield limit than rift-perpendicular extension. This factor can be significant in magma-poor regions, like the Brazilian Equatorial margin.

The earlier rifting stages of the Equatorial Atlantic had an intra-continental dextral shear component, described in the onshore basins of northeast Brazil (Magnavita, 1992, Darros de Mattos, 1999, Destro et al., 2003), in the South American margin between Northeast Brazil and the Guinean coast of Africa (Greenroyd et al., 2008), and in the counterpart Guinean coast of Africa (Antobreh et al., 2009). The fault geometries associated to the earlier stages of the rift have been described in detail in the onshore basins of northeast Brazil (e.g. the Recôncavo-Tucano-Jatobá Basins and the Cariri-Potiguar Basins) (Magnavita, 1992, Darros de Mattos, 1999, Destro et al., 2003). The geometry of these intra-cratonic basins consist of asymmetric half grabens separated by

basement highs, transfer faults, and/or accommodation zones with a spectrum of normal and strike-slip basement-involved faults (Darros de Matos, 1999).

This work was the first attempt to describe in detail the geometries of the rift faults in the Brazilian Equatorial margin, as opposed to the work from Greenroyd et al., (2008) and Antobreh et al. (2009) that focused on the mapping of the COTZ regionally and not detail mapping of the faults that comprise the COTZ. Greenroyd et al., (2008) described internal deformation on the South American margin, from the French Guiana to northeast Brazil margin, during the earlier stages of rifting. The authors were the first to describe the segmentation of the margin as a series of rift-dominated and transform-dominated segments, that they named rifted and sheared segments respectively. Antobreh et al. (2009) described similar segmentation in the counterpart Guinean coast of Africa and used the same nomenclature. Antobreh et al. (2009) used the term sheared margin to describe the segments of the Ghanaian margin that are parallel to the main fracture zone traces, and rifted margins to describe the segments in between. Sheared margins trace and are parallel to major oceanic fracture zones that offset the Mid-Atlantic Ridge up to several hundreds of kilometers.

Here we used the same terminology used by Greenroyd et al. (2008) and Antobreh et al. (2009) to describe the Brazilian margin. Segments with basement faults parallel to the basinward fracture zones, correspond to sheared segments (Greenroyd et al., 2008, Antobreh et al., 2009) and segments with basement faults oblique to the

direction of sea-floor spreading correspond to rifted segments (Greenroyd et al., 2008, Antobreh et al., 2009). From south to north, from the Piauí-Ceará to offshore Amapá, shear-dominated and rift-dominated segments of the margin alternate. We describe the Piauí-Ceará margin and the southern portion of the Barreirinhas margin as a sheared segment and the Barreirinhas, Pará-Maranhão, and Amapá as rifted margins. The East-West geometry of the COTZ under the Foz do Amazonas, suggests the possibility of a buried sheared segment between Pará-Maranhão and the Amapá margin. The continental margin is wider, and the basement is heavily faulted in the rifted segments and is narrow with fewer faults on the sheared segments.

The Piauí-Ceará shear segment of the margin has been described by Bird (2001) as a transform margin; that segment is particularly well developed as it is bounded by the Romanche Fracture Zone. The shear segments of the margin (Piauí-Ceará Basin and possibly a buried segment between Pará-Maranhão and the Amapá North Rift) are large scale features of what has been described by McClay and White (1995) as accommodation zones separating rifted segments.

The rifted segments of the Brazilian Equatorial margin are oblique rifts composed by shorter, segmented border faults with major rift faults forming en-echelon arrays parallel to the underlying zone of extension as described by Umhoefer et al. (2002). Basement fault dips are similar in all segments, but displacement and strike varies. Characteristics of faults per segment are represented in the table below.

Segment	Mean fault strike direction (azimuth)	Faults mean dip	Faults mean displacement	Faults length
Piauí-Ceará	~278^{o}	~15 ^{o} to 20 ^{o}	4 seconds	180 to 210 km
Barreirinhas	~337^{o}	~15 ^{o} to 20 ^{o}	3 seconds	5 to 50 km
Pará-Maranhão	~304^{o}	~15 ^{o} to 20 ^{o}	1.5 to 2.5 seconds	5 to 50 km
Amapá	~345^{o}	~15 ^{o} to 20 ^{o}	1 second	40 to 180 km

Table 2-1 geometries of the basement faults in the Brazilian equatorial margin.

2.7.2 Basement Fault Geometry and Obliquity of the Rift

The geometric distribution of the sheared segment faults arranged between rifted segments in the Brazilian Equatorial margin is similar to what was described as accommodation zones by McClay and White (1995). The authors proposed that accommodation zones consisting of systems of conjugate extensional faults accommodate the polarity reversals between rift segments in oblique rifts. Because of the strong strike-slip component on oblique divergent passive margins, many characteristics of strike-slip basins are observed in oblique rifts: 1) widespread structural segmentation with a possible alternating vergence in the segmentation (Umhoefer et al., 2002); and 2) episodic development of the plate boundary with progressive concentration of plate motion onto the main boundary (Hayward and Ebinger, 1996), stress rotation (Bergerat, 1989), and en-echelon arrangements of normal faults and rhombohedric arrangements of horsts (Bergerat, 1989) in which elongation is controlled by the displacement along strike-slip faults (Bergerat, 1989).

The Barreirinhas Basin has the shape of half a rhombohedron that indicates a role for a strike-slip component active during the earlier stages of rifting, as described by Bergerat (1989) in the Pannonian Basin.

In the whole Brazilian Equatorial margin the edge of the continental crust corresponds to a series of normal fault zones. The difference is that in the transform segment of the margin the total displacement (sum of the displacement in the dip

direction of all faults) which adds to approximately 4 seconds is distributed by fewer fault zones than in the rest of the margin. Basement fault dip angles range between 15^{o} to 20^{o} (table 2-1) in all segments of the margin, but fault displacement differs and are higher (4 seconds) in the transform segment of the margin (table 2-1), intermediate on the oblique segments (1.5 to 3 seconds), and smaller (1 second) on the more orthogonal segment of the margin.

The Amapá margin is very wide, consistent with a higher crustal stretching on the rifted segments, as opposed to the sheared segments, as shown by the Greenroyd et al. (2008) crustal models. Greenroyd et al. (2008) made two 2D magnetic models, one on the rifted margin and one on the transform margin of French Guiana. The rifted segment model shows that the crust thins from 37 km to 7.5 km over a distance of 317 km, and on the transform segment model, the crust thins from 37 km to 7.5 km over a distance of 70 km (Greenroyd et al., 2008).

Clifton and Schlische (2001), using scaled physical models, demonstrated that there is a geometric upper limit to fault length in oblique rift zones causing fault length to be inversely proportional to obliquity. That relationship is observed in the basement fault geometries of the Brazilian Equatorial margin. There is a correlation between obliquity and strike length basement faults in the Brazilian Equatorial margin. Offshore Piauí-Ceará is a transform margin and basement faults strike-lengths are very long from 180 to 210 km (table 2-1) (Fig. 2-14). In the oblique-rifted segments of the Barreirinhas and

Pará-Maranhão fault strike lengths range from 5 to 50 km (Fig. 2-14). Offshore Amapá the rifting geometry was less oblique, than in the Barreirinhas and Pará-Maranhão segments and basement faults strike lengths are as long as 180 km (table 2-1) (Fig. 2-14). Because basement faults formed and grew during the rifting process, their geometries represent the geometry at the time of rifting and an argument can be made that there is an observed upper limit of ~ 50 km to fault length in the oblique-rifted segments of the Brazilian Equatorial margin.

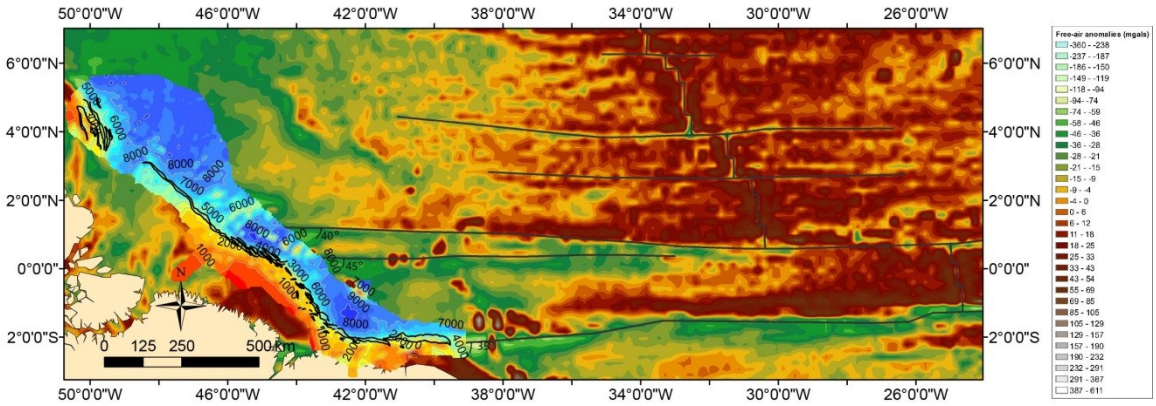

Figure 2-14. Structural map of the Brazilian Equatorial margin and adjoining oceanic basins, depicting the structure of the ocean floor between the mid-oceanic ridge and the continent-ocean transition zone. Map shows depth to basement in miliseconds mapped on the seismic data set superimposed on the free-air gravity anomalies data set (Sandwell and Smith, 2009). Fracture zones and mid-ocean ridge displacements are interpreted based on the free-air gravity anomalies. Basement faults on the continental margin and slope are interpreted on the seismic data set. Map shows that the continent-oceanic transition zone (COTZ) is highly segmented and faulted, and that segmentation is observed at the present day boundary at the mid-oceanic ridge.

2.7.3 The Geometry of the COTZ to the Opening of the Equatorial Spreading

In oblique-rifted margins, like the Brazilian Equatorial margin, the COTZ is not normal to the direction of spreading and to the fracture zones. The COTZ forms an oblique angle with the fracture zones, and the angles between COTZ and the fracture zones vary among different segments of the margin.

We used the free-air map (Fig. 2-5) together with free-air gradient map (Fig. 2-6) to map the main fracture zones in the area, and the mid-ocean ridge displacements (Fig. 2-14). The free-air gravity anomaly map proved very useful in mapping seabed topography in areas beyond seismic coverage, and in appreciating the relationship of the structures on the continental margins to those on the adjacent abyssal plain from the northern Brazilian margin offshore Amapá to the Piauí-Ceará Basin (Fig. 2-14).

The angle between the continent ocean transition zone (COTZ) and Saint Paul Fracture Zone is 40^{o} in the north branch and 45^{o} in the southern branch. The angle between the COTZ and the Romanche Fracture Zone is 35^{o} (Fig. 2-14). Oblique rifting is followed by oblique sea-floor spreading, but the angle between the fracture zones and the mid-oceanic ridge is orthogonal, indicating present day orthogonal spreading. Due to the thick sedimentary sequence associated to the prograding Amazon Delta, it was not possible to map the extension of the 4^{o}N Fracture Zone west of the Ceará Rise using the potential fields data. In the Amazon Delta area, in the absence of mapped fracture zones, we used flow lines to estimate the obliquity (Fig 2-15). Flow lines were calculated using

poles of rotation from (Bird and Hall, 2010) using Bird Geophysical software that uses the methodology from Cox and Hart (1986).

The fracture zones in the Equatorial Atlantic (Fig. 2-15) have an unusual geometry. They are perfectly parallel to each other close to the mid-Atlantic ridge, but diverge from each other as they extend in direction of the margin, a consequence of the oblique spreading in the Equatorial Atlantic. In oblique spreading the angle between oceanic fracture zones and mid-oceanic ridge is oblique at a regional scale, but is scale dependent. In order to spread with a regionally oblique angle, the mid-oceanic ridge is interpreted to break into numerous short segments (Fig. 2-15); in the Equatorial Atlantic these segments are as short as 50 km (Fig. 2-15). When the segments are examined at a larger scale, the mid-oceanic ridges appear to be oriented normal to transform faults that bound them, though the mid-ocean ridge system of small segments trends oblique to the main fracture zones.

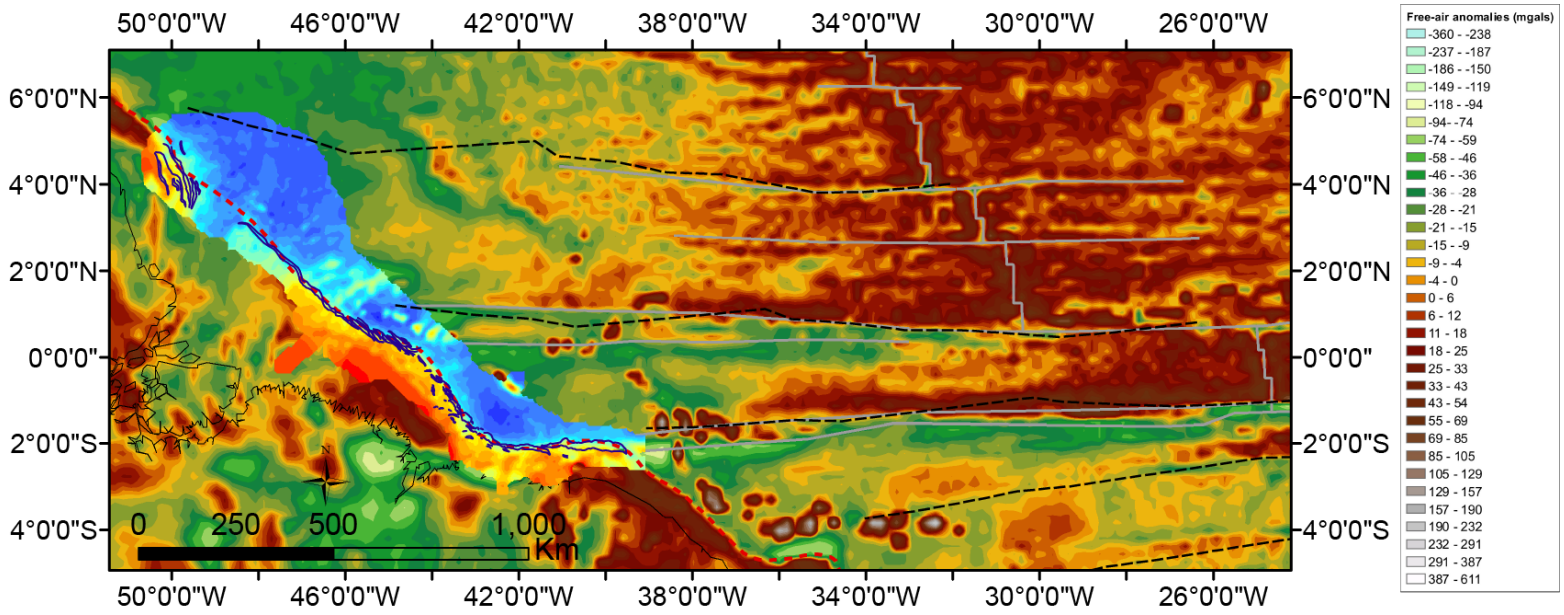

Figure 2-15. Flow lines plotted on top of the structural map of the Equatorial margin and adjoining oceanic basins. Map shows depth to basement in milliseconds mapped on the seismic data set superimposed on the free-air gravity anomalies data set (Sandwell and Smith, 2009). Interpreted fracture zones and mid-ocean ridge displacements are represented in gray. Overlaying the mapped fracture zones are flow lines represented in a black dashed line. Flow lines were calculated using poles of rotation from (Bird and Hall, 2010) using Bird Geophysical software that uses the methodology from Cox and Hart (1986). Basement faults are represented in dark blue. The continent-oceanic transition zone (COTZ) is represented in a red dashed line.

2.8 SUMMARY AND CONCLUSIONS

The segmentation of the margin is a combination of perpendicular rifting and dextral shear at the time of the rifting, and the basement fault geometry provides a snapshot in time to the geometry of the margin at the time of rifting.

The study area can be divided into four segments: 1) the Piauí-Ceará segment (Fig. 2-10); 2) the Barreirinhas segment (Fig. 2-11); 3) Pará-Maranhão segment (Fig. 2-12); and 4) the Amapá segment (Fig. 2-13). The COTZ in the Piauí-Ceará Basin segment corresponds to the Romanche Fracture Zone and therefore constitutes a transform margin. The Barreirinhas and Pará-Maranhão segments constitute oblique-rifted margins, faults are more segmented and there is an observed upper limit of ~ 50 km to fault length in the basement faults.

CHAPTER 3: DEPOSITION AND DEFORMATION IN DEEP-WATER SEDIMENTS OF THE OFFSHORE BARREIRINHAS BASIN

ABSTRACT

Regional seismic reflection profiles across the Barreirinhas Basin on the Brazilian Equatorial margin reveal two major deep-water fold and thrust belts linked landward to extensional fault systems. Thrust faults are interpreted to be products of shortening caused by gravity-driven extension on the continental margin that involve rocks at both the shelf and the slope. Results show two main deformation events during the Cretaceous (99.6 to 83.5 Ma) and the Cenozoic (65.5 to 0 Ma). Both events were characterized by displacement along a detachment fault linking a landward system of normal faults to a basinward system of folds and thrust faults. The Cretaceous deformation involved a thin sequence, less than 1.5 km thick, deformed in a 30 km wide set of listric normal faults (extensional domain) on the outer continental shelf and top of slope that merge into a bed-parallel detachment surface, forming a 30 km wide translational domain, that is linked to a 30 km wide zone of imbricate thrust faults (compressional domain) on the toe of slope. The Tertiary structural system has a different geometry involving thick (over 4km) sedimentary sequence of Turonian to Miocene age, and cross-cuts the pre-existing Cretaceous deformed sequence. Normal faults connect to the thrust faults at depth, forming two discrete bowl-shaped fault systems, linked at depth at different stratigraphic

levels. Plots of displacement versus time show normal and thrust faults growth in the same time intervals, supporting linkage between extensional stress on the continental shelf with compressional stress on the continental slope.

Deformation has increased dramatically during the last ten million years, with movement in all earlier and some newly formed faults. The increased deformation coincided to paleogeographic changes in the north South America in the Late Miocene that led to an increase in the sediment supply in the Barreirinhas Basin.

3.1 INTRODUCTION

Gravity gliding covers a wide range of temporal and spatial scales, from geologically instantaneous, small (up to hundreds of square meters in area), shallow slides associated with mass wasting on land, to giant submarine slides that can cover hundreds of square kilometers (Morley et al., 2011). These slides are commonly triggered by catastrophic events such as storms, earthquakes, high rainfall, and contrast with gravity gliding systems on passive margins that extend for tens of kilometers and develop as a result of long term geological processes that can develop over up to tens of millions of years (Morley et al., 2011).

The presence of large-scale compressional provinces linked to shelf extensional provinces, also known as deep-water foldbelts, at the toe of the slope according to Morley et al. (2011) can be described in terms of the critical taper angle model (Davis et al., 1983; Dahlen, 1984). A combination of a steep surface slope with a low-angle oceanward or landward basal slope in the presence of an efficient detachment will reduce basal friction and allow for gliding and compression at the toe of the slope. The detachment is usually on evaporites or thick shales (Rowan et al., 2004).

Shale detachments are normally associated with overpressure: examples are the Amazon Delta (Cobbold et al., 2004), the Niger Delta (Corredor et al., 2005; Billotti and Shaw, 2005), and the Mexican ridges (Weimer and Buffler, 1992). Fluid overpressures carry part of the weight and reduce the frictional resistance at the base of sediments

(Mourgues et al., 2009). That is the most likely case for the Barreirinhas Basin, but we have no data that would demonstrate overpressure in the sediments to be modeled.

The Barreirinhas Basin is located in a transform margin (Fig.3-1) with, consequently, a very narrow and steep slope. The zone of highly thinned continental transitional crust underlying the slope is locally as narrow as 12 kilometers. We consider the steep gradient in the slope to be the main cause for instability on the margin and a key factor for generating the down slope mass transport flows. In the Barreirinhas Basin the conditions are ideal for the formation of deep-water foldbelts. Two episodes of compressional deformation in the Cretaceous (~89.3 Ma to 83.5 Ma) and Cenozoic (~65.5 Ma to 0 Ma) have been identified.

In areas of very thick sediments, as in the Amazon Delta (Araujo et al., 2009; Perovano et al., 2009) and Niger Delta (Corredor et al., 2005; Billoti and Shaw, 2005), the weight of the sediments has depressed the lithosphere (Morley et al., 2011) so that the basal slope of the sediments dips landward. Bending of the lithosphere by sediment loading is minor in the Barreirinhas Basin, because the sedimentary sequence is not thick enough. The observed landward dipping basal slope of 0.5 degrees seems to be more of a feature of the thinned oceanic crust topography.

All the deformation by thrusting and folding has taken place during the deposition of the sequence (89.3 to 0 Ma), and post-dates intra-cratonic rifting of the basin. The gradient of the top of the sedimentary basement on the continental slope is very steep at

the transform boundary and shallow at the toe of the slope. After oceanic crust emplacement, sediments prograded into the basin, sedimentation rate varied in discrete episodes. During rapid progradation the surface slope has become sufficiently steep to form a critically tapered wedge, with sufficient shear stress along the basal detachment to initiate thrusting. The Barreirinhas Basin archives two main shelf collapse events, an early collapse during the late Mesozoic (~ 99.6 to 83.5 Ma) and a later event in the Cenozoic (42 to 0 Ma). These two events led to the formation of the Barreirinhas Basin deep-water fold and thrust belts on the toe of slope. Both events are shale-detached, but are quite different in terms of geometry (Fig. 3-2).

The post-rift geology of this part of the Barreirinhas Basin can be viewed as consisting of two shale-detached collapse systems. All mapped faults in this study are listric detachment faults of those two systems. Similar shale-detached systems have been described from many basins worldwide, such as; Niger Delta (Damuth, 1994; Rowan et a., 2004; Krueger and Gilbert, 2006 and 2009; Sultan et al., 2007), Pará-Maranhão (Zalan, 2005), and Namibia (Butler and Payton, 2010) (Fig. 3-3).

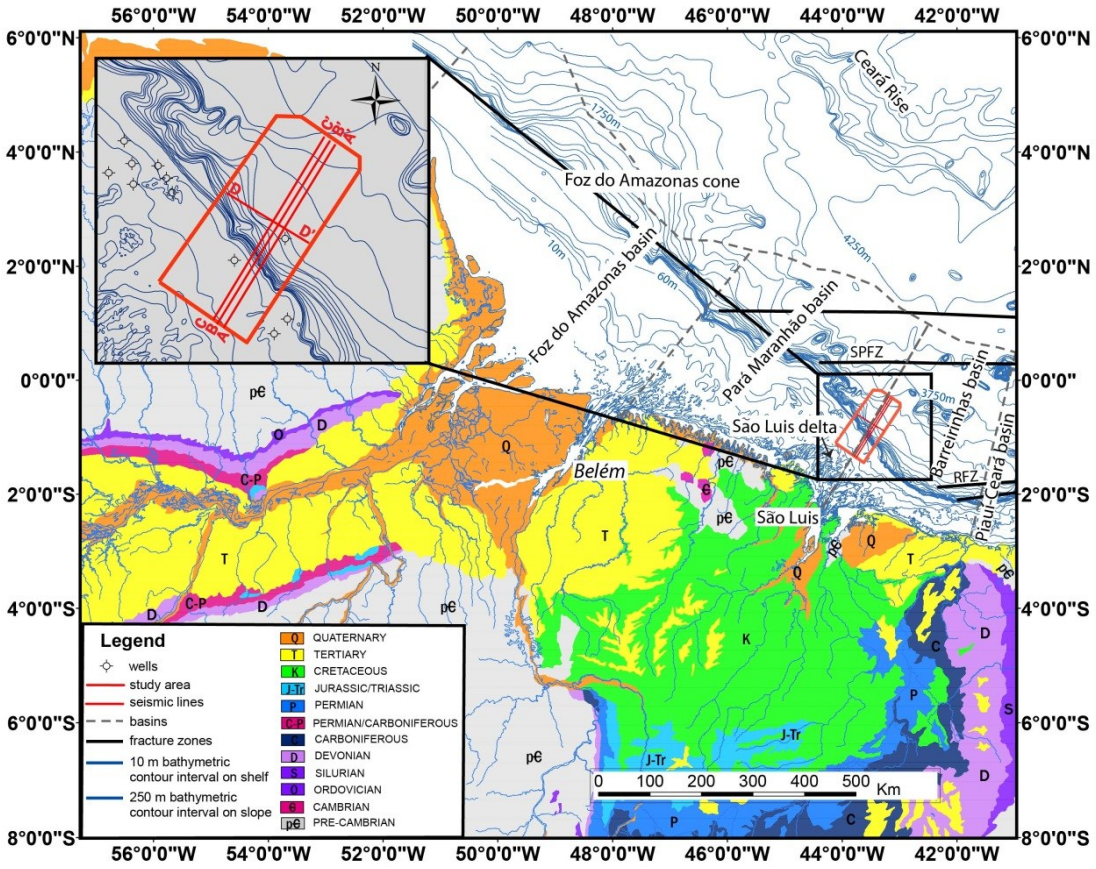

Figure 3-1. Location map in the northeastern margin of Brazil depicting onshore surface geology, offshore bathymetry, main physiographic features, and offshore basin outlines. Detail box depicts work area with available wells, and seismic lines. Surface geology is based on the Geologic Map of South America (Schobbenhaus and Bellizia, 2001) (www.cprm.gov.br). Bathymetric data are derived from ETOPO 1 grid (Amante and Eakins, 2009). Well locations and offshore basin limits are from Agência Nacional de Petróleo (www.anp.gov.br).

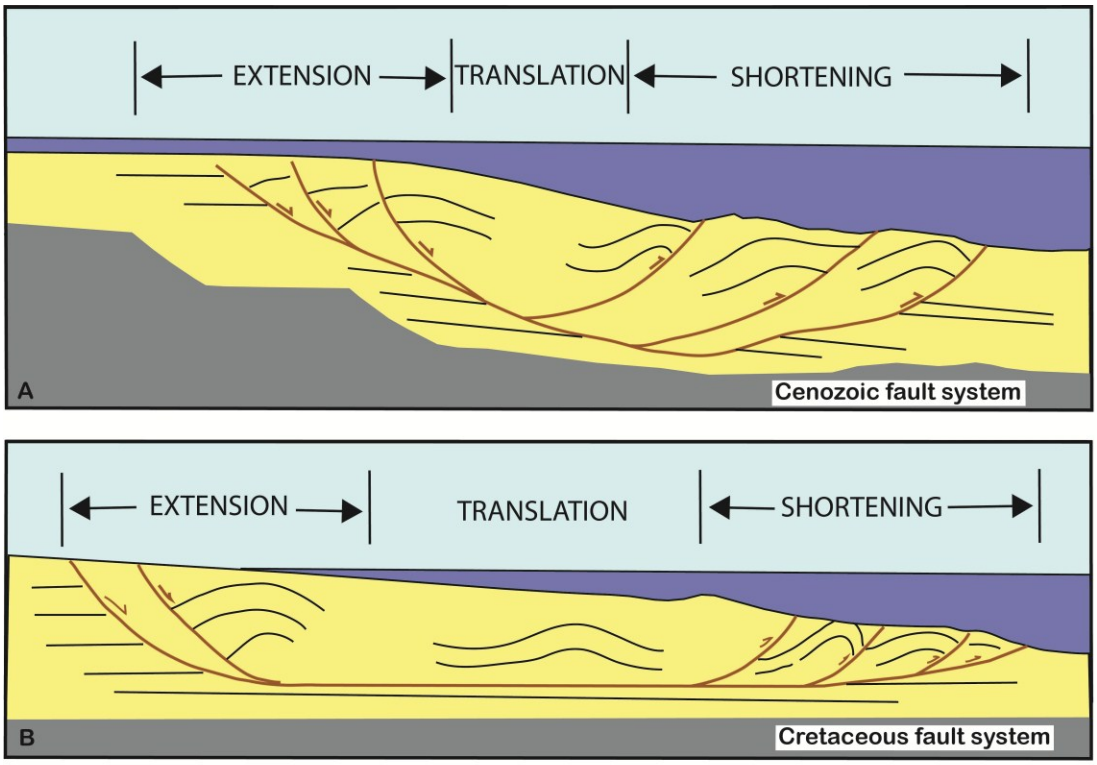

Figure 3-2. Geometry of the two fault-linked systems that form the Barreirinhas fold and thrust belt located in the study area. **A.** Cenozoic age fault system. Normal faults on the continental shelf link at depth with thrust faults on the continental slope forming a concave detachment fault. The detachment fault cross-cuts stratigraphy and has normal displacement updip and reverse displacement down dip. **B.** Cretaceous fault system. Normal and thrust faults detach at a parallel to bed detachment.

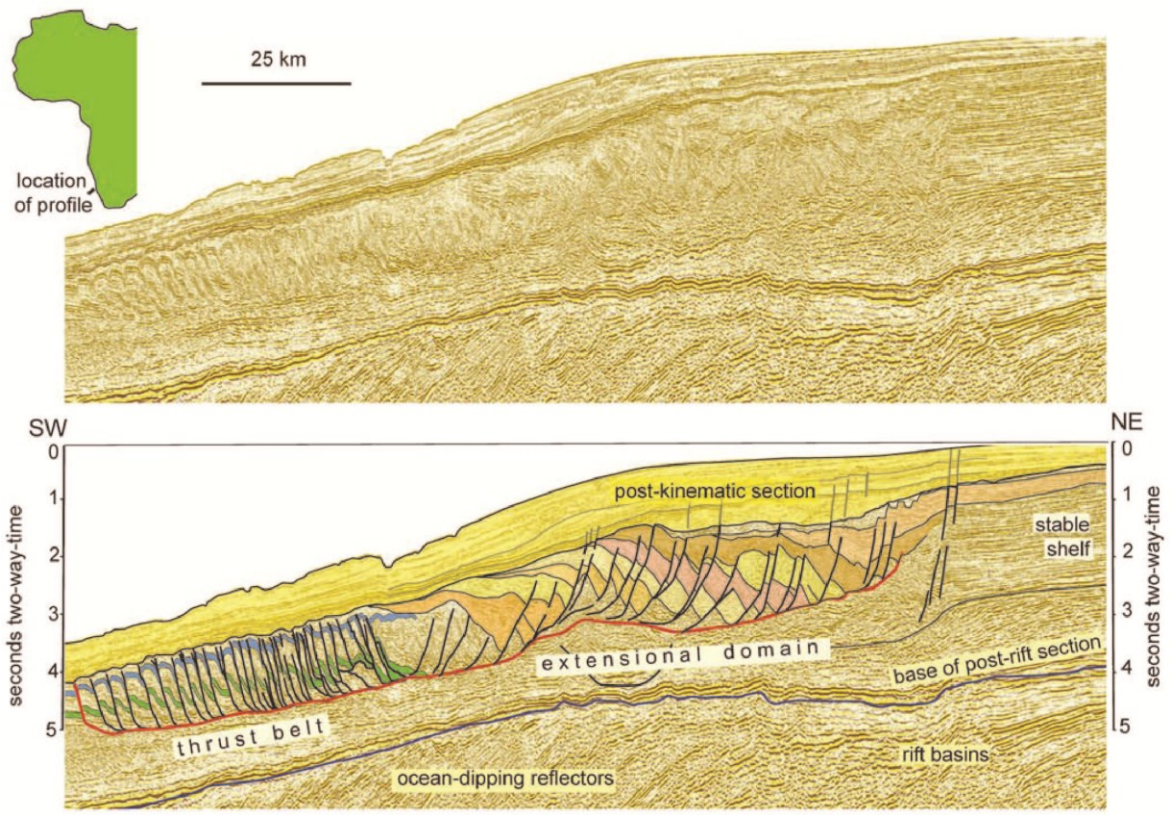

Figure 3-3. A prograding continental shelf offshore Namibia caused slope instability that generated a set of normal listric faults on the continental shelf linked by a translational domain to thrust faults on the toe of slope (Butler and Payton, 2010).

3.2 REGIONAL TECTONICS AND STRATIGRAPHY

The Barreirinhas Basin is one of a set of basins on the Equatorial Brazilian margin and the Amazon Delta, and west of the onland projection of the Romanche Fracture Zone (Fig. 3-1). The Barreirinhas Basin on the south is separated from the Ceará Basin by the Tutóia High, but the limit to the north with the Pará-Maranhão Basin is arbitrary. In this paper we consider the Barreirinhas and Pará-Maranhão Basins as one basin.

The Barreirinhas Basin has a tectonic history distinct from the more familiar basins of the Southeastern Brazilian margin. The initial Aptian rifting phase of the Equatorial Atlantic margin had a dextral shear component that led to the creation of small pull-apart basins filled by thick, unnamed continental sedimentary sequences (Trosdtorf et al., 2007) (Fig. 3-4). Following the deposition of this continental sequence, a shallow ocean invaded the basin in the Late Aptian from north to south and a lagoonal anoxic sequence was deposited, the Codó Formation (Trosdtorf et al., 2007) (Fig. 3-4), followed by the marine Canárias and Cajú Groups (Fig. 3) in Albian time (112-99.6 Ma). Above the Canárias Group is the break-up unconformity above which the Cajú Group continued to be deposited as the drift section. Oceanic crust accretion initiated around Late Aptian-Early Albian (102 Ma) time (Trosdtorf et al., 2007). By Late-Albian (102 Ma), Brazil had finally broken away from West Africa, ending the dextral shear in the margin (Antobreh et al., 2009). The oceanic connection between Central Atlantic and South Atlantic was established during Cenomanian/Turonian time (~99.6 to 89.3 Ma) (Antobreh et al., 2009).

Above the Cajú Group is the Turonian to Oligocene Humberto de Campos Group, with proximal deposition of the Areinhas formation, the Ilha de Santana Formation on the platform, and distal deposition of the deep-water Travossas Formation (Trosdtorf et al., 2007) (Fig. 3-4). The Travossas Formation is locally highly deformed, and understanding the deformation of the Travossas Formation is one of the main objectives of this study.

The Brazilian Equatorial margin went through extreme progradation starting at Late Miocene (~5.5 Ma) causing high sedimentation rates at the Amazon Delta and in the much smaller São Luís Delta. The progradation lead to a very broad continental shelf (over 300 km) in the Foz do Amazonas in a transform margin that is very narrow (less than 100 km) in the Ceará Basin away from the sediment sources (Fig. 3-1). The extreme progradation that took place in the Late Miocene on the Brazilian Equatorial margin seems to be a product of not only the global cooling, but also rearrangements on the drainage system due to an Andean tectonic event (Altamira-Areyan, 2009).

Figueiredo et al. (2009) compared biostratigraphic data with isotopic data to establish provenances and times of erosion and re-deposition of sediments on the Amazon Delta and constructed paleogeographic maps for the Miocene (Fig. 3-5). Figueiredo et al. (2009) Miocene paleogeographic maps show a change of drainage direction from the Western Amazonia wetlands to the Amazon Delta as well as the São Luís fan (Figueiredo et al., 2009) (Fig 3-5).

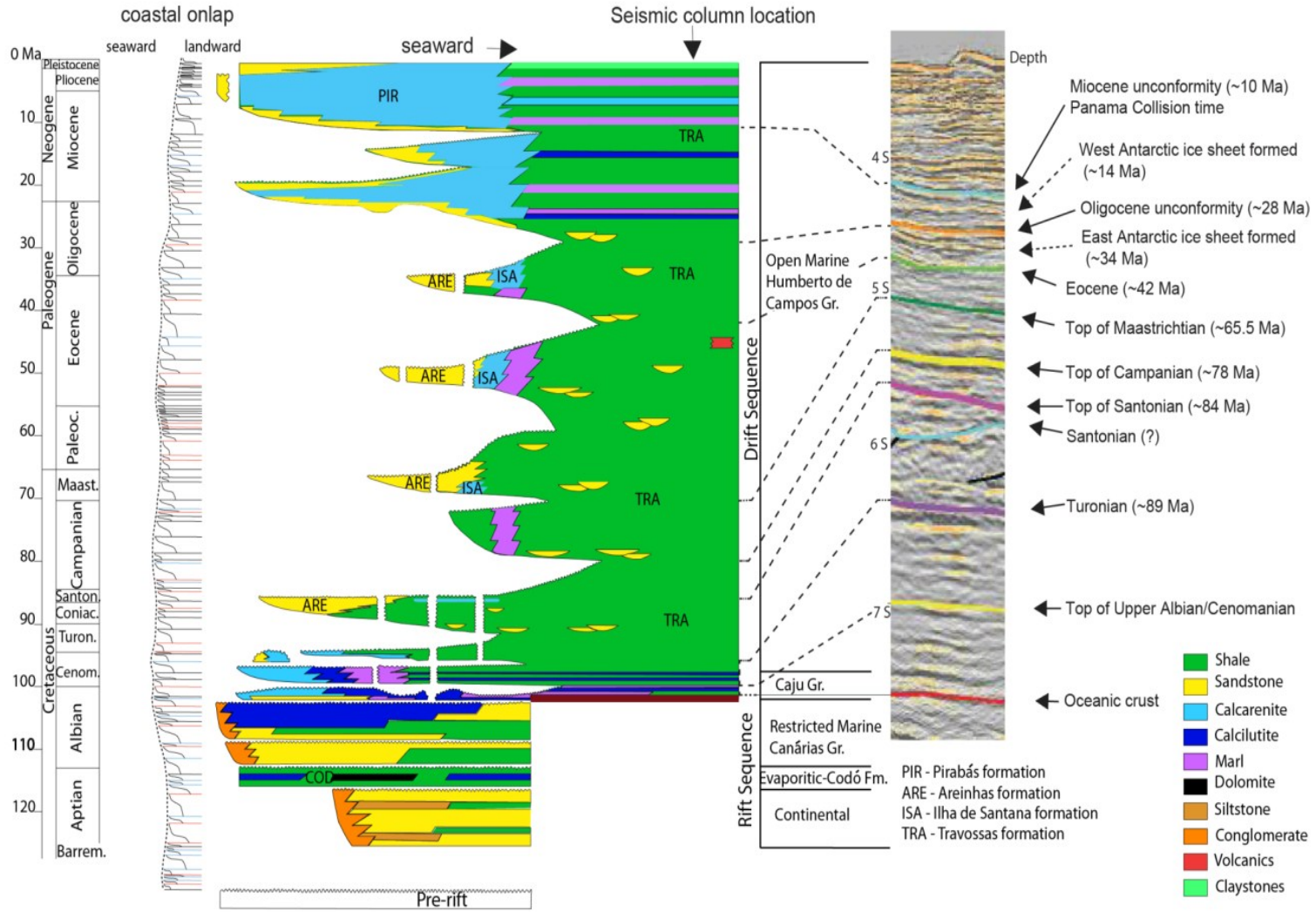
coastal onlap
seaward
landward
Seismic column location
seaward
0 Ma
10
20
30
40
50
60
70
80
90
100
110
120
Pleistocene
Pliocene
Neogene
Miocene
Oligocene
Paleogene
Eocene
Paleoc.
Maast.
Campanian
Santon.
Coniac.
Turon.
Cenom.
Cretaceous
Albian
Aptian
Barrem.
PIR
TRA
ARE
ISA
COD
Pre-rift
Drift Sequence
Rift Sequence
Open Marine
Humberto de
Campos Gr.
Caju Gr.
Restricted Marine
Canárias Gr.
Evaporitic-Codó Fm.
Continental
4 S
5 S
6 S
7 S
Depth
Miocene unconformity (~10 Ma)
Panama Collision time
West Antarctic ice sheet formed
(~14 Ma)
Oligocene unconformity (~28 Ma)
East Antarctic ice sheet formed
(~34 Ma)
Eocene (~42 Ma)
Top of Maastrichtian (~65.5 Ma)
Top of Campanian (~78 Ma)
Top of Santonian (~84 Ma)
Santonian (?)
Turonian (~89 Ma)
Top of Upper Albian/Cenomanian
Oceanic crust
PIR - Pirabás formation
ARE - Areinhas formation
ISA - Ilha de Santana formation
TRA - Travossas formation
Shale
Sandstone
Calcarenite
Calcilutite
Marl
Dolomite
Siltstone
Conglomerate
Volcanics
Claystones

Figure 3-4. Stratigraphic chart of the Barreirinhas Basin (Trosdtorf et al., 2007), with sea-level curve (Haq et al., 1987), and interpreted horizons. Seismic column with the interpreted horizons was extracted along the continental slope portion of line B-B' (Fig. 3-1). The nature of the basement at the chosen location is oceanic, therefore the Aptian and Albian rift sequences lie landward and are not represented in the seismic column

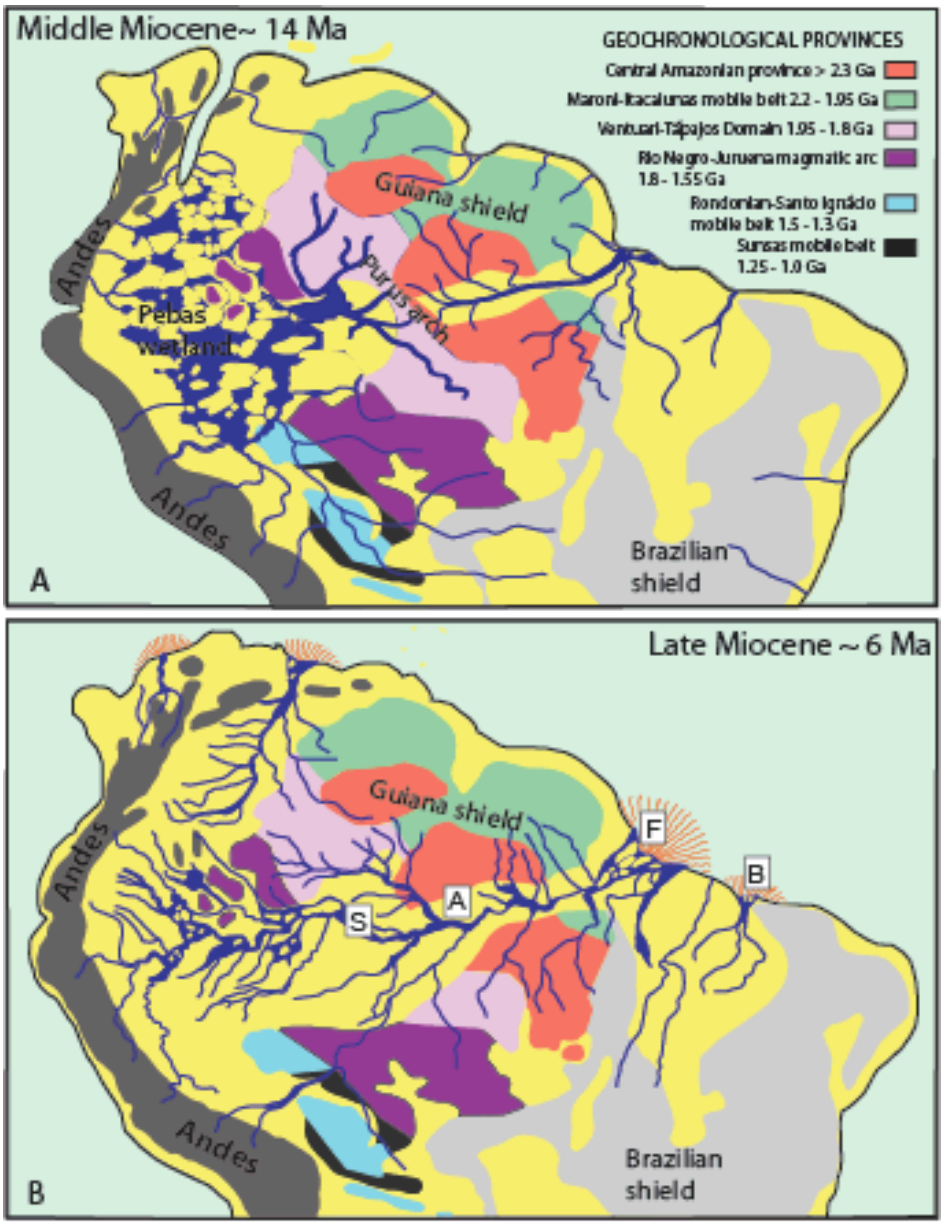
Middle Miocene~ 14 Ma
GEOCHRONOLOGICAL PROVINCES
Central Amazonian province > 2.3 Ga
Maroni-Itacaiunas mobile belt 2.2 - 1.95 Ga
Ventuari-Tapajos Domain 1.95 - 1.8 Ga
Rio Negro-Juruena magmatic arc 1.8 - 1.55 Ga
Rondonian-Santo Ignácio mobile belt 1.5 - 1.3 Ga
Sunsas mobile belt 1.25 - 1.0 Ga
Guiana shield
Andes
Pebas wetland
Andes
Brazilian shield
A
Late Miocene ~ 6 Ma
Guiana shield
Andes
F
B
A
S
Andes
Brazilian shield
B

Figure 3-5. Paleogeography for northern South America (Figueiredo et al., 2009) and Amazonian geochronological provinces (Almeida et al., 2007). **A.** During the Middle Miocene (~14 Ma) the Purus Arch worked as a drainage continental divide for east and west Amazonia. Rivers west of the Purus Arch used to flow to the Pebas wetlands and rivers east of the Purus Arch used to flow to the Atlantic Ocean (Figueiredo et al., 2009). **B.** Starting at Late Miocene (~6 Ma) a drainage rearrangement caused all rivers as far west as the Andes to flow east, causing the Pebas wetlands to dry and the birth of the Amazon River in its modern shape (Figueiredo et al., 2009). This drainage rearrangement is also the probable cause for the formation of the Sao Luis Delta and increased sedimentation on the Barreirinhas Basin. The Amazon Delta in the Foz do Amazonas Basin is labeled in the figure with an F and the Sao Luiz Delta in the Barreirinhas Basin is labeled with a B.

3.3 DATA AND METHODOLOGY

Our dataset consists of four 2D pre-stack time migrated sections provided by WesternGeco, three dip lines with a line spacing of 4 km between lines and one strike line (Figs. 3-6, 3-7, 3-8, 3-9, and 3-10). The seismic lines are pre-stack time migrated. These lines are part of a larger 4x8 km grid of 2D seismic lines covering the whole deformational system that was also interpreted courtesy of Devon and is part of our dataset.

Ten regional seismic stratigraphic horizons roughly corresponding to the main sequences described by Trosdtorf et al. (2007) (Fig. 3-4) are tied to wells on the shelf and one in deep- water are mapped throughout the area (Fig. 3-1). Interpreted horizons are: 1) basement, 2) Albian (~100 Ma), 3) Turonian (~89 Ma), 4) Santonian (~84 Ma), 5) Campanian (~78 Ma), 6) Maastrichtian (~66 Ma), 7) Eocene (~42 Ma), 8) Oligocene (~27 Ma), 9) Miocene (~10 Ma), and 10) Sea-floor.

One regional cross section 130 km long was depth converted using constant average interval velocities for each layer. This cross-section was restored using Lithotect, (Geo-Logic Systems Inc., Halliburton), assuming plane-strain deformation.

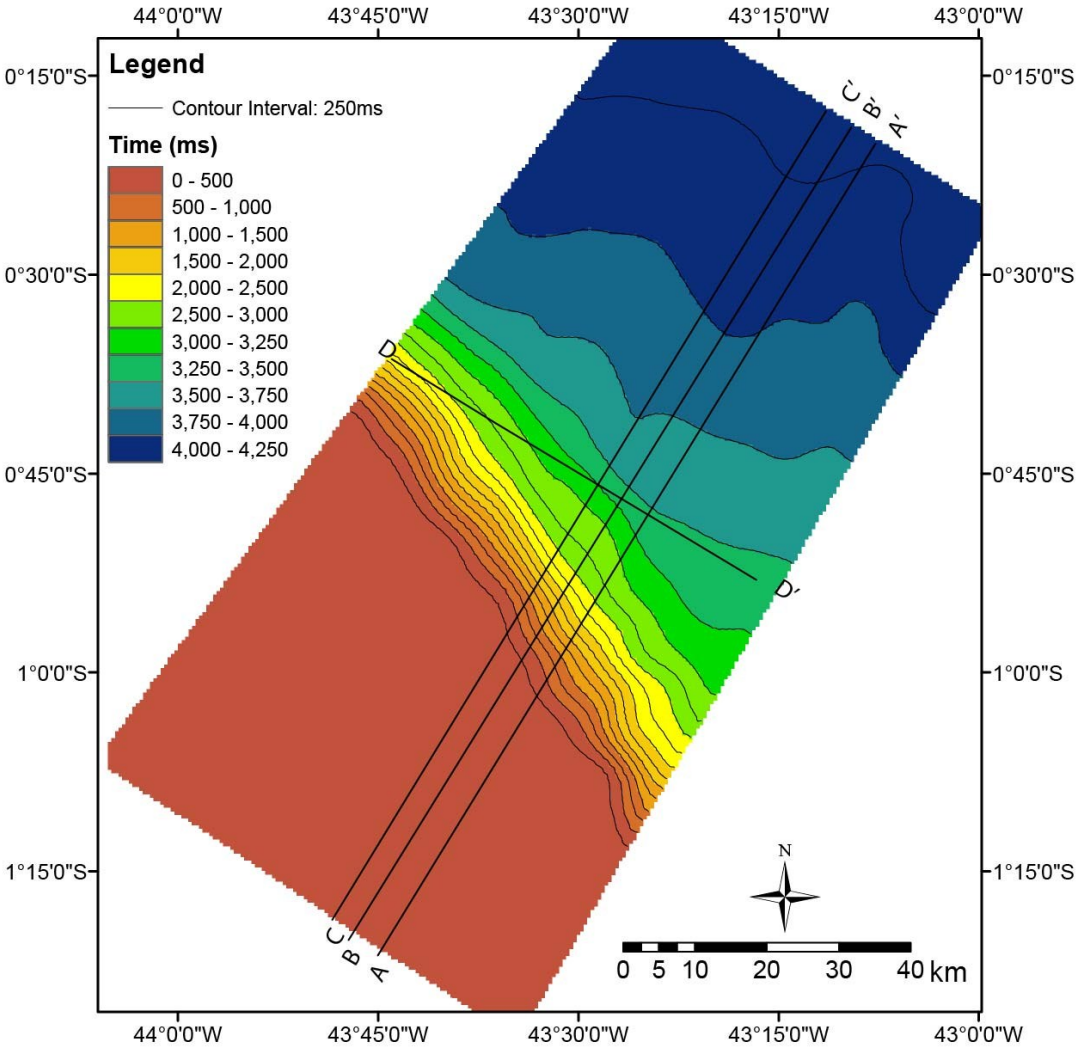

Figure 3-6. Location of the seismic lines and bathymetry of the study area.

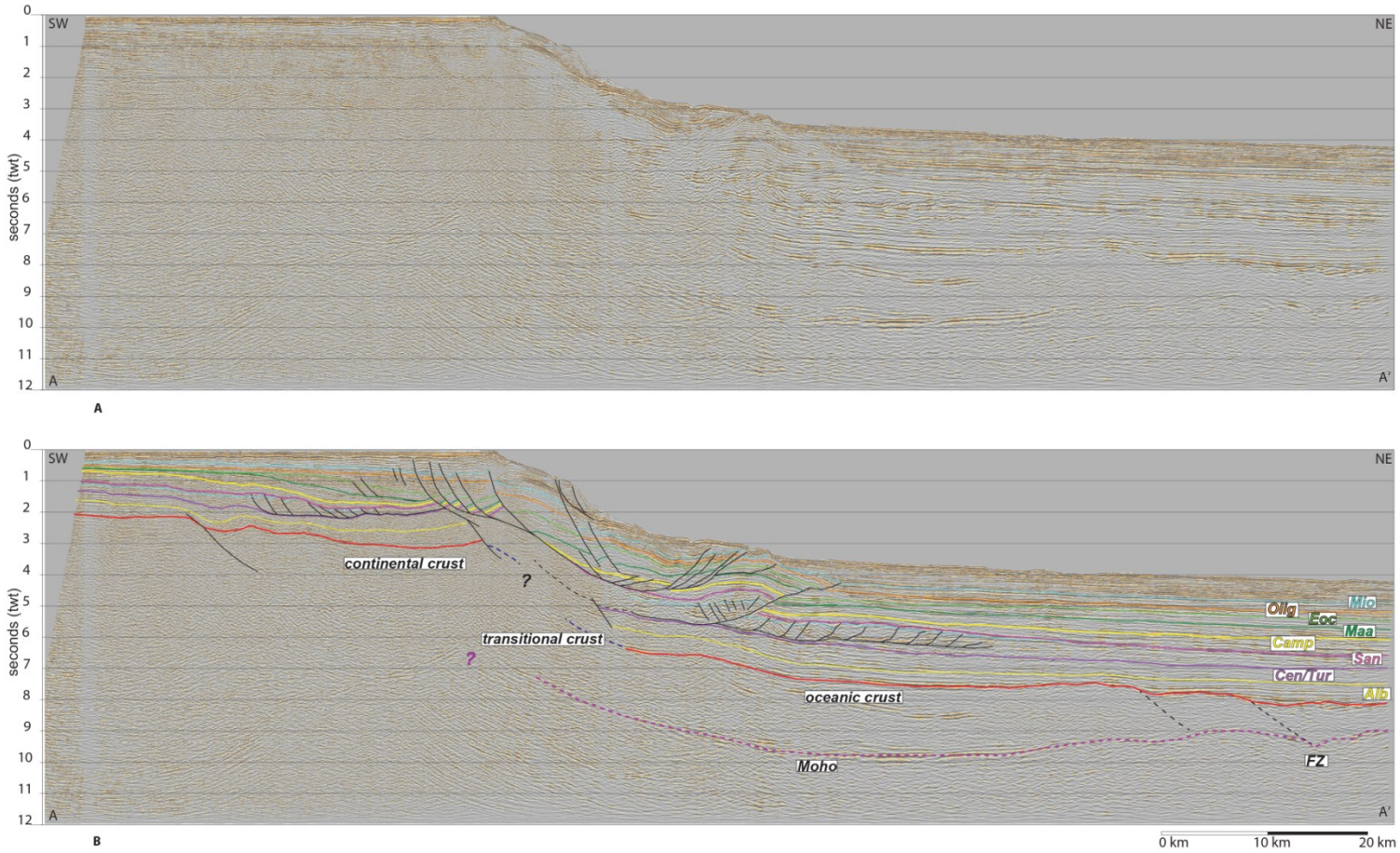
SW
NE
A
A'
seconds (twt)
0
1
2
3
4
5
6
7
8
9
10
11
12
A
SW
NE
A
A'
seconds (twt)
continental crust
?
transitional crust
?
oceanic crust
Moho
FZ
Olig
Eoc
Mio
Maa
Camp
San
Cen/Tur
Alb
B
0 km
10 km
20 km

Figure 3-7. Regional pre-stack time migrated seismic line A-A'. Location of the line is represented on figure 3-6. Vertical scale is in seconds and horizontal scale is in kilometers, average vertical exaggeration is approximately 1:5. Line is courtesy of WesternGeco. **A.** Seismic line without interpretation. **B.** Interpreted line shows a very narrow transition from a shallow continental crust to a deeper oceanic crust, measured at 15 km along strike, resulting in a narrow and steep continental slope. Large grabens and horsts common in other continental margins are absent, and the rift sequence on the continental margin represented between the yellow and red horizon is less than one second thick. Interpreted horizons are labeled on the line Miocene (MIO), Oligocene (OLIG), Eocene (EOC), Maastrichtian (MAA), Campanian (CAMP), Santonian (SAN), Cenomanian/Turonian (CEN/TUR) and Albian (ALB

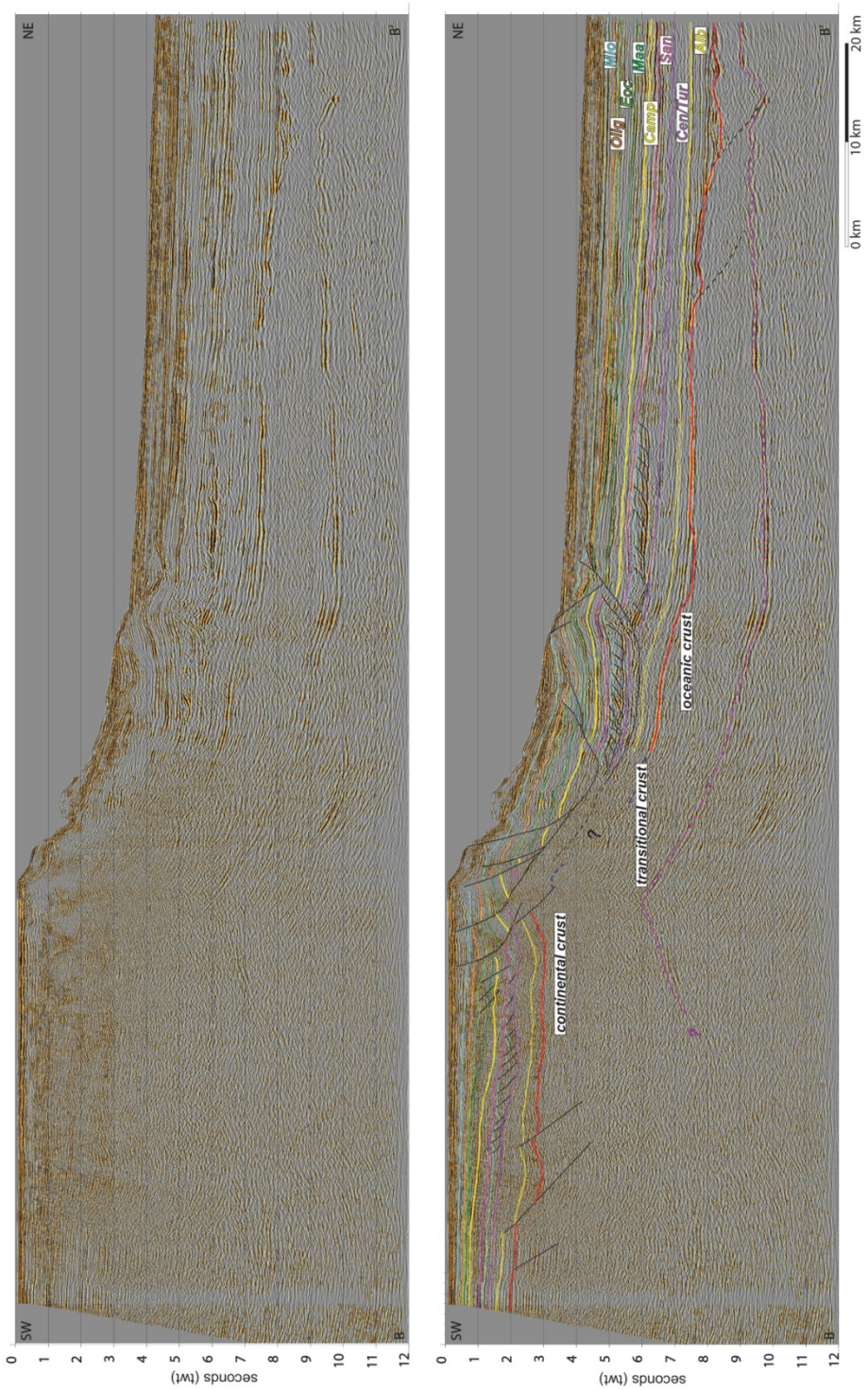
NE
SW
B
B'
seconds (twt)
0
1
2
3
4
5
6
7
8
9
10
11
12
continental crust
transitional crust
oceanic crust
?
Mio
Olig
Eoc
Mes
Camp
Sant
Cen/Tur
Alb
0 km
10 km
20 km

Figure 3-8. Regional pre-stack time migrated seismic line B-B'. Location of the line is represented on figure 3-6. Vertical scale is in seconds and horizontal scale is in kilometers, average vertical exaggeration is approximately 1:5. Line is courtesy of WesternGeco. **A.** Seismic line without interpretation. **B.** Interpreted line shows a series of smaller normal faults on the shelf limited to a thin Cretaceous sequence from Turonian (purple horizon) to Santonian age (pink horizon) connected to a series of thrusted imbricates located on the same sequence on the toe of slope. The detachment surface for the normal and thrust faults sole in a bed-parallel detachment close to the Turonian age (purple horizon). This Cretaceous system is crosscut by a younger Tertiary fault system. FZ- corresponds to the location of an oceanic fracture zone. Interpreted horizons are labeled on the line Miocene (MIO), Oligocene (OLIG), Eocene (EOC), Maastrichtian (MAA), Campanian (CAMP), Santonian (SAN), Cenomanian/Turonian (CEN/TUR) and Albian (ALB).

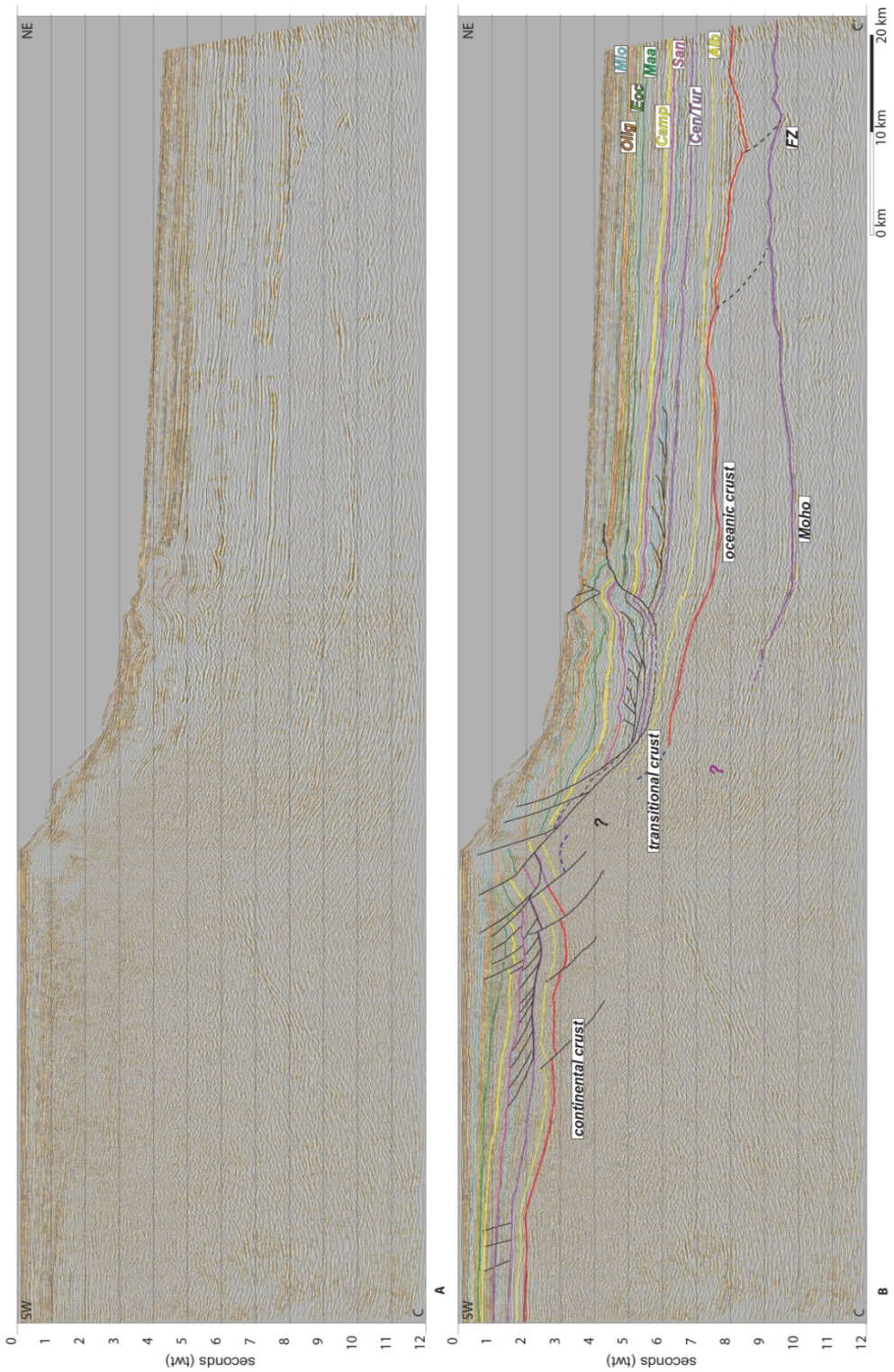
NE
SW
A
C
seconds (twt)
0
1
2
3
4
5
6
7
8
9
10
11
12
NE
SW
C
C'
B
Mio
Olig
Eoc
Mea
Camp
San
Cen/Tur
Alb
FZ
continental crust
transitional crust
oceanic crust
Moho
?
?
0 km
10 km
20 km

Figure 3-9. Regional pre-stack time migrated seismic line C-C'. Location of the line is represented on figure 3-6. Vertical scale is in seconds and horizontal scale is in kilometers, average vertical exaggeration is approximately 1:5. Line is courtesy of WesternGeco. **A.** Seismic line without interpretation. **B.** Interpreted line shows large normal faults on the shelf and continental slope linked in depth to a large fold on the base of the continental slope. Interpreted horizons are labeled on the line Miocene (MIO), Oligocene (OLIG), Eocene (EOC), Maastrichtian (MAA), Campanian (CAMP), Santonian (SAN), Cenomanian/Turonian (CEN/TUR) and Albian (ALB).

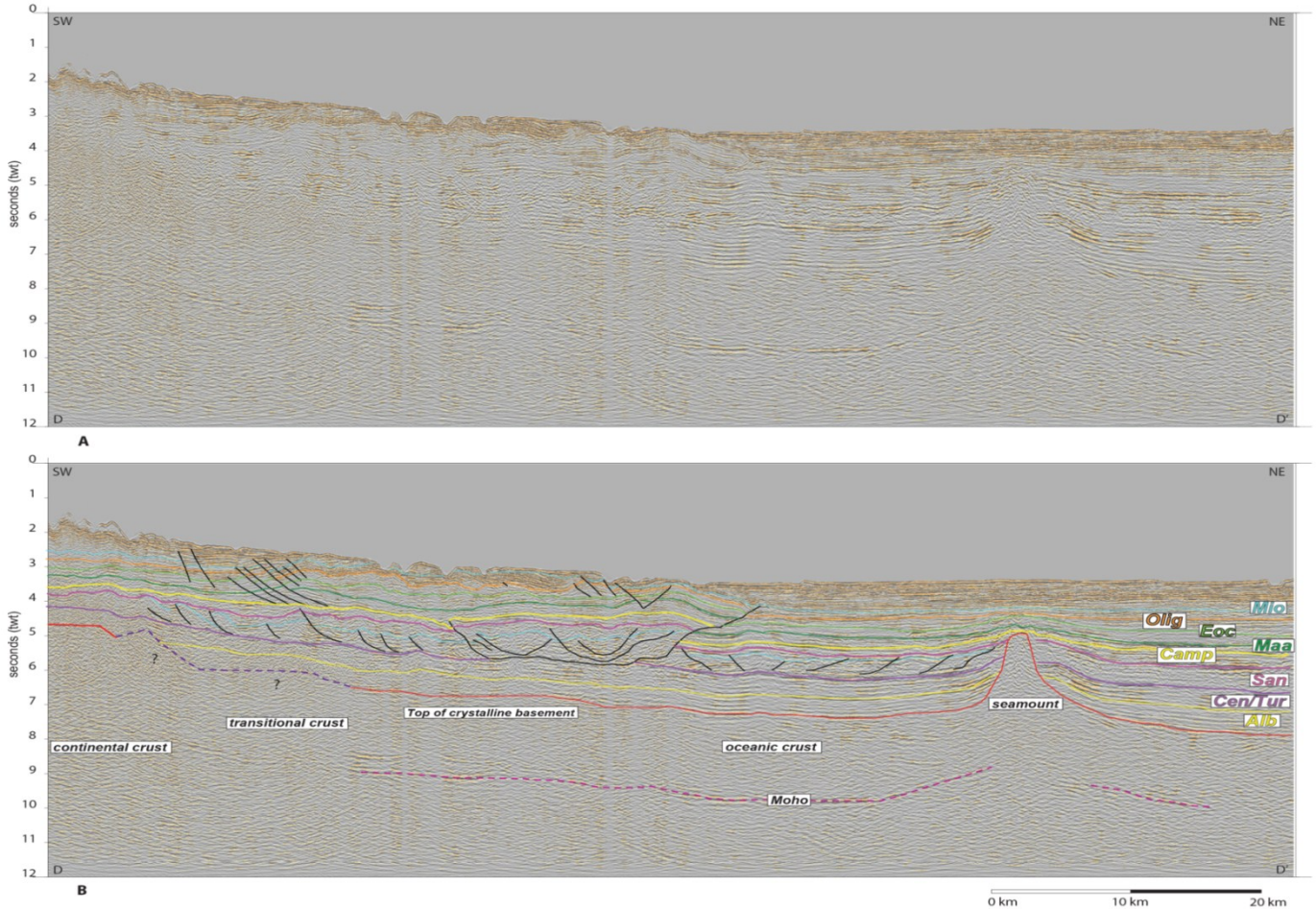
SW
NE
seconds (twt)
D
D'
A
B
Mio
Olig
Eoc
Camp
Maa
San
Cen/Tur
Alb
?
?
transitional crust
Top of crystalline basement
seamount
continental crust
oceanic crust
Moho
0 km
10 km
20 km

Figure 3-10. Regional pre-stack time migrated seismic line D-D'. Location of the line is represented on figure 3-6. Vertical scale is in seconds and horizontal scale is in kilometers, average vertical exaggeration is approximately 1:5. Line is courtesy of WesternGeco. **A.** Seismic line without interpretation. **B.** Line is located in strike to a large fold and shows the linkage in depth between the normal and thrust faults. It also shows a seamount and its very minor influence on the deformed sequence. The line represents the lateral extent of the deformation in the Tertiary rocks of the study area that over-prints the pre-existing Cretaceous deformation. Interpreted horizons are labeled on the line Miocene (MIO), Oligocene (OLIG), Eocene (EOC), Maastrichtian (MAA), Campanian (CAMP), Santonian (SAN), Cenomanian/Turonian (CEN/TUR) and Albian (ALB).

3.4 SEISMIC INTERPRETATION OF THE BARRERINHAS BASIN

3.4.1 Basement

The interpreted basement horizon is a combination of the pre-rift mega-sequence on the continental margin, described by Trosdtorf et al. (2007) (Fig. 3-4) but not discussed in this work, and the top of oceanic crust as defined seismically (Figs. 3-7, 3-8, 3-9, and 3-10). The transitional zone between oceanic and continental crust in this basin is very narrow (10 to 20 km) (Fig. 3-7), as a result of being located along a transform margin (Fig. 3-1). In the basement structural map (Fig. 3-11), the transition from continental crust to oceanic crust corresponds to a change from basement depths of less than 3000 ms on the continental shelf to depths of more than 6000 ms on the toe of slope in less than 20 km.

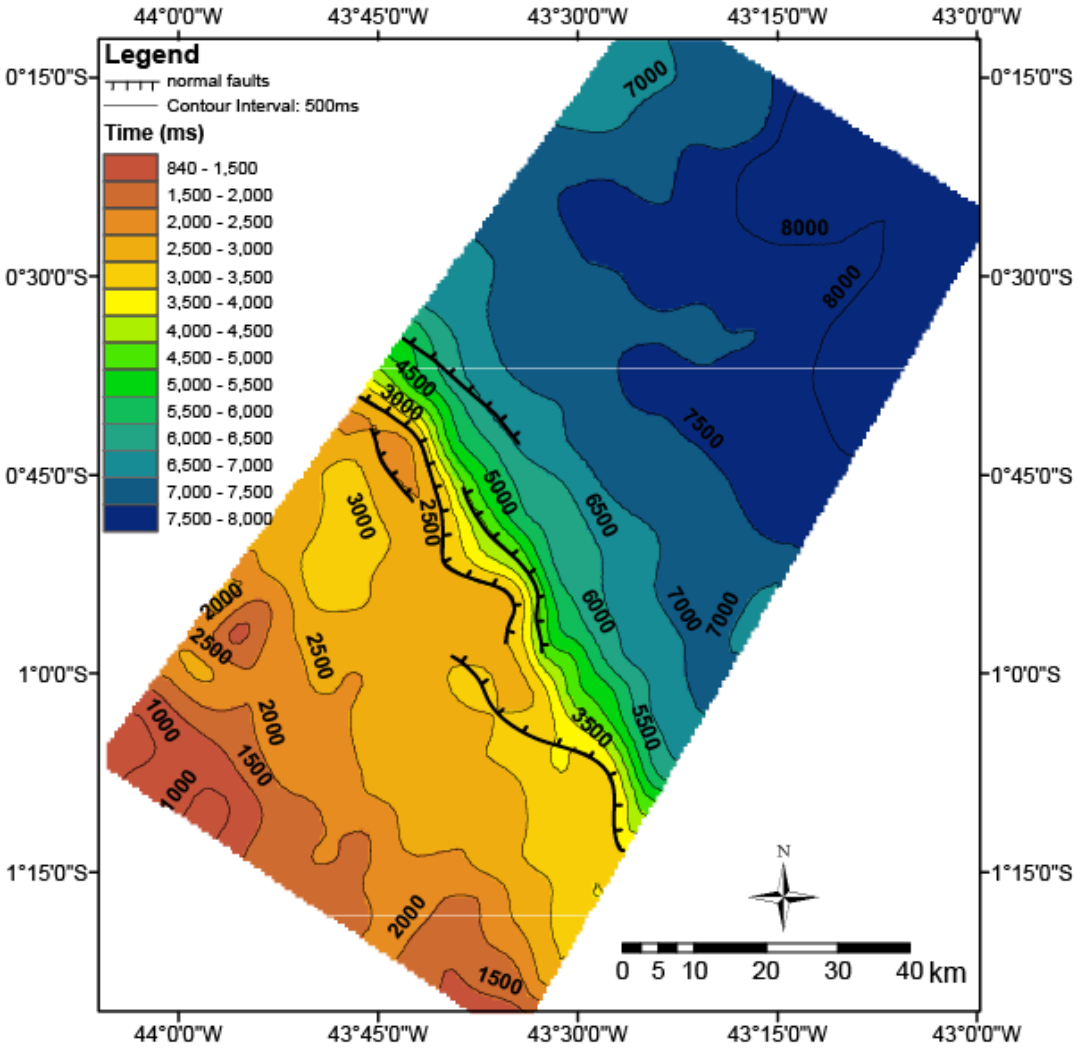

Figure 3-11. Basement structural map. Basement structural map depicts a narrow continental slope with depths changing from 2500 ms in the continental margin to 7000 ms in the abyssal plains in a distance of less than 20 km.

3.4.2 Albian (112 to 99.6 Ma)

The Albian age (~100 Ma) structural map (Fig. 3-12) (deeper yellow horizon on the seismic lines, Figs. 3-7, 3-8, 3-9 and 3-10) marks the beginning of the drift sequence, and is the first truly time-correlative sequence in both the shelf and deep-water (Fig 3-2). It also corresponds to the top of the rift sequence on the shelf.

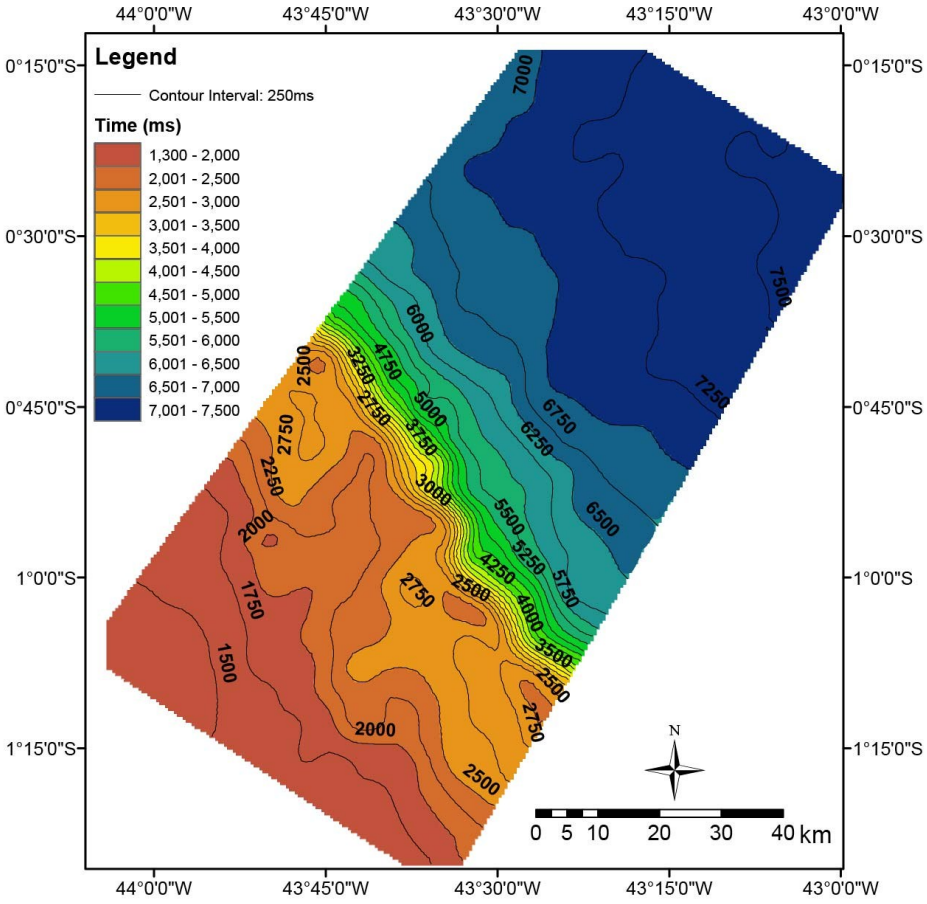

Figure 3-12. Albian age (~100 Ma) structural map

3.4.3 Cenomanian/Turonian (99.6 to 89.3 Ma)

The Turonian age horizon (~89 Ma) (Fig. 3-13) (purple horizon on the seismic lines, Figs. 3-7, 3-8, 3-9 and 3-10) corresponds to a maximum flooding surface and anoxic event that has a very characteristic high-amplitude seismic character, and can be easily correlated throughout the Equatorial margin. Lithologically this sequence is composed mainly of mudstones and marls (Trosdtorf et al., 2007) (Fig. 3-4). The Turonian mapped surface is the detachment surface beneath the Cretaceous deformed unit. The surface follows the abrupt changes in morphology of the transform margin with a difference in total depth of approximately 3000 ms between the continental shelf and the toe of slope being accommodated very abruptly in less than 20 km (Fig. 3-13).

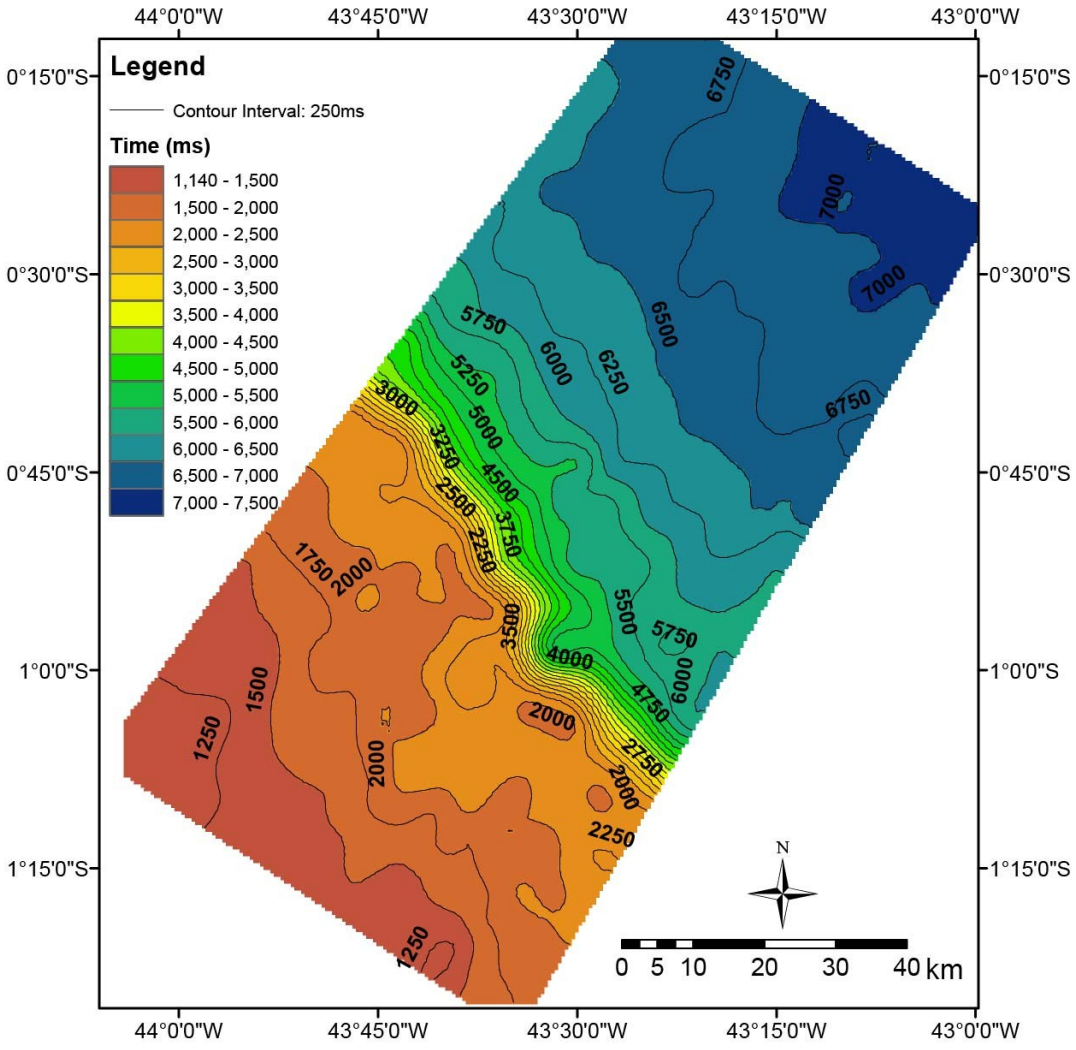

Figure 3-13. Turonian age (~89 Ma) structural map.

3.4.4 Coniacian/Santonian (89.3 to 83.5 Ma)

Two horizons were interpreted on this sequence: 1) top of the Cretaceous deformed sequence (cyan horizon on the seismic sections, Figs. 3-7, 3-8, 3-9, and 3-10), and 2) top of Santonian age rocks (~84 to 83.5Ma) (Fig. 3-14) (pink horizon on the seismic sections, Figs. 3-7, 3-8, 3-9, and 3-10). The deformed Cretaceous rock age is uncertain, but resides below our interpreted top of Santonian horizon and above the Cenomanian/Turonian sequence (Figs. 3-7, 3-8, 3-9, and 3-10) implying a probable age for the deformed sequence younger than 89.3 and older than 83.5 Ma.

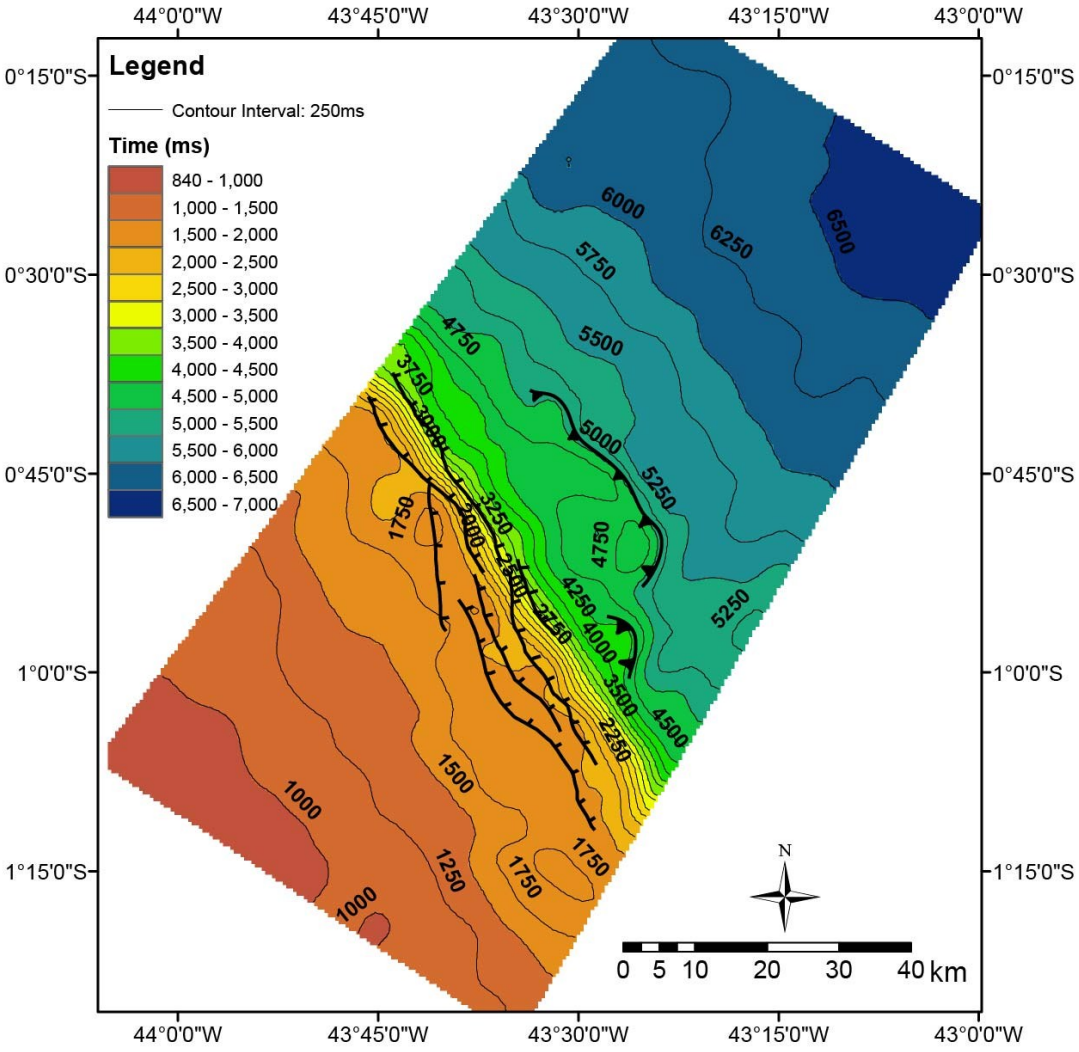

Figure 3-14. Santonian age (~84 Ma) structural map.

3.4.5 Campanian/Maastrichtian (83.5 to 65.5 Ma)

During the Campanian (~78 Ma) the sea level dropped, marking the change from mainly transgressive to mainly regressive sequences (Trosdtorf et al., 2007 after Haq et al., 1987) (Fig. 3-4). The base of this regressive sequence is the Campanian horizon (~78 Ma) (Fig. 3-15) (yellow horizon on the seismic sections, Figs. 3-7, 3-8, 3-9, and 3-10) and the top of the sequence is the Maastrichtian horizon (~66 Ma) (Fig. 3-16) (green horizon on the seismic sections, Figs. 3-7, 3-8, 3-9, and 3-10). In our seismic lines that change is characterized by the progradation of the hinge of the shelf break from the yellow horizon to the dark green horizon (Figs. 3-7, 3-8, 3-9, and 3-10).

The Campanian sequence onlaps the top of the Santonian deformed sequence (Fig. 3-7). The Maastrichtian is a time of tectonic quiescence on the basin, and the Maastrichtian sequence buries the Campanian ponded mini-basins (Fig. 3-7). The top of Maastrichtian/ top of Cretaceous (~66 Ma) (Fig. 3-16), is the closest mapped horizon to the top of the rocks that were deposited prior to the Cenozoic folding and faulting, and is identified in the seismic lines as a sequence without growth (Fig. 3-7).

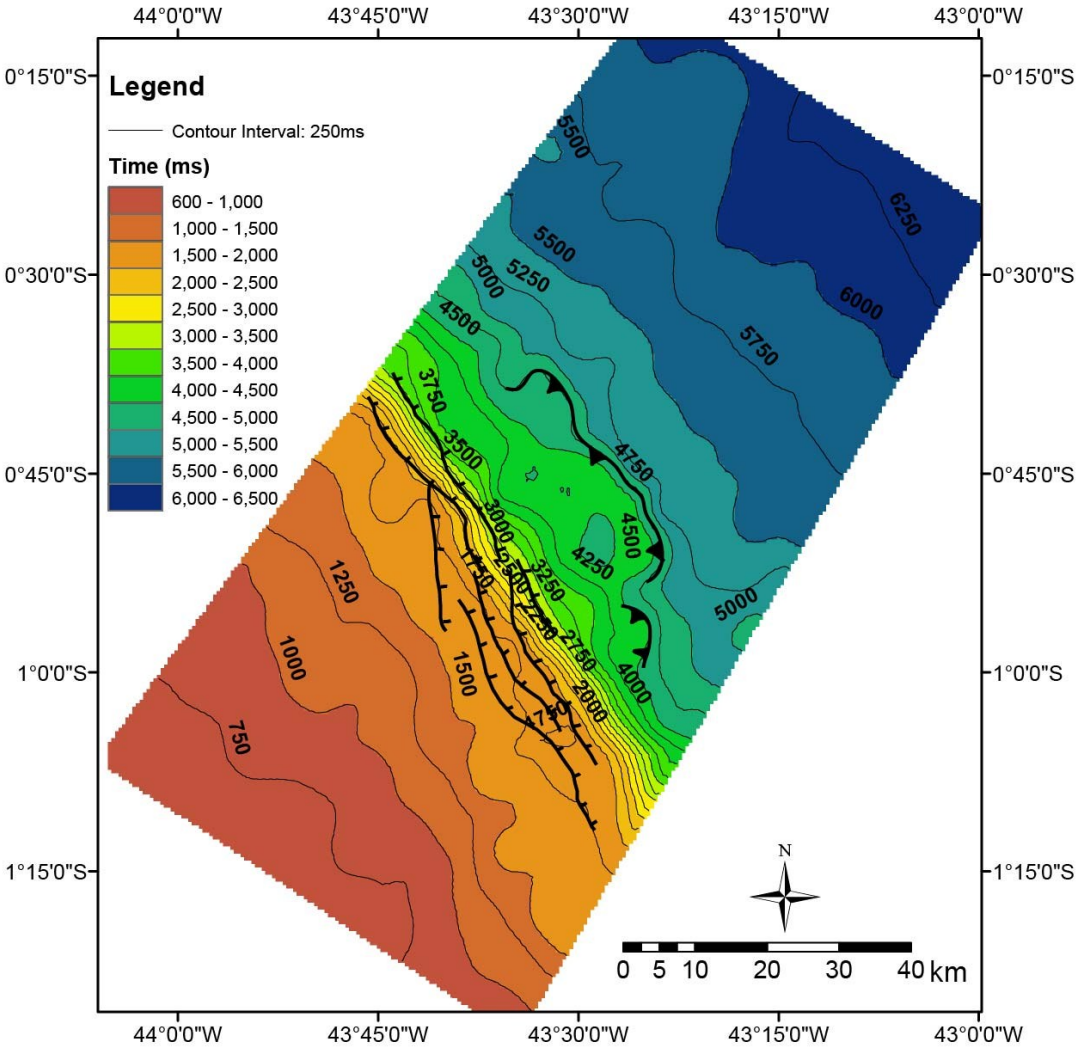

Figure 3-15. Campanian age (~78 Ma) structural map.

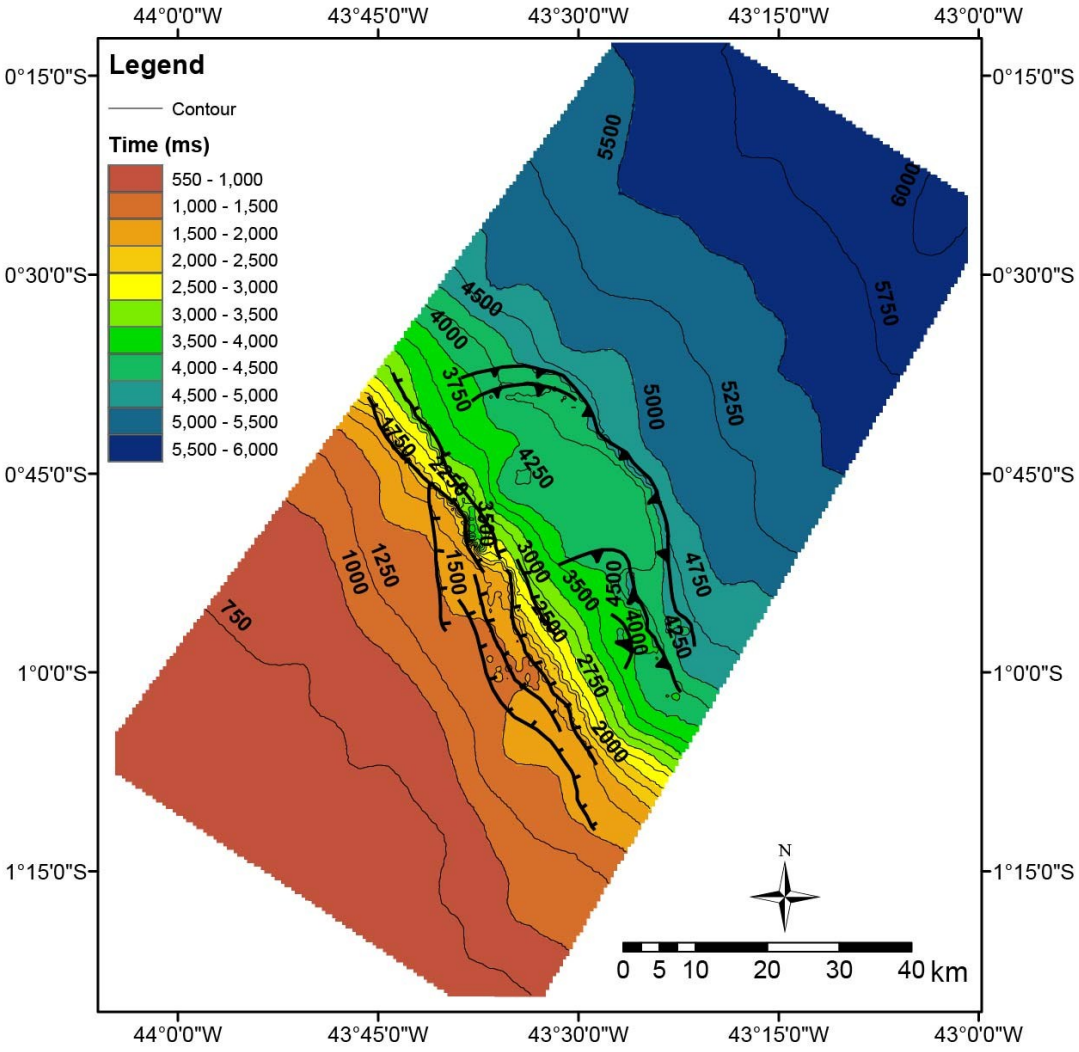

Figure 3-16. Maastrichtian age (~66 Ma) structural map.

3.4.6 Paleocene/Eocene (65.5 to 37.2 Ma)

The Eocene age (~42 Ma) structural map (Fig. 3-17) (light green horizon on the seismic sections, Figs. 3-7, 3-8, 3-9, and 3-10) corresponds to the base of the first sequence we can identify as a structural growth sequence for the Cenozoic fault movement.

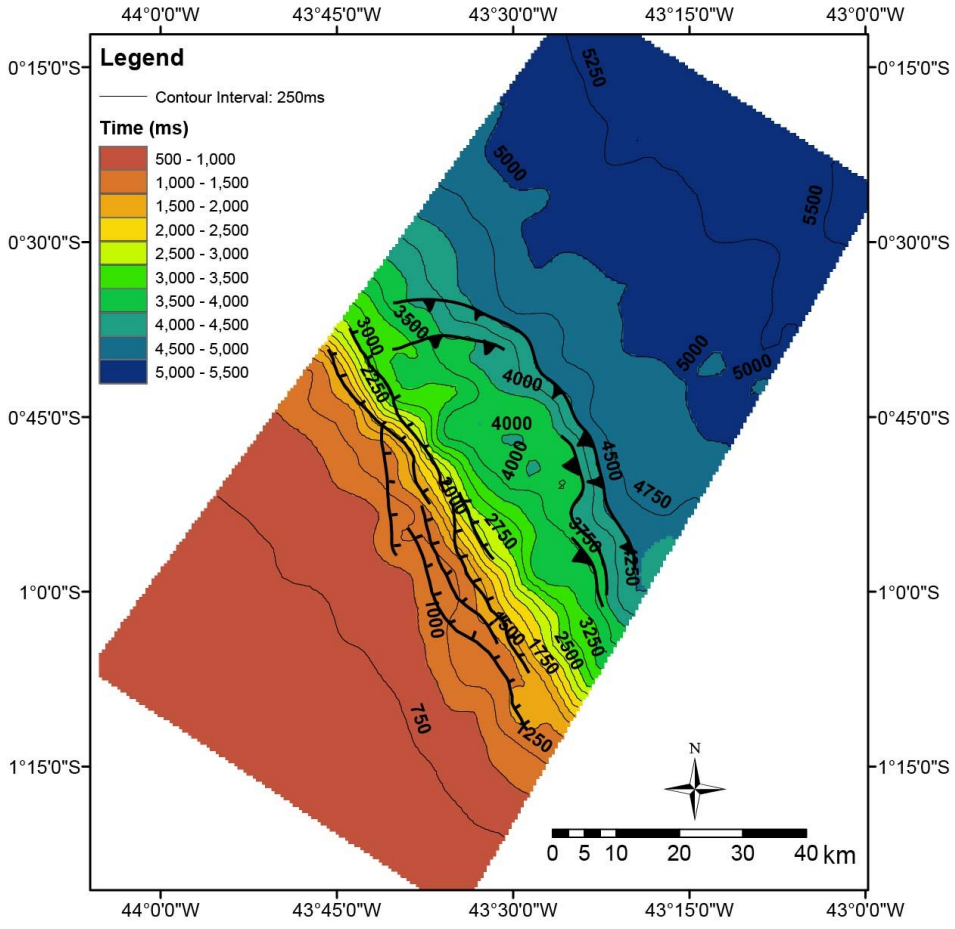

Figure 3-17. Eocene age (~42 Ma) structural map.

3.4.7 Oligocene (33.9 to 23.03 Ma)

The Oligocene age (~27 Ma) horizon (Fig. 3-18) (orange horizon on the seismic sections) (Figs. 3-7, 3-8, 3-9, and 3-10) corresponds to the Rupelian-Chattian boundary (28.4 Ma) unconformity (Trosdtorf et al., 2007) (Fig. 3-4). During the Oligocene conditions changed from regressive in the Rupelian (33.9 to 28.4 Ma) to transgressive in the Chattian (28.4 to ~23.0 Ma), and formed the Oligocene unconformity (Fig. 3-4) (Trosdtorf et al., 2007 after Haq et al., 1987).

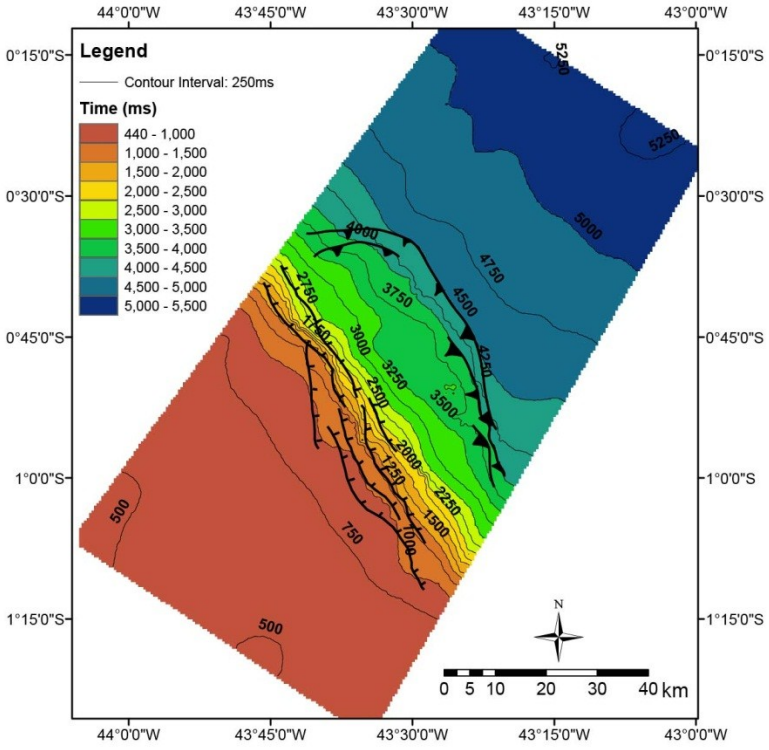

Figure 3-18. Oligocene age (~27 Ma) structural map.

3.4.8 Miocene (~23.0 to ~5.3 Ma)

The Miocene age horizon (~10 Ma) (Fig. 3-19) (cyan horizon on the seismic sections) (Figs. 3-7, 3-8, 3-9, and 3-10) corresponds to the top of a large transgressive event on the whole Brazilian Equatorial margin that gave origin to a large carbonate ramp (Trosdtorf et al., 2007).

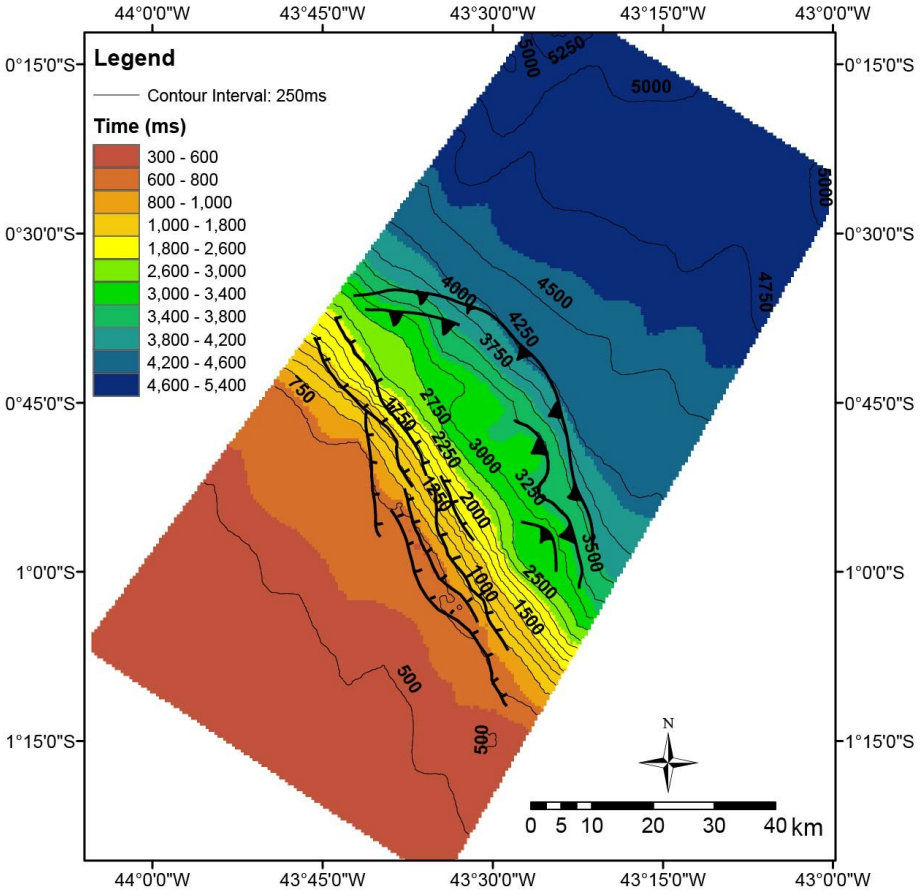

Figure 3-19. Miocene age (~10 Ma) structural map.

3.4.9 Upper Miocene to Present (~11.6 To 0 Ma)

The sequence above the Miocene age horizon (Fig. 3-19) is a prograding deep-water unconsolidated ponded basin mud and clay sequence that fills accommodation spaces created by folds (Fig. 3-7). Present day sea floor is a highly eroded surface cut by canyons (Fig. 3-20).

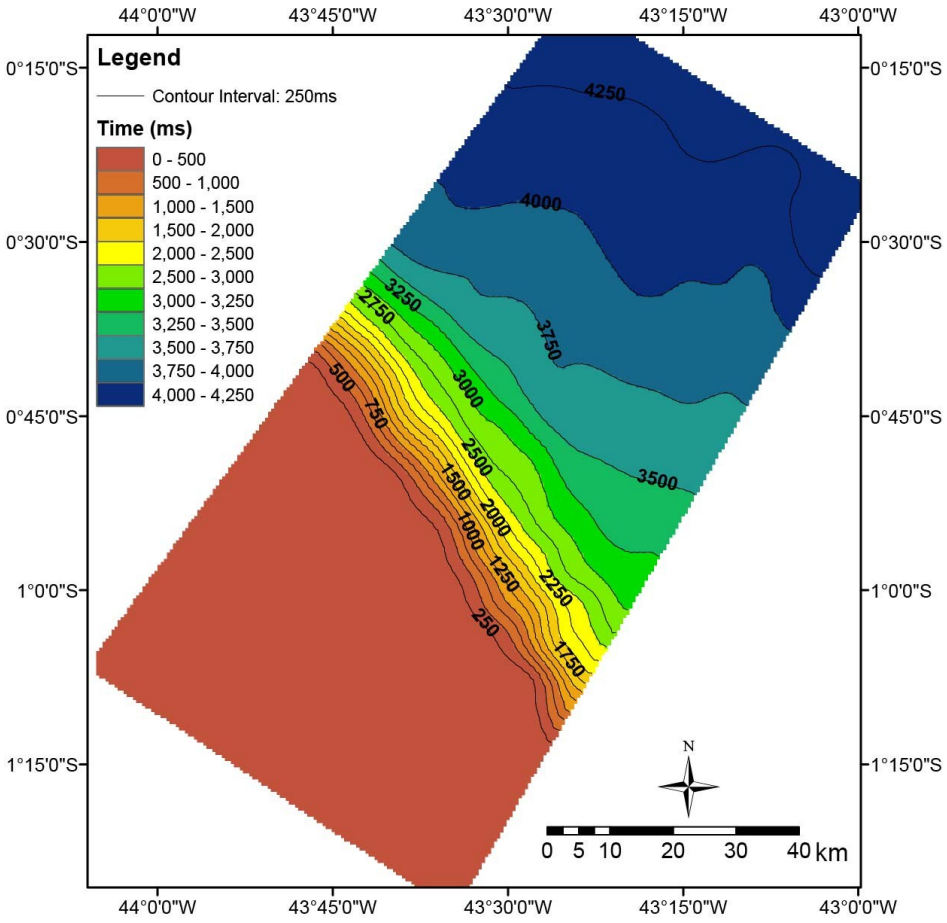

Figure 3-20. Sea-floor structural map

3.5 SEDIMENTATION RATES OF THE BARRERINHAS BASIN

Sedimentation rates were calculated for the deep-water well location using the ages and thicknesses of the horizons on the depth converted line, tied to the only deep-water well in the study area. The calculated sedimentation rates are summarized in Table 1 and plotted on Figure 3-21.

The higher sedimentation rate occurred at the earlier stages of the drift phase on the basin with a sedimentation rate as high as 226 m/my (Table 1) during the Coniacian (89 to 84.6 Ma) (Fig. 3-21). These high rates of sedimentation coincided with the Cretaceous deformation of the Travossas Formation (89.3 to 83.5 Ma). The deformed Coniacian-Santonian interval is a mud-dominated interval with a very high sedimentation rate, similar to the Amazon Delta today (Nancy Engelhardt-Moore, personal communication). Fossil recovery from well cuttings is poor, consistent with an environment of rapid deposition.

Campanian to Maastrichtian (70 to 67 Ma) sedimentation rates were also high (86 m/my) (Table 1) (Fig. 10), and could be associated with tectonic uplift that affected the whole Brazilian Equatorial Margin, as described by Zalan (2004).

Two more pulses of high sedimentation are observed in the Cenozoic during Oligocene and Miocene times, with sedimentation rates of 45 m/my during the Oligocene (34 to 23 Ma) and 37.5 m/my from Miocene to present (10 to 0 Ma) (Table 1). However,

the calculated sedimentation rates for the Cenozoic are dependent on our seismic stratigraphic model and our time-depth model, since no biostratigraphic data was available for the interval. The Miocene high sedimentation pulse coincides with the time of rearrangement of the drainage system east of the Andes, and the birth of the Amazon River (Figueiredo et al., 2009) (Fig. 3-5), suggesting the Miocene drainage rearrangement affected areas farther south than previously recognized.

Stage name	Age (my)	Time of deposition	Rate of deposition (m/my)
Miocene to Present	10 to 0	10 my	37.5
Oligocene to Miocene	23 to 10	13 my	30.7
Eocene to Oligocene	34 to 23	11 my	45.5
Top Paleocene to Eocene	55 to 34	21 my	24.8
Maastrichtian to Top Paleocene	67 to 55	12 my	7.5
Campanian to Maastrichtian	70 to 67	3 my	86
Upper Santonian to Campanian	83.5 to 70	6.5 my	13.5
Lower Santonian to Upper Santonian	84.6 to 83.5	1.1 my	92.72
Turonian/Cenomanian to Lower Santonian/Coniacian	89 to 84.6	4.4 my	226
Albian to Turonian/Cenomanian	102 to 89	3 my	19

Table 1. Sedimentation rate Barreirinhas Basin. Sedimentation rates are in meters/million years and are calculated for a point at the toe of slope in the middle of the study area. Sedimentation rates for the Cretaceous stratigraphy were calculated using biostratigraphic data from a deep-water well in the area. Cenozoic sedimentation rates were calculated using the age and thickness of the seismically defined units. The result of the different resolutions of the methodology is a higher frequency curve for the cretaceous and lower frequency curve for the Cenozoic.

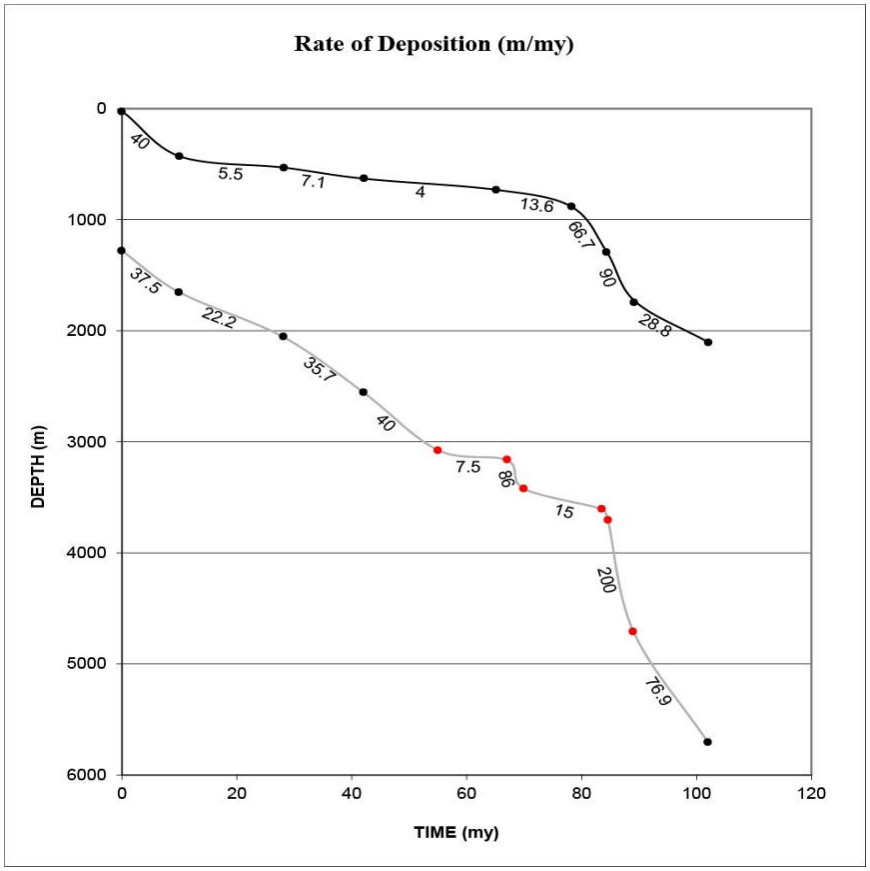

Figure 3-21. Rate of deposition plot for two locations: 1) deep-water well location (gray curve), and, 2) a location on the shelf (black curve). Points in black correspond to depth of measured horizons in meters versus their age in million years. Points in red correspond to rock samples depths on the well and interpreted ages based on the biostratigraphy. Points are plotted for their age in millions of years versus their current depth in meters. The shallowest point is the present day sea-floor (1279 m in deep-water and 50 m on the shelf) and the deeper point, the Turonian (detachment surface). Steep slopes correspond to high sedimentation rates and low angle slopes correspond to low sedimentation rates.

3.6 STRUCTURAL HISTORY OF THE BARREIRINHAS BASIN

3.6.1 Cretaceous Structural History

This wide system of folds and thrusts generated significant topographic relief at the sea-floor during deformation. On the continental shelf rotated blocks created topography at the sea-floor that caused preferential erosion of the footwall. Some of the sediments filled the accommodation space at the hanging wall (Fig. 3-22 and 3-23), but most of the sediments bypassed the shelf and were deposited at the toe of the slope (Fig. 3-23). On the toe of the slope folds created anticlines at the sea-floor that were buried by sediments coming from the shelf (fig. 3-25). Because deformation occurred within a very brief interval, the sequence deposited on the top of the rotated blocks on the shelf and on the top of the folds at the toe of slope onlaps the cyan horizon (Figs. 3-26, 3-27, and 3-28). The top of this onlapping sequence was mapped as the pink horizon (Fig. 3-22) at the top of the Santonian (~84 Ma) sequence. The paleo-sea-floor topography controlled the deposition of the upper part of the Santonian sequences on the toe of the slope (Fig. 3-23).

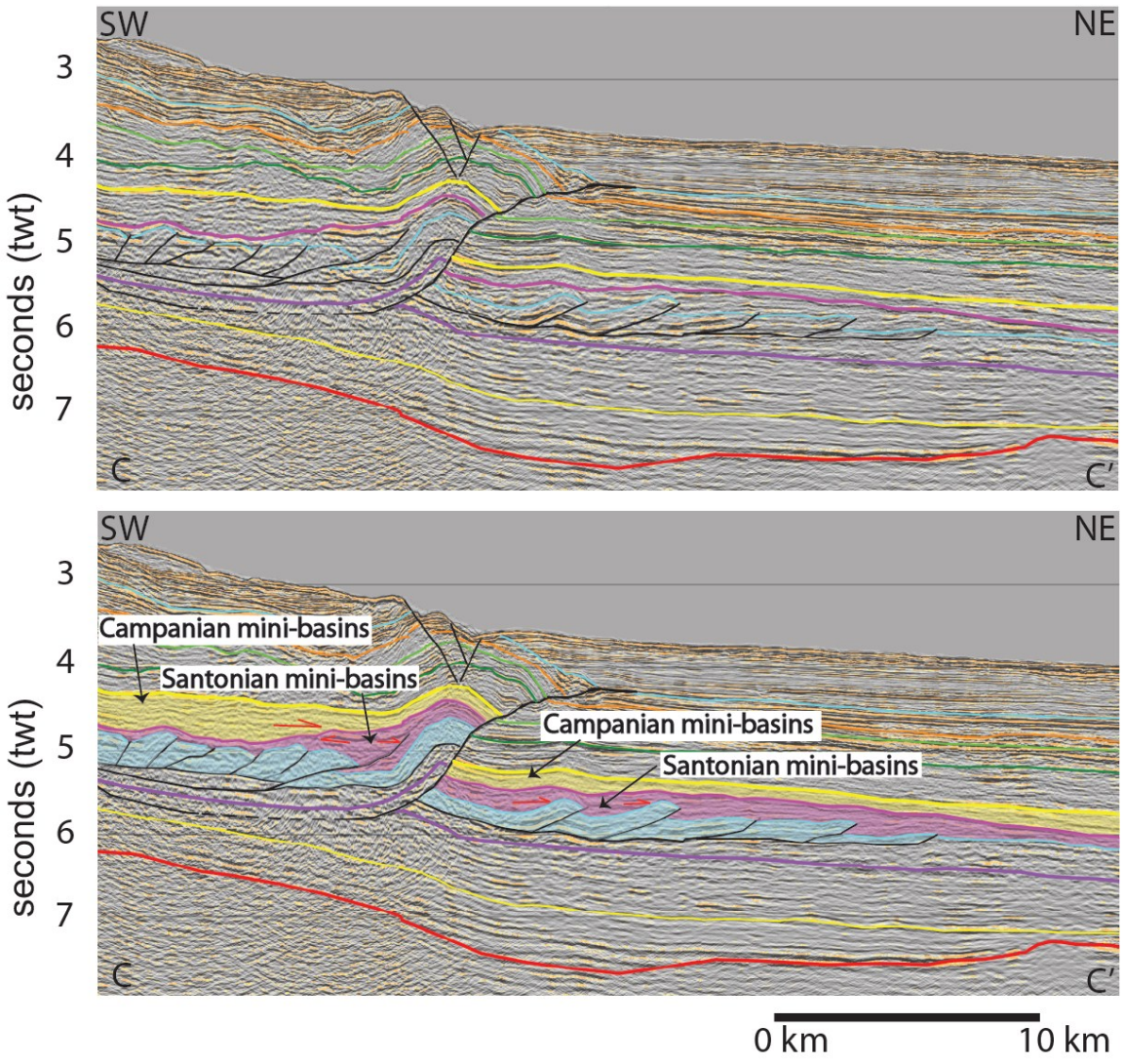

Figure 3-22. A. Detail of pre-stack time migrated dip seismic line C-C'. Vertical scale is in seconds and horizontal scale is in kilometers, average vertical exaggeration is approximately 1:5. Line shows accommodation space was being created on the paleo sea-floor, and infilled by the purple sequence during the Santonian. B. Cyan sequence corresponds to the Coniacian/Santonian deformed sequence. Sequence in pink was

probably deposited during a deformational hiatus and onlaps the cyan sequence, forming a series of ponded mini-basins filling the accommodation space created by faulting and folding. Sequence in yellow corresponds to Lower Campanian sediments and infills remaining paleo water-bottom topography. Campanian sequence was deposited post-deformation of Coniacian/Santonian sequences in cyan and pink. Notice that sediments landward of the last fold on the bottom of the sequence represented in yellow onlaps the pink sequence, but not basinward suggesting movement on the folds continued longer landward.

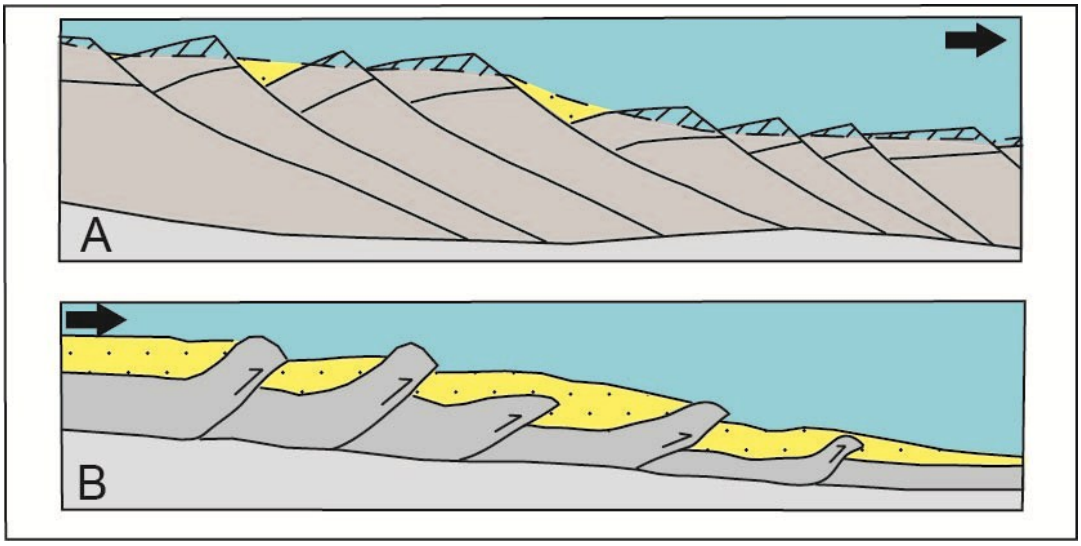

Figure 3-23. Schematic depiction of erosion and deposition on the Cretaceous deformed sequence. A. On the continental shelf rotated blocks created topography at the sea-floor, with structural highs on the footwalls and lows on the hanging walls. Sediments were eroded from the footwall and deposited on the hanging wall. As erosion of the shelf proceeded sediments bypassed the shelf and were deposited at the toe of the slope. B. On the toe of the slope folds created anticlines at the sea-floor that were buried by sediments coming from the shelf, forming an onlapping sequence in the back limbs of the folds.

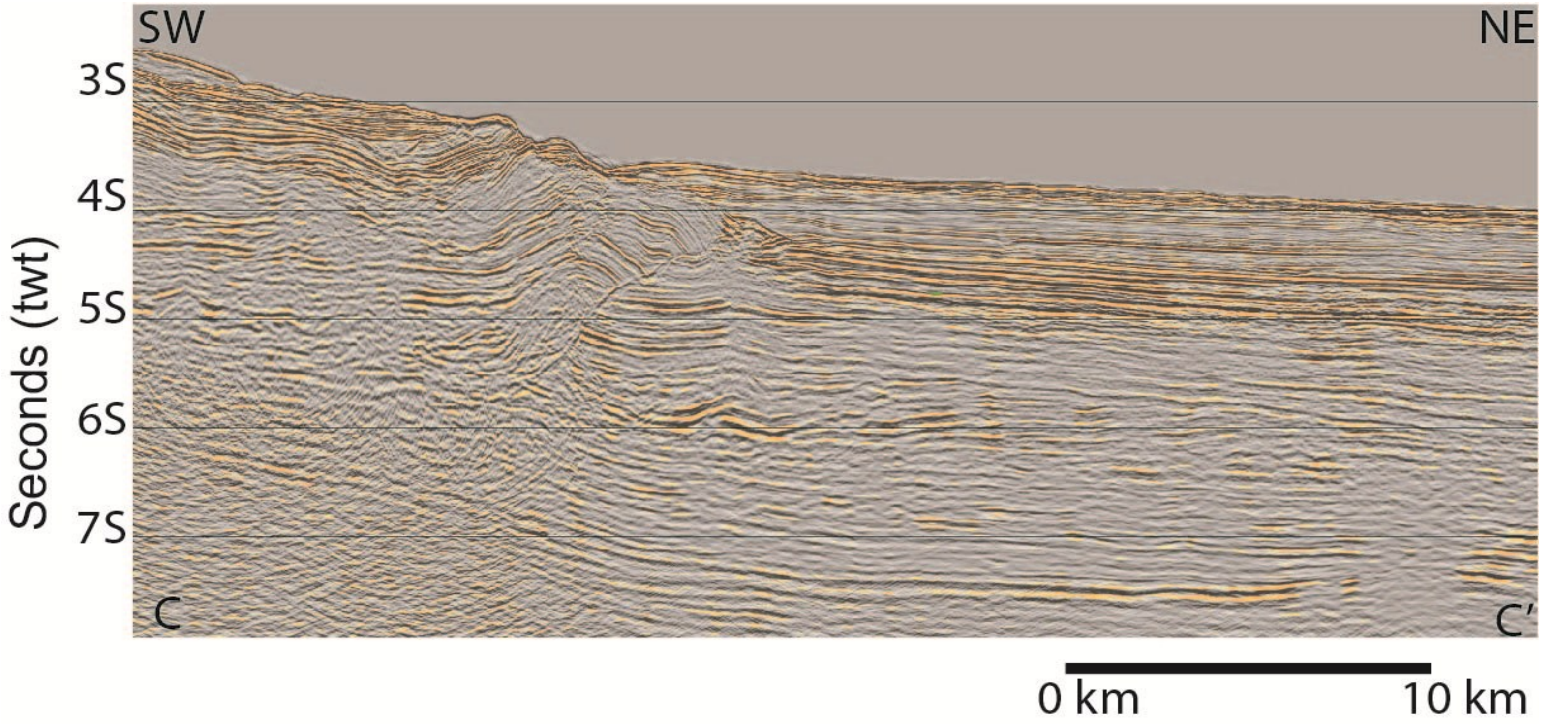

Figure 3-24. Detail on pre-stack time migrated dip seismic line C-C' without interpretation. Vertical scale is in seconds and horizontal scale is in kilometers, average vertical exaggeration is approximately 1:5.

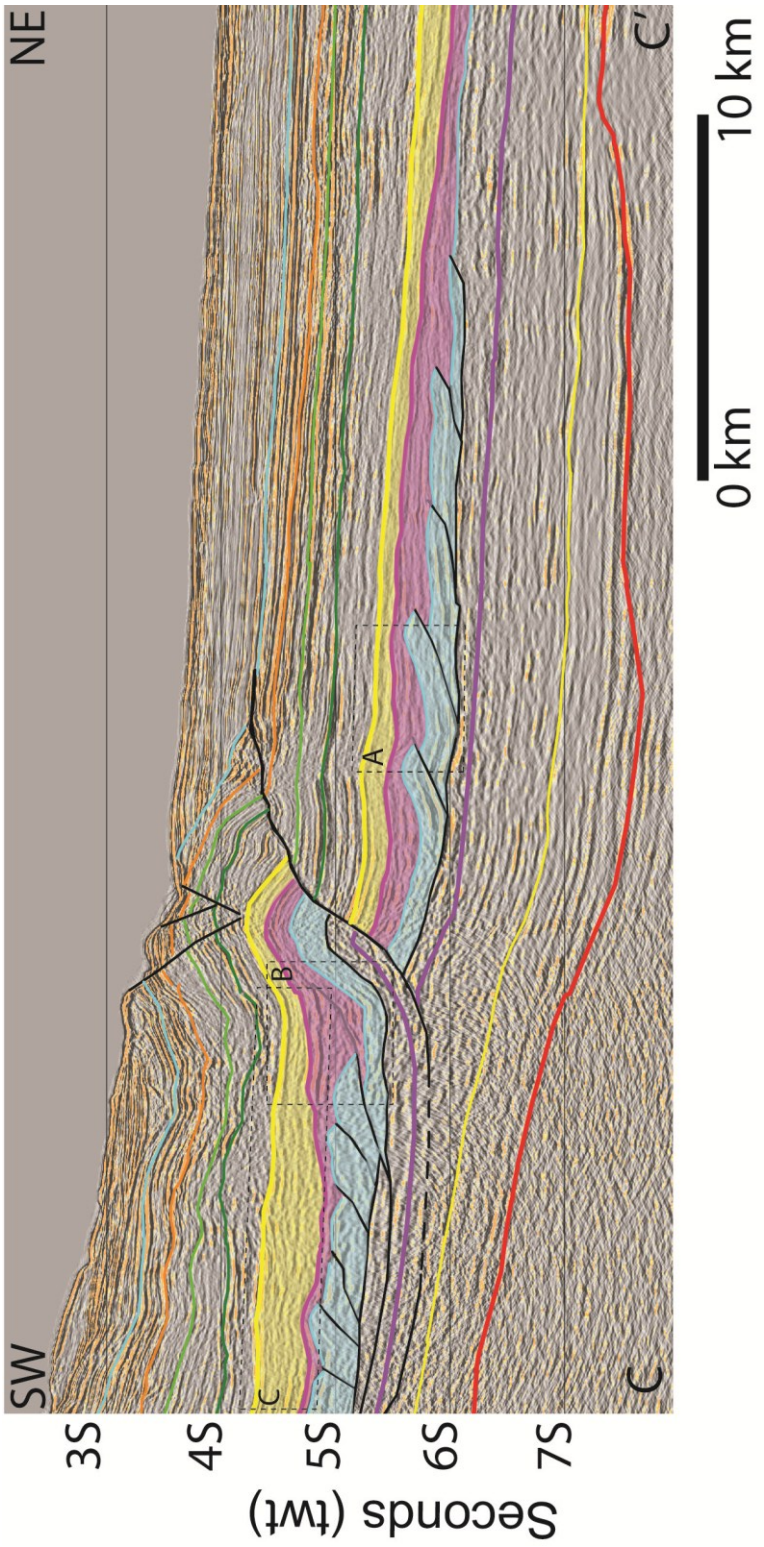
NE
SW
C
C'
A
B
C
3S
4S
5S
6S
7S
Seconds (twt)
0 km
10 km

Figure 3-25. Detail on pre-stack time migrated dip seismic line C-C'. Vertical scale is in seconds and horizontal scale is in kilometers, average vertical exaggeration is approximately 1:5. We interpret accommodation space being created on the paleo sea-floor and infilled by the pink sequence during the Santonian. Cyan corresponds to the Coniacian/Santonian deformed sequence. Sequence in pink was probably deposited during a deformational hiatus and onlaps the cyan sequence, forming a series of ponded mini-basins filling the accommodation space created by faulting and folding. Sequence in yellow corresponds to Lower Campanian sediments and infills remaining paleo water-bottom topography at Campanian time. Campanian sequence was deposited post-deformation of Coniacian/Santonian sequences in cyan and pink. Notice that sediments landward of the last fold at the bottom of the sequence represented in yellow onlap the pink sequence, but not basinward sequence suggesting movement on the folds continued longer landward.

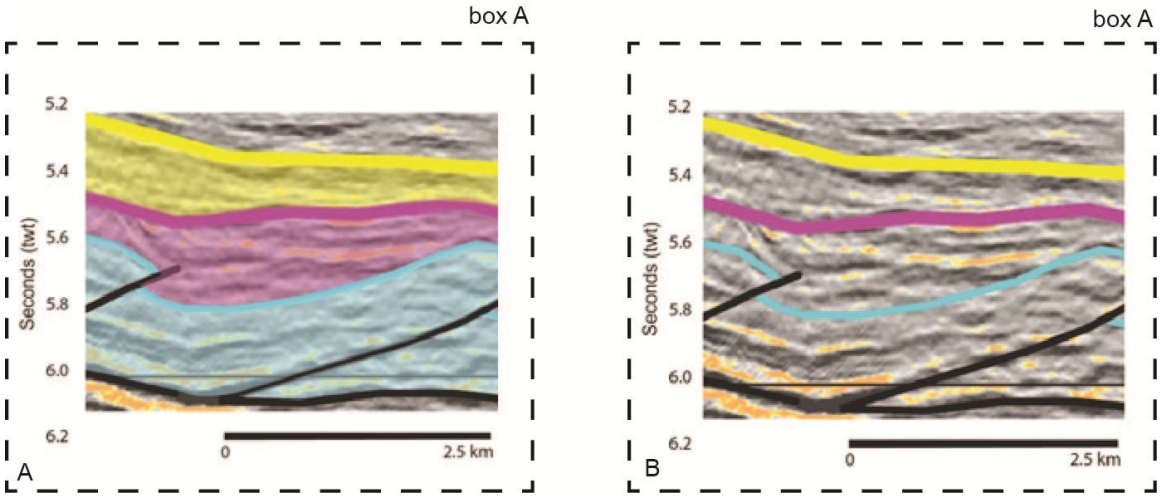

Figure 3-26. Detail on ponded mini-basin, box A on figure 3-25. Vertical scale is in seconds and horizontal scale is in kilometers, average vertical exaggeration is approximately 1:5. A- Line shows accommodation space was being created on the paleo sea-floor, and infilled by the purple sequence during the Santonian. Cyan corresponds to the Coniacian/Santonian deformed sequence. Sequence in pink was deposited during a deformational hiatus and onlaps the cyan sequence, forming a series of ponded mini-basins filling the accommodation space created by faulting and folding. Sequence in yellow corresponds to Lower Campanian sediments and infills remaining paleo water-bottom topography during Campanian time. B- Same as A without color.

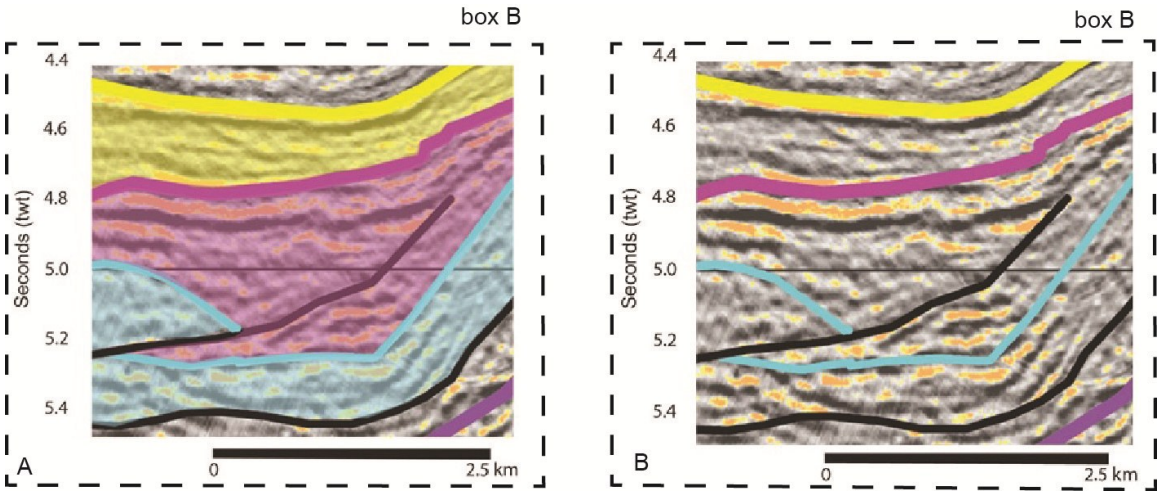

Figure 3-27. Detail of ponded mini-basin, box B on figure 3-25. Vertical scale is in seconds and horizontal scale is in kilometers, average vertical exaggeration is approximately 1:5. Line shows syn-deformation thrusting with duplicate sections of sequences represented in cyan Coniacian/Santonian age and pink of Santonian age. But pre-dating deposition of the Sequence in yellow of Campanian age.

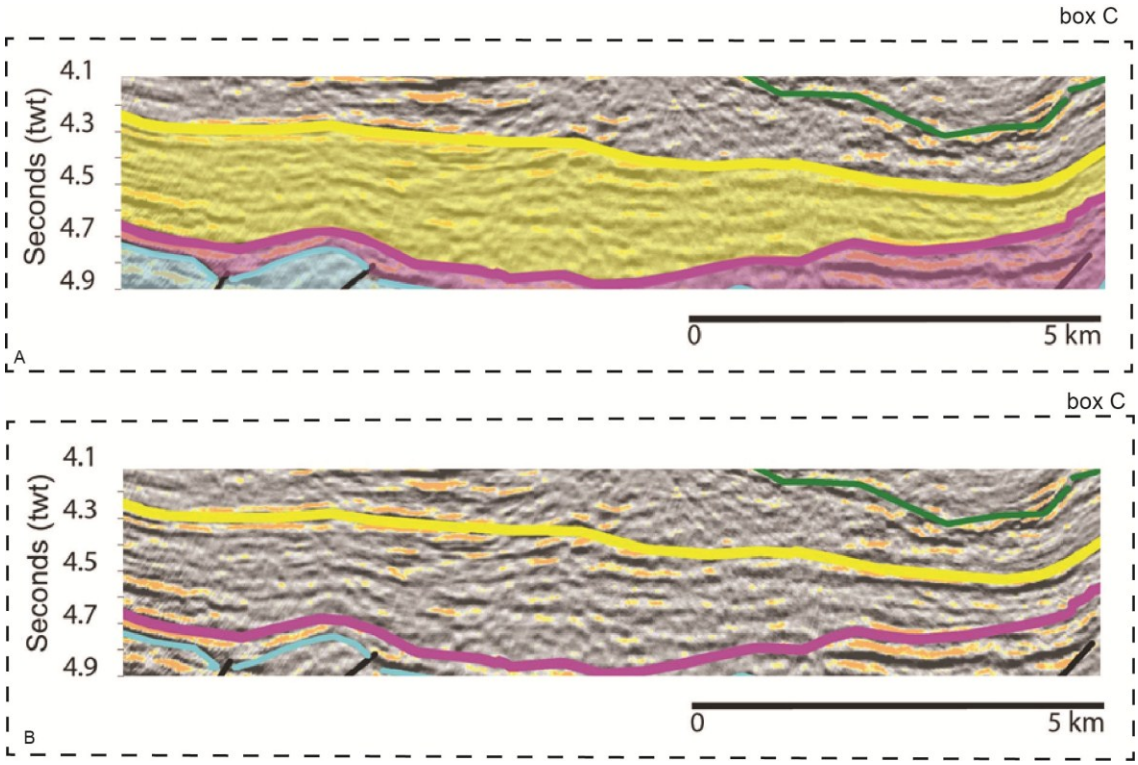

Figure 3-28. Detail of ponded mini-basin. Vertical scale is in seconds and horizontal scale is in kilometers, average vertical exaggeration is approximately 1:5. Line shows deposition of Campanian mini-basin represented by the sequence in yellow. Campanian sequence was deposited post-deformation of Coniacian/Santonian sequences in cyan and purple.

3.6.1.1 *Aptian/Albian (125 to 99.6 Ma)*

The Albian horizon represents the top of the rift sequence on the shelf and the beginning of the marine influx in the deep-water. Rift-related basement faults formed horsts and grabens on what is now the continental shelf (Fig. 3-11). Rift faults cut through the top basement surface (red surface) and mostly die out upward below the top of the rift sequence (yellow horizon, Fig. 3-8). The rift sequence, mapped as the interval between the basement and the Albian horizons, is not very thick in the study area, less than 1000 ms (Fig. 3-29).The main characteristic of the Barreirinhas Basin is an abrupt transition zone between oceanic and continental crust as a result of being located on a transform margin (Fig. 3-1). The transition between oceanic and continental crust takes place over a distance of 10 to 20 km, resulting in a slope of 10 to 15 degrees measured on the basement level (Fig. 3-9).

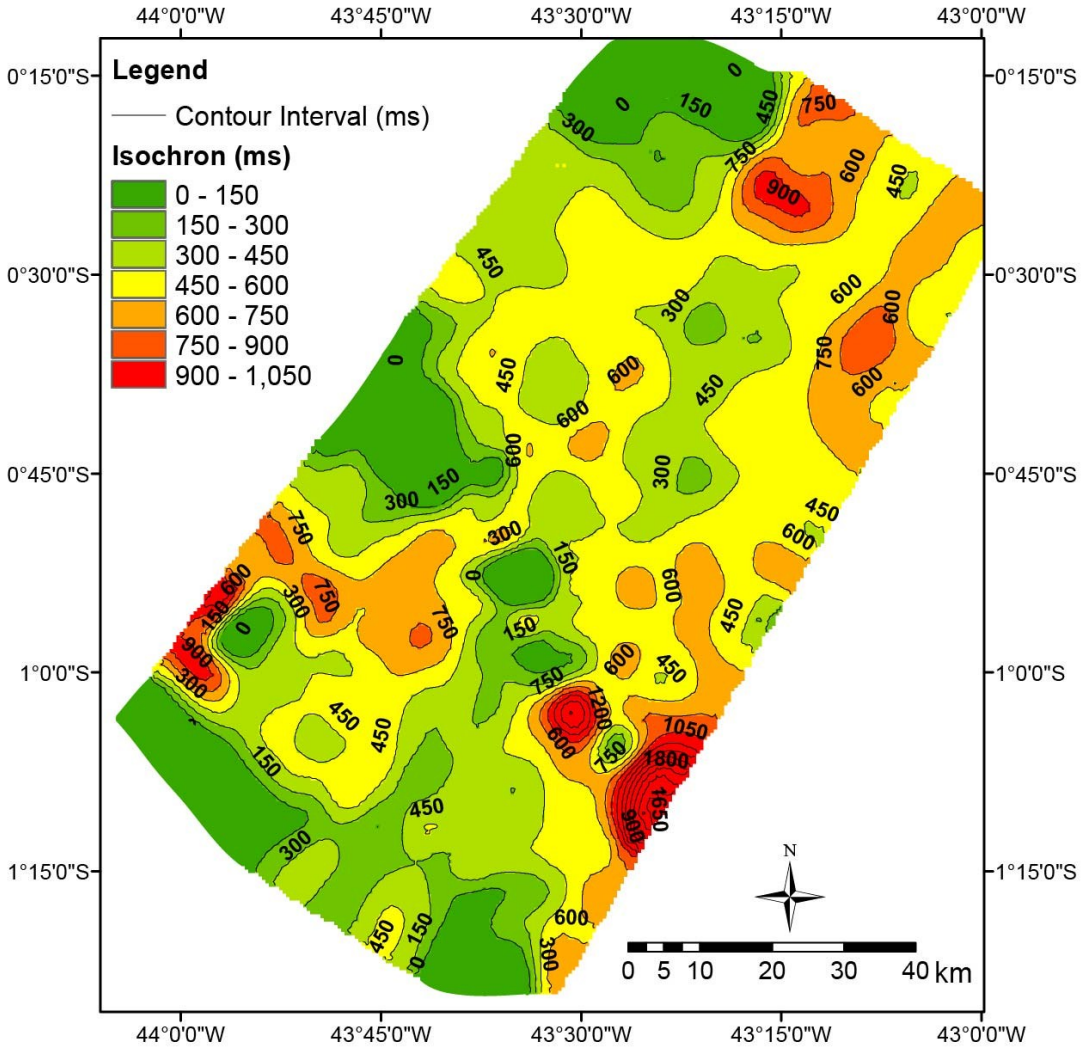

Figure 3-29. The isochron from basement to top of Albian age (~100 Ma) horizon represents the thickness of the rift sequence on the shelf and thickness of first marine sediments on the slope and oceanic basin.

3.6.1.2 *Cenomanian/Turonian (99.6 to 89.3 Ma)*

The Cenomanian/Turonian (Fig. 3-13) was a time of deep-water deposition of shales and marls in the area (Fig. 3-4). The Turonian consists in well-section of 1100 meters of mudstones interbedded with thin layers of sandstone, siltstones, limestones, and marls. The Cenomanian/Turonian sequence corresponds to continuous, parallel-bedded horizons on the seismic that cover the whole study area (Fig 3-30). Turonian rocks form the detachment surface for the Santonian deformed rocks (85.8 to 83.5 Ma) (Fig. 3-25).

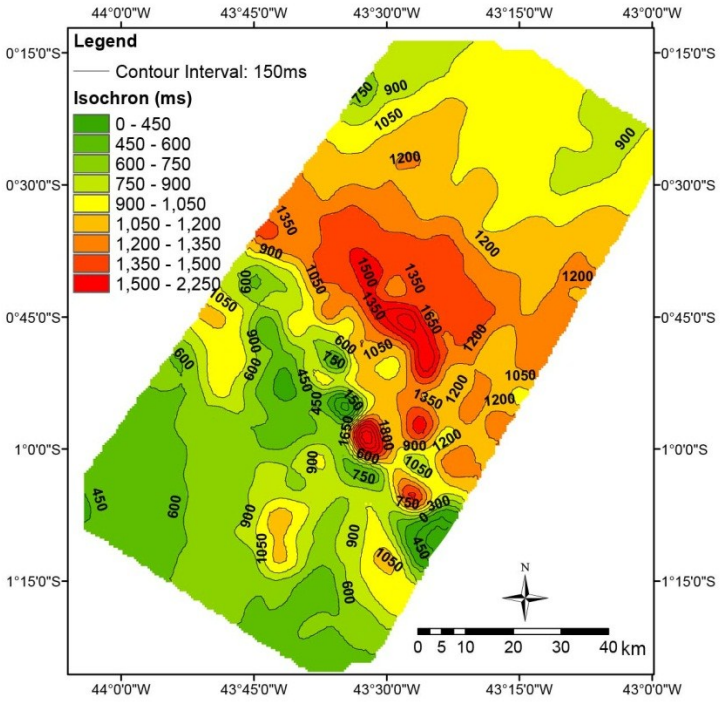

Figure 3-30. Isochron map between the Albian (~100 Ma) and Turonian age (~89 Ma) horizons.

3.6.1.3 *Coniacian/Santonian (89.3 to 83.5 Ma)*

The combination of a steep basal slope (10 to 15 degrees) due to a narrow transition zone (10 to 20 km) (Fig. 3-7) with intervals of high sedimentation (Fig. 3-21), and consequently steep surface-slope led to instability of the overlying sediments, making them prone to gravity-driven slumps and slides (Fig. 3-22). During the Santonian (85.8 to 83.5 Ma) a prograding shelf and a high sedimentation rate (226 m/my) (Fig. 3-21) in deep-water caused slope instability that generated a set of linked listric normal faults on the shelf and thrust faults on the toe of slope (Fig. 3-7). On the shelf a thin deformed sequence is characterized by listric normal faults detached on a discrete stratigraphic horizon within the sequence of Cenomanian to Turonian shales (96 to 91.5 Ma) (Fig. 3-22). The faults form basinward-dipping rotated blocks over a distance of ~30 km in the dip direction (Fig. 3-7). The extensional domain on the shelf is linked by a 30 km wide translational domain without visible faults to a compressional domain at the toe of slope (Fig. 6). On the toe of the slope the sequence is deformed by a set of landward-dipping thrust faults, forming a 30 km long and 30 km wide belt of folded imbricates with duplicated sections (Fig. 3-7).

The sequence deposited on the top of the rotated blocks on the shelf and on the top of the folds at the toe of slope onlaps the deformed sequence (Figs. 3-26, 3-27, and 3-28). The onlapping sequence is highlighted in pink in figure 3-22, the top of the onlapping sequence corresponds to the top of the Santonian (~84 Ma) (Fig. 3-14). The paleo-sea-floor topography controlled deposition of this upper part of the Santonian

sequences on the toe of the slope and the sequence infills the spaces created by the normal faults on the continental shelf and the thrust folds on the toe of slope (Fig. 3-32).

The isochron map between the Turonian and the Santonian horizons (Fig. 3-31) shows the thickness of the Cretaceous syn-deformational sequence and part of the post-deformational sequence. Most of the sediments, up to 1000 ms (Fig. 3-31), accumulated on the slope on pocket mini-basins (Fig. 3-32).

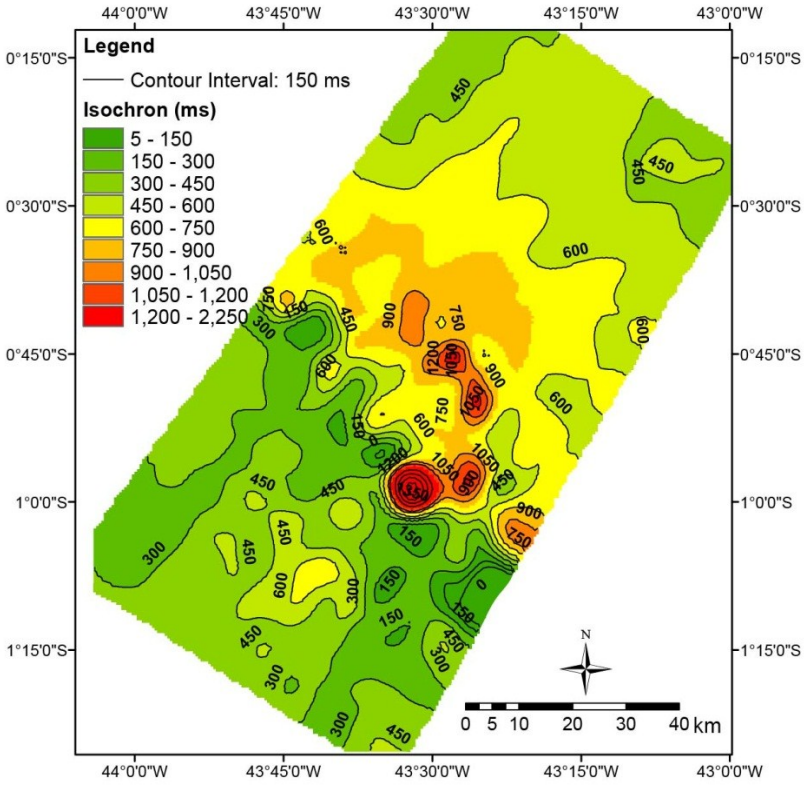

Figure 3-31. Isochron map between Turonian (~89 Ma) and Santonian age (~84 Ma) horizons.

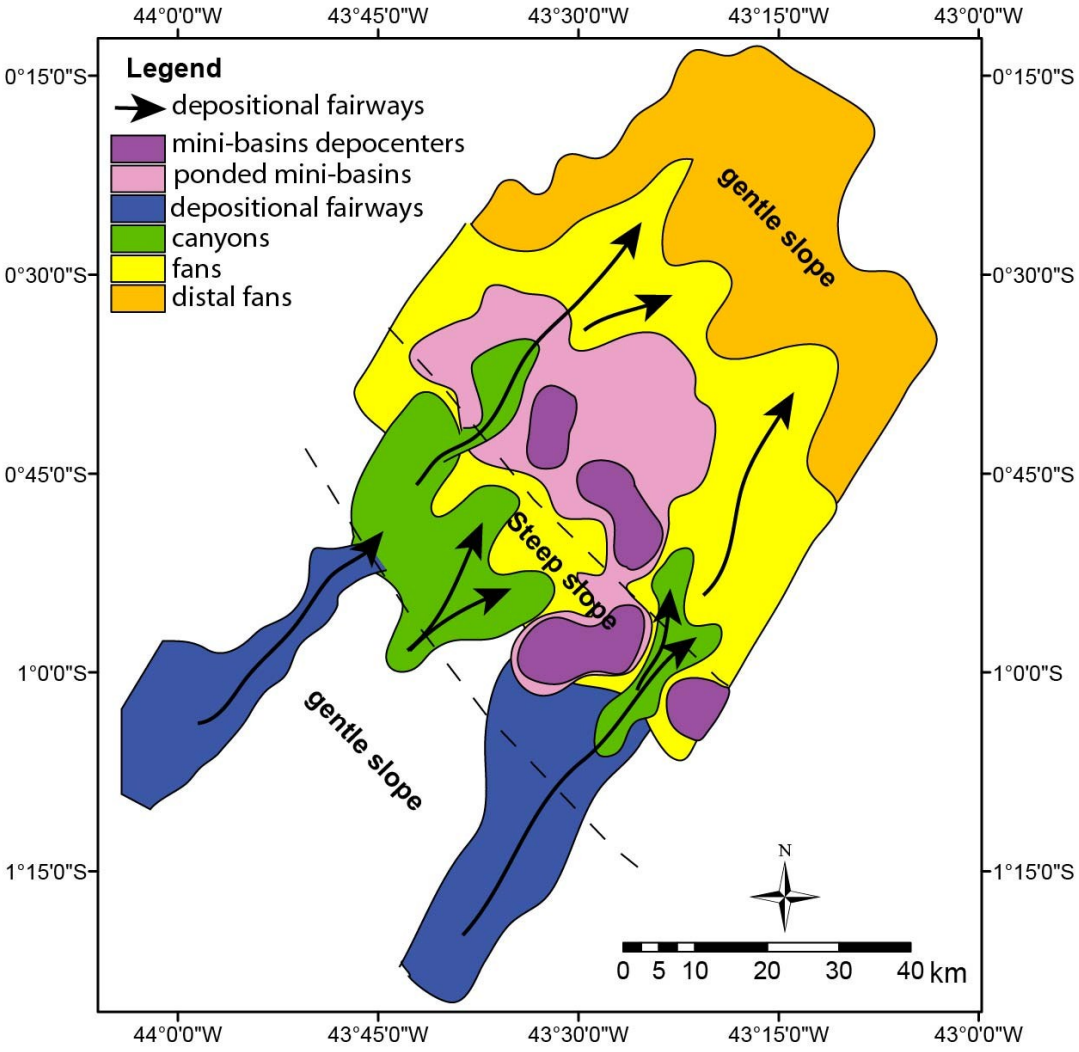

Figure 3-32. Depositional environments from ~89 to ~84 Ma.

3.6.1.4 *Campanian/Maastrichtian (83.5 to 65.6Ma)*

The Campanian sediments infill the space created by normal faults on the shelf and thrusted folds in the toe of slope (Fig. 3-33); and is a growth sequence (Fig. 3-8). The isochron map between the Santonian and Campanian (Fig. 3-33) shows depositional thicks forming Campanian ponded mini-basins (Fig. 3-34). Mini-basins (Fig. 3-34) are wider than the Santonian mini-basins (Fig. 3-32), represented on the Turonian to Santonian isochron (Fig. 3-31). Santonian ponded mini-basins coalesced into larger basins during Campanian time (Fig 3-34). The isochron map (Fig. 3-33) between the Campanian horizon (Fig. 3-15) and the Maastrichtian horizon (Fig. 3-16) shows burial of the multiple ponded mini-basins (Fig. 3-22). Depositional thicks are observed in deep-water, suggesting sediments also bypassed the area into deep-water (Fig. 3-33).

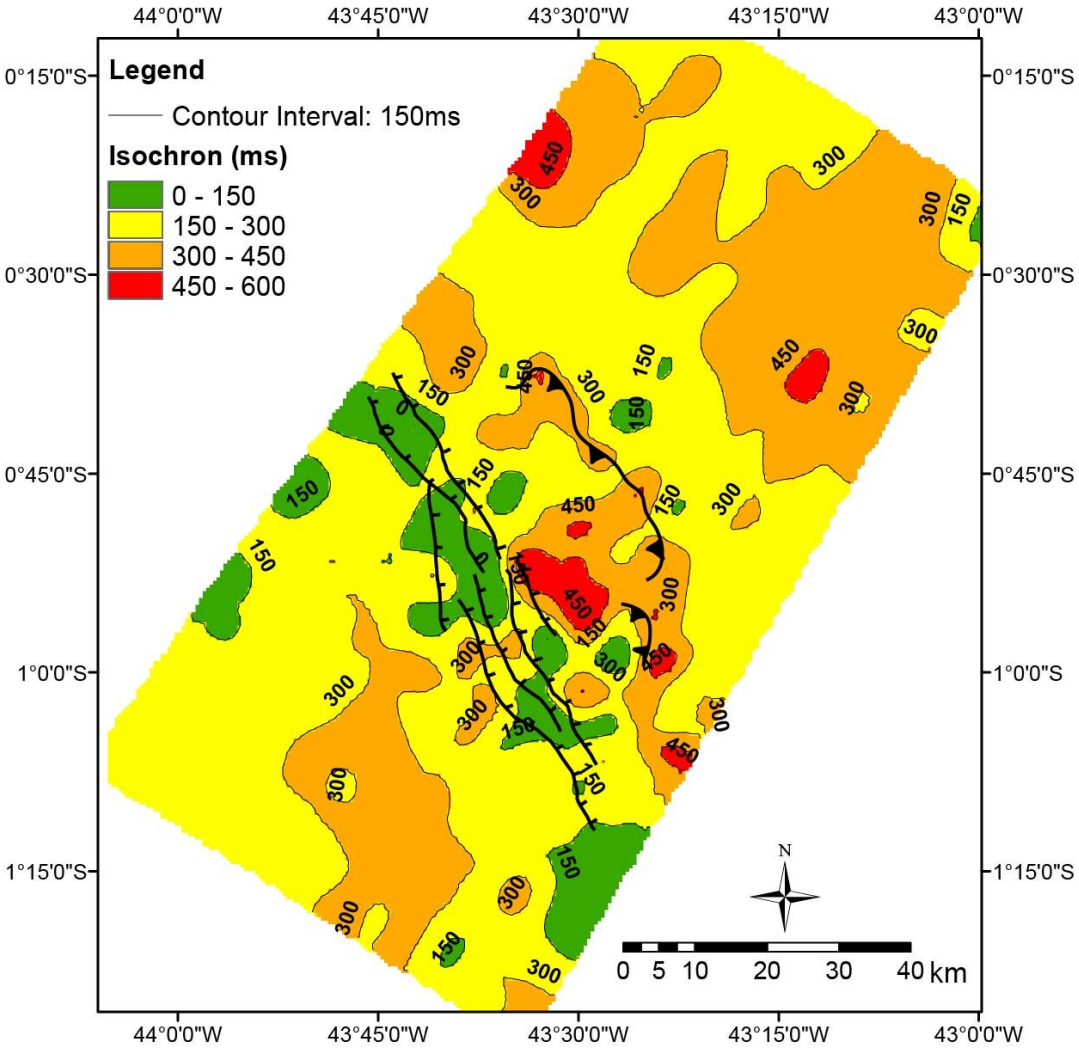

Figure 3-33. Isochron map between the Santonian (~84 Ma) and Campanian age (~78 Ma) horizons.

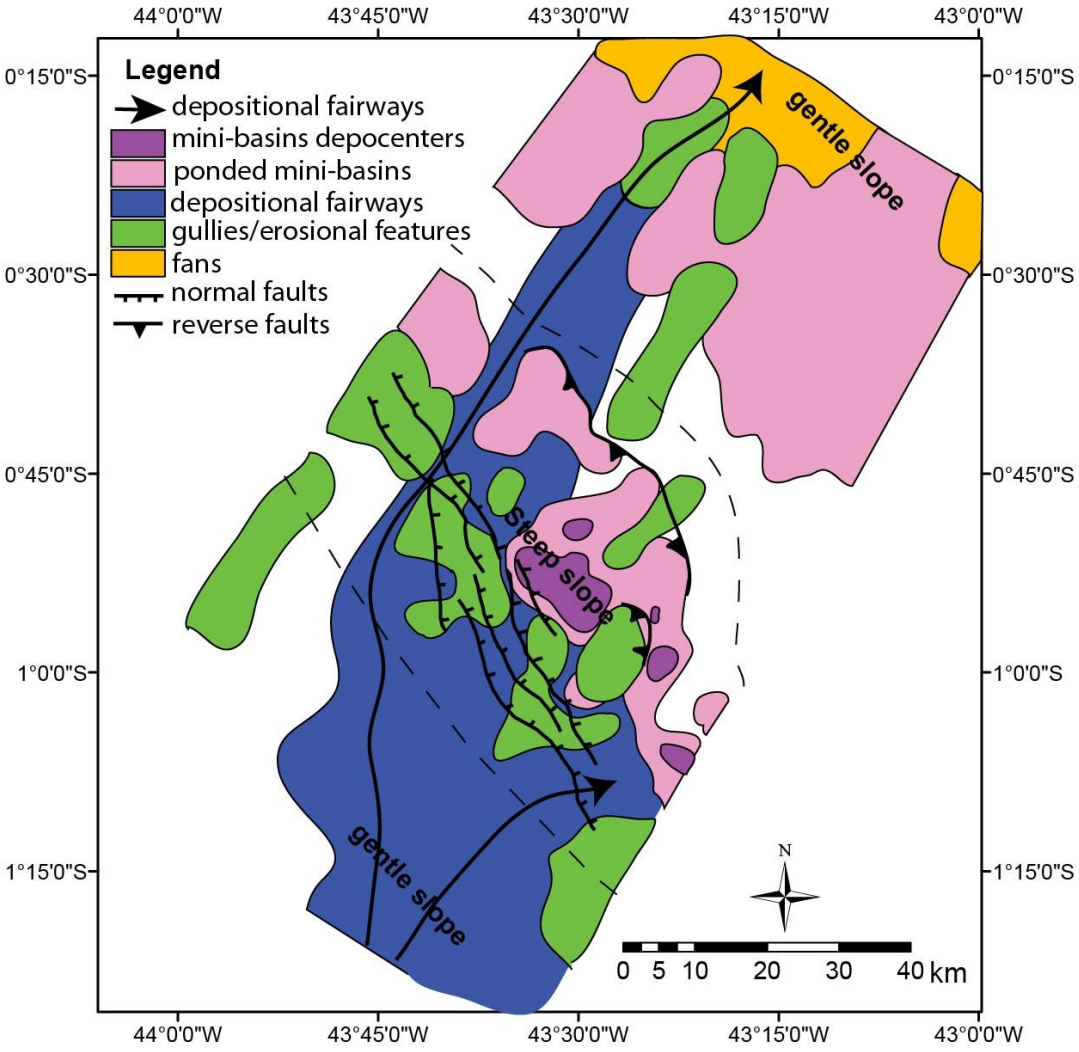

Figure 3-34. Depositional environments from ~84 to ~78 Ma.

3.6.2 Cenozoic Structural History

The Cenozoic sequences, from Turonian to Pleistocene were subjected to a second phase of deformation (Fig. 3-35). Sequences from Cenomanian (99.6 Ma) to Paleocene (55.8) ages (Fig. 3-4) were deposited before Cenozoic deformation, while sequences from Eocene to present (55.8 to 0 Ma) (Fig. 3-4) were deposited during deformation (Fig. 3-35). On the continental shelf, sediments were eroded from the footwalls and deposited on the hanging walls of normal faults (Fig. 3-36). On the toe of the slope thrust faults created anticlines at the sea-floor that were partially eroded (Fig.3-36).

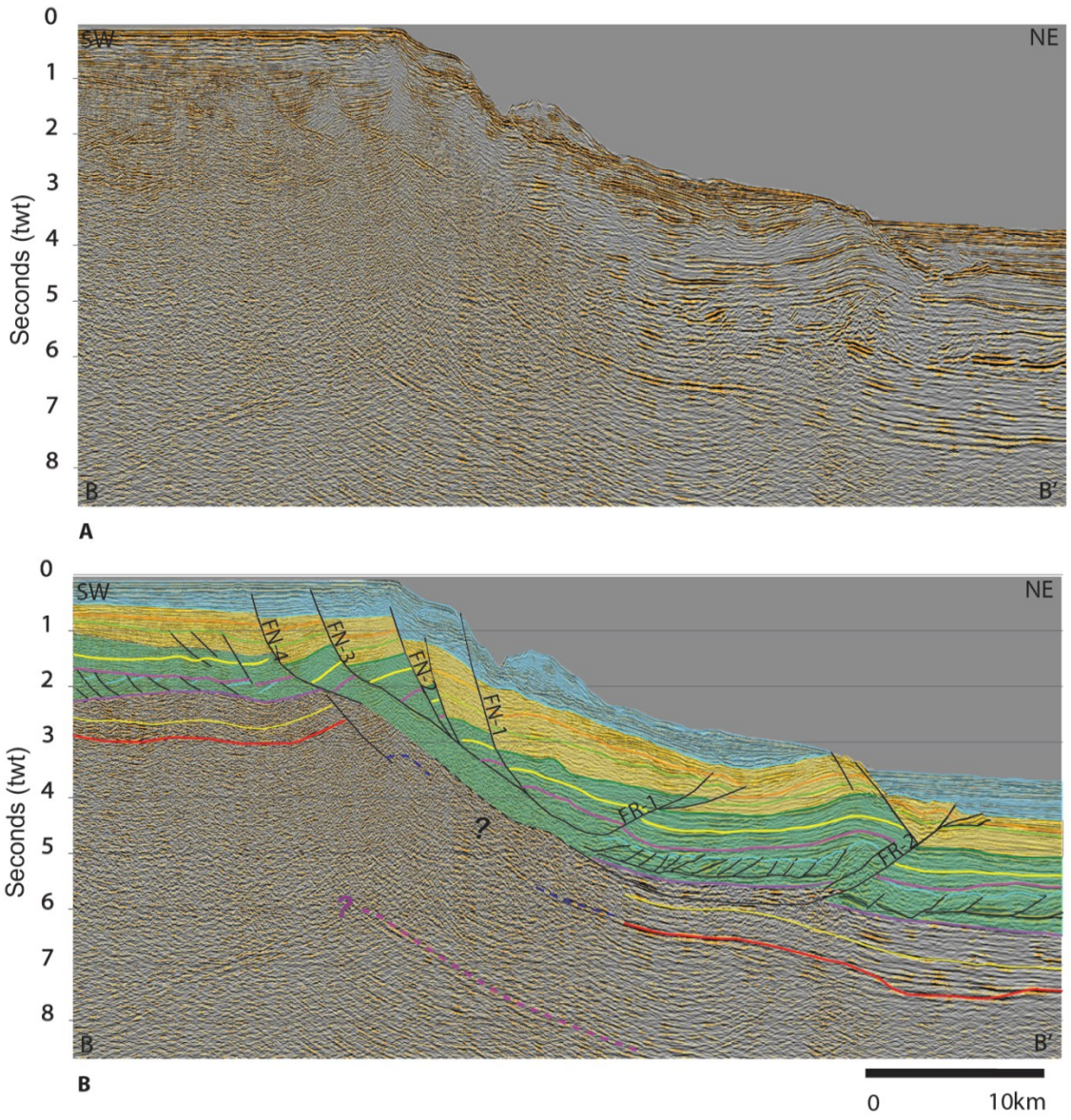

Figure 3-35. Detail of the pre-stack time migrated dip seismic line B-B'. Vertical scale is in seconds and horizontal scale is in kilometers, average vertical exaggeration is approximately 1:5. Cenozoic deformation is highlighted, the pre-growth sequences in green and growth sequences in yellow and blue.

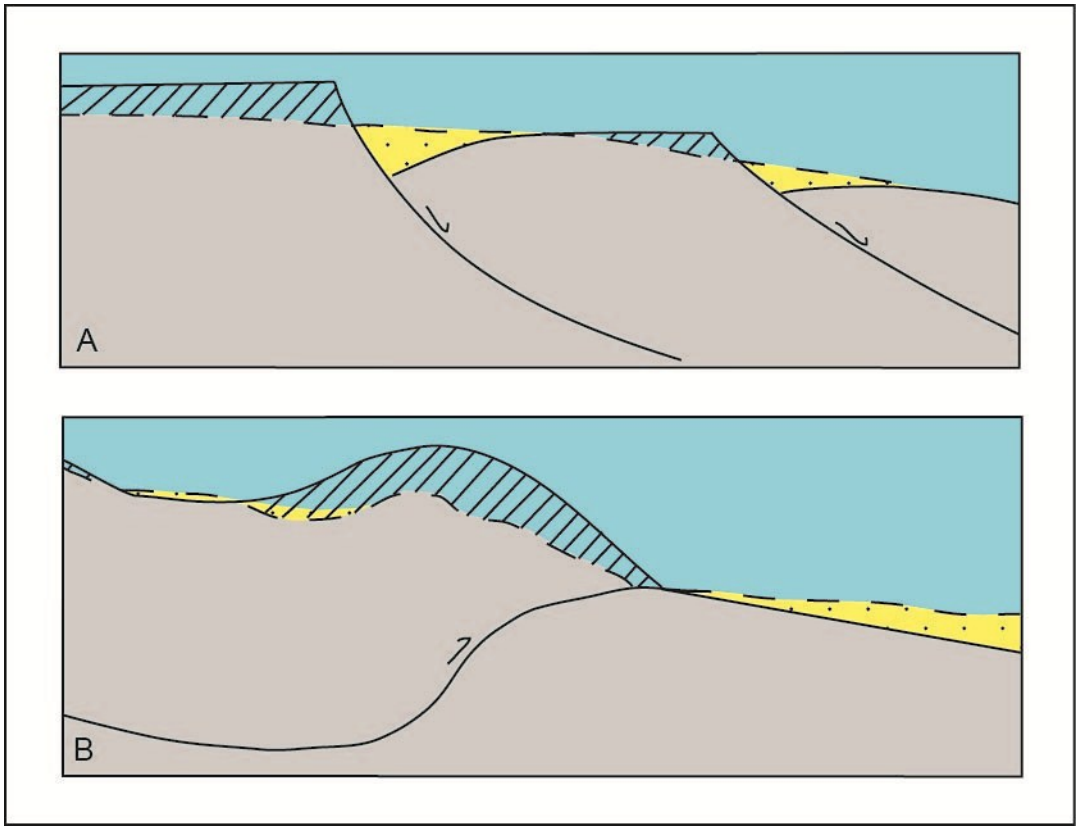

Figure 3-36. Erosion and deposition on the Cenozoic deformed sequence. A. On the continental shelf listric faults created accommodation space on the hanging wall, sediments were eroded from the footwall and deposited on the hanging wall as faults moved through time. B. On the toe of the slope thrust faults created anticlines at the sea-floor that were partially eroded and material re-deposited around the anticlines.

3.6.2.1 *Paleocene/Eocene (65.5 to ~42 Ma)*

The isochron map between the Eocene and the Maastrichtian horizons (Fig. 3-37) show thicks and thins over the Paleocene/Eocene sequence top (65.5 to 37.2 Ma). On the shelf break sediments were eroded from the footwall and re-deposited on the hanging wall of the normal faults, forming elongated depocenters parallel to the shelf break (Fig. 3-38). On the continental slope sediments were deposited as thrust faults moved, resulting in a growth sequence (Fig. 3-37). Sediments deposited on the hanging-wall of the thrust faults formed ponded-mini-basins (Fig. 3-38). Thrust fault movement formed folds on the hanging wall that created anticlines at the Paleocene/Eocene sea-floor. These anticlines were partially eroded and sediments were locally re-deposited on the thrust faults footwalls (Fig. 3-36).

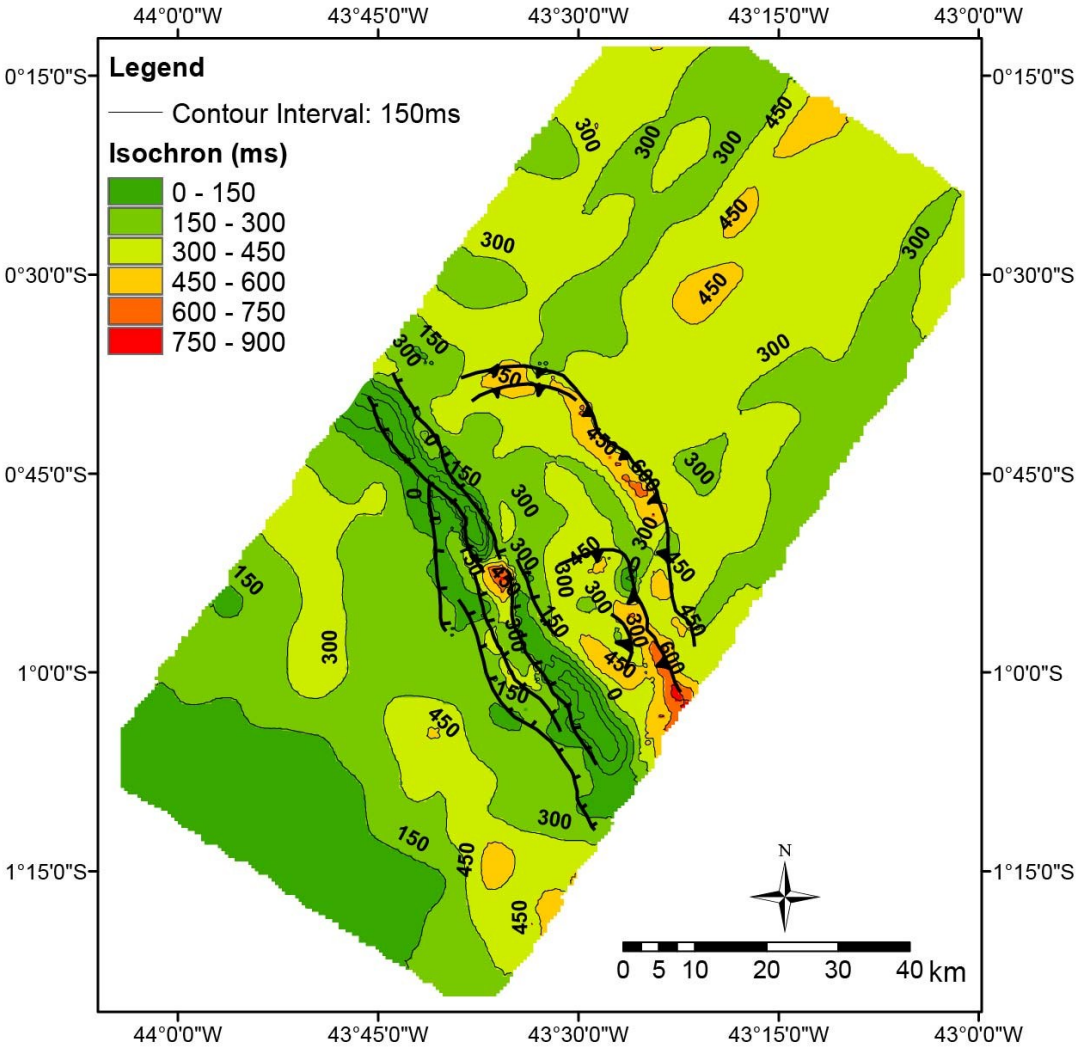

Figure 3-37. Isochron map between the Eocene (~42 Ma) and Maastrichtian age (~66 Ma) horizons.

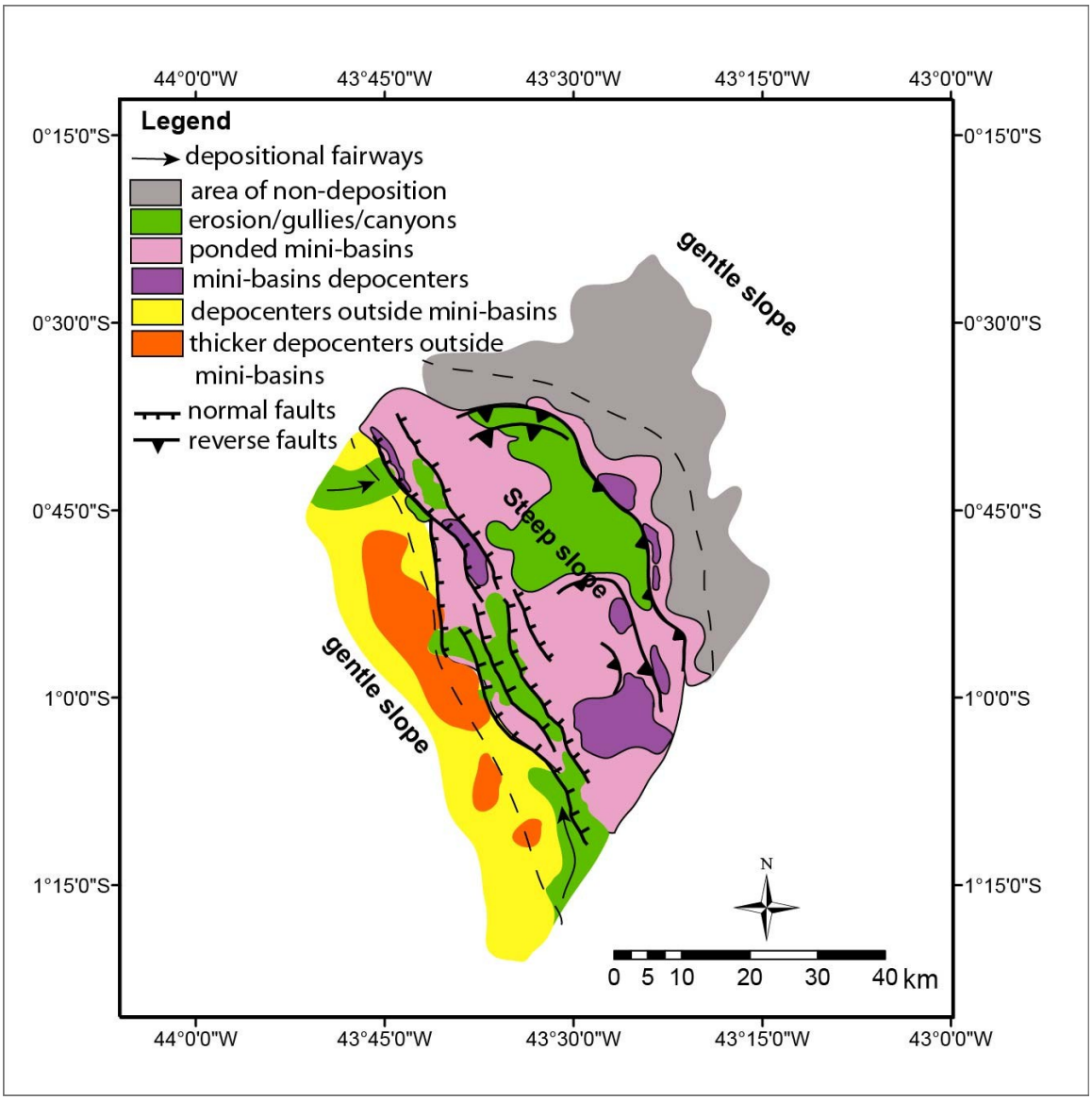

Figure 3-38. Depositional environments from ~66 to 42 Ma.

3.6.2.2 *Upper Eocene/Lower Oligocene (~42 to28.4 Ma)*

The isochron map (Fig. 3-39) between the Lower Eocene top (Fig. 3-17) and the Oligocene (Fig. 3-18) horizons represents thickness of the Upper Eocene/Lower Oligocene sequence (42 to 28.4 Ma) (Fig. 3-39). Because of an Oligocene regression most of the sediments are trapped on the continental shelf and on the continental slope (Fig. 3-40). On the continental slope sediments continued to be trapped in space created by normal and thrust faults forming ponded mini-basins (Fig. 3-40). Erosion and gulling of the ponded mini-basins also occurs and the larger fold is partially breached causing sediments to bypass to the abyssal plain (Fig. 3-40).

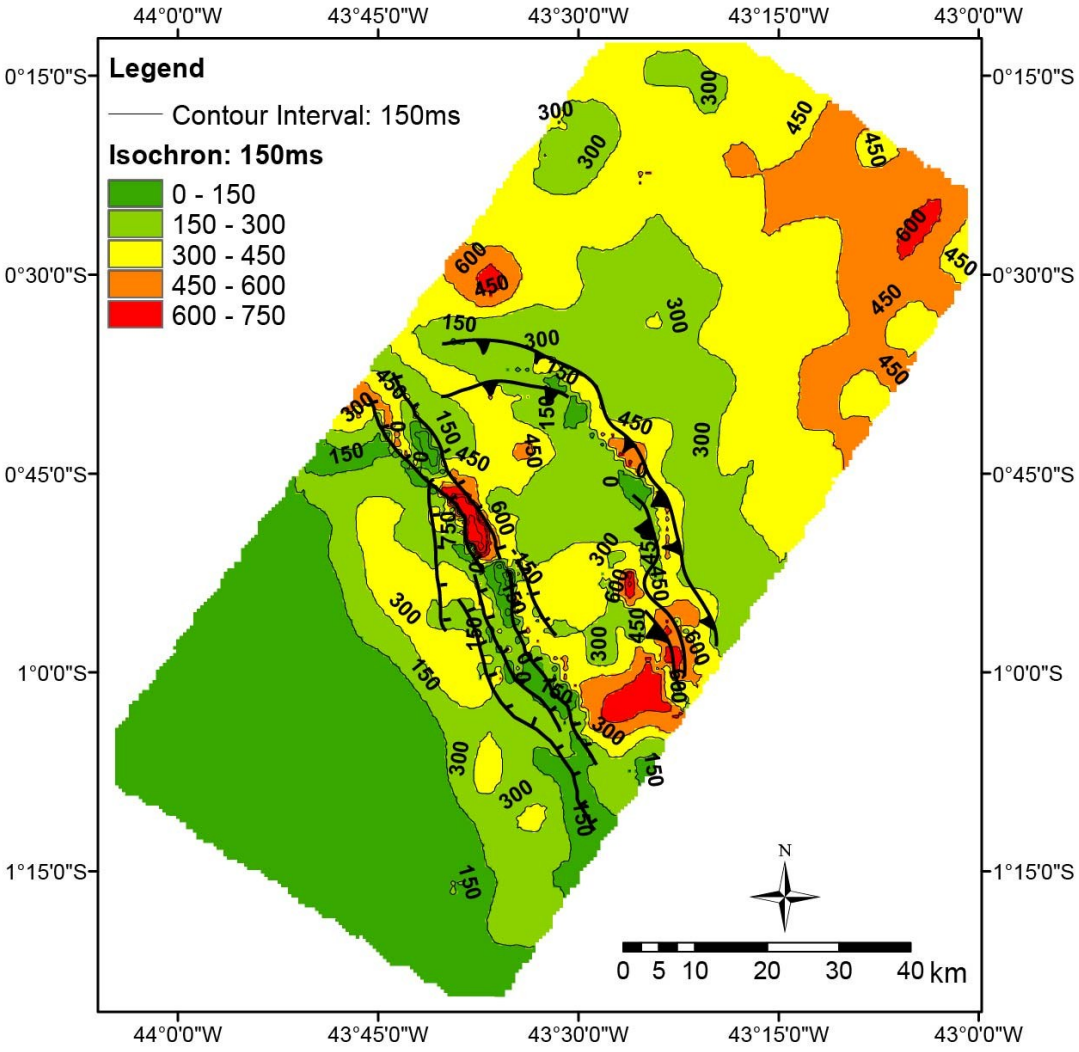

Figure 3-39. Isochron map between the Eocene (~42 Ma) and Oligocene age (~27 Ma) horizons.

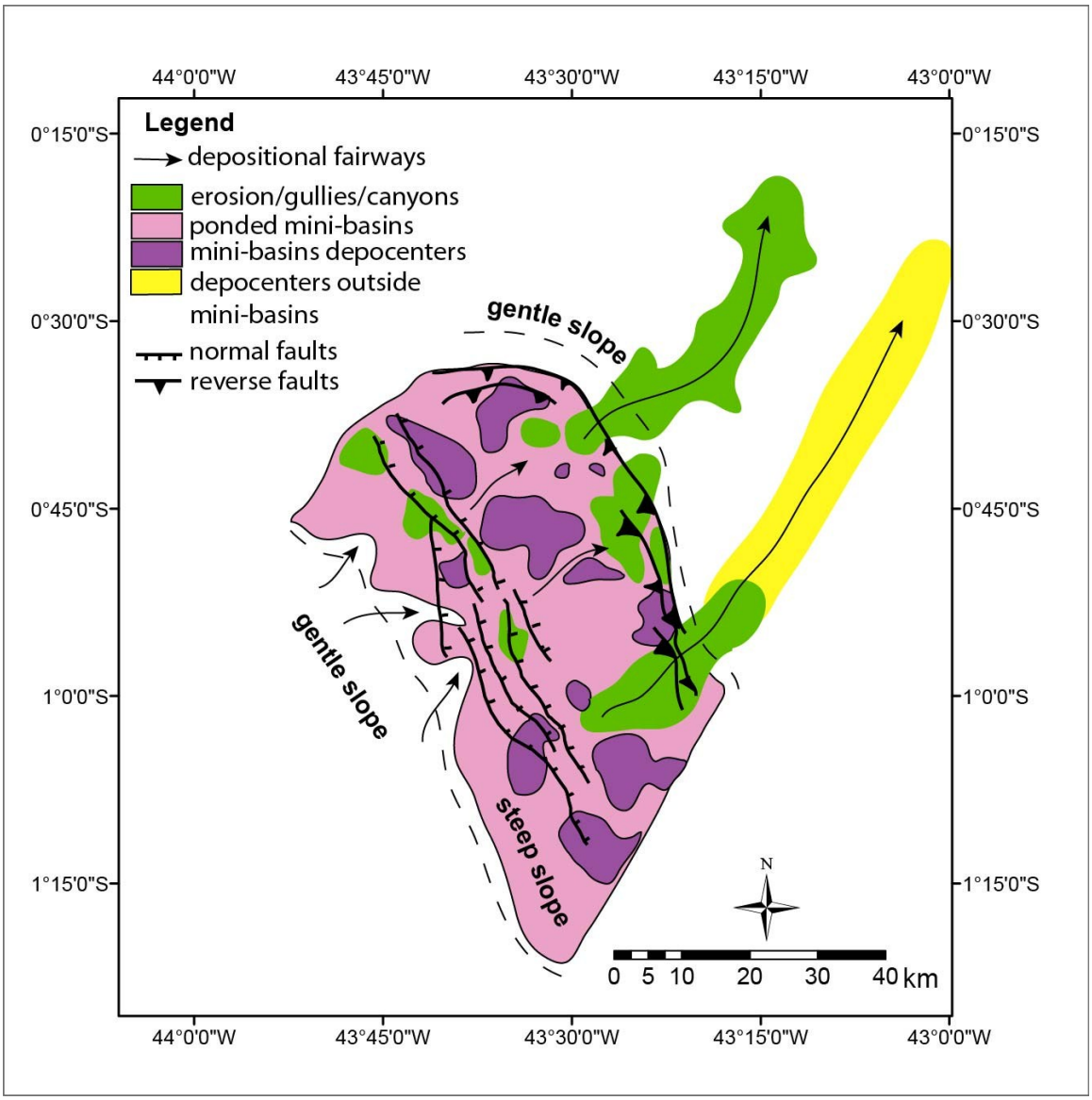

Figure 3-40. Depositional environments from ~42 to 27 Ma.

3.6.2.3 *Upper Oligocene/Lower Miocene (28.4 to 11.608 Ma)*

The isochron map (Fig. 3-41) between the Oligocene unconformity (~27 Ma) and the Mid-Miocene unconformity horizons (~10 Ma) (Fig. 3-19) represents thicks and thins of the Upper Oligocene/Lower Oligocene sequence (28.4 to 11.608 Ma). This was a time of erosion on the shelf and deposition in deep water, gulling and channeling are observed on the continental shelf and slope, and depositional fairways are observed in the abyssal plains (Fig. 3-42). The isochron map For the Upper Oligocene/Lower Miocene sequence (Fig. 3-41) shows that sediments continued to be trapped in the continental shelf and on the ponded mini-basins of the continental slope. The larger fold on the toe of the slope continued to be breached allowing sediments to reach the abyssal plains (Fig. 3-42).

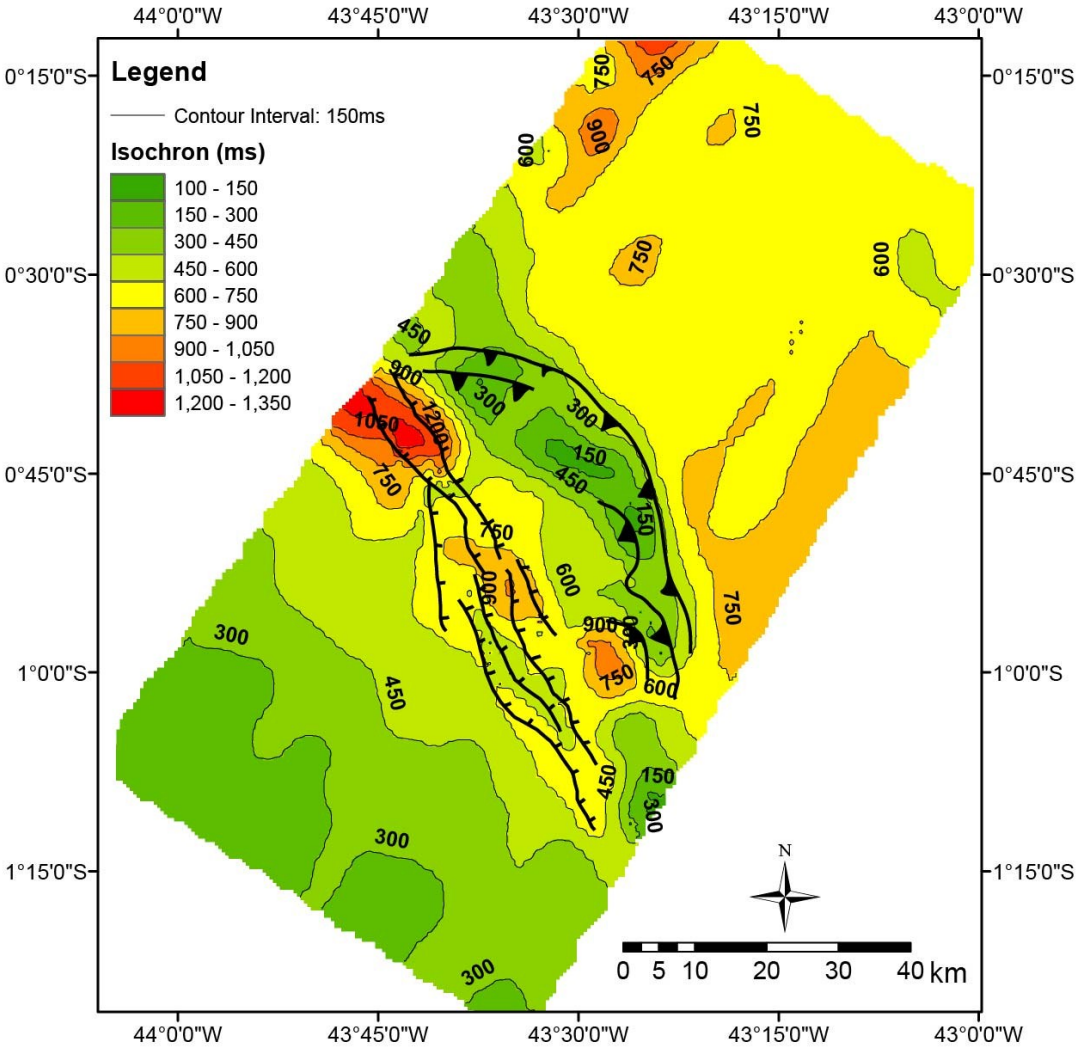

Figure 3-41. Isochron map between the Oligocene (~27 Ma) and the Miocene age (~10 Ma).

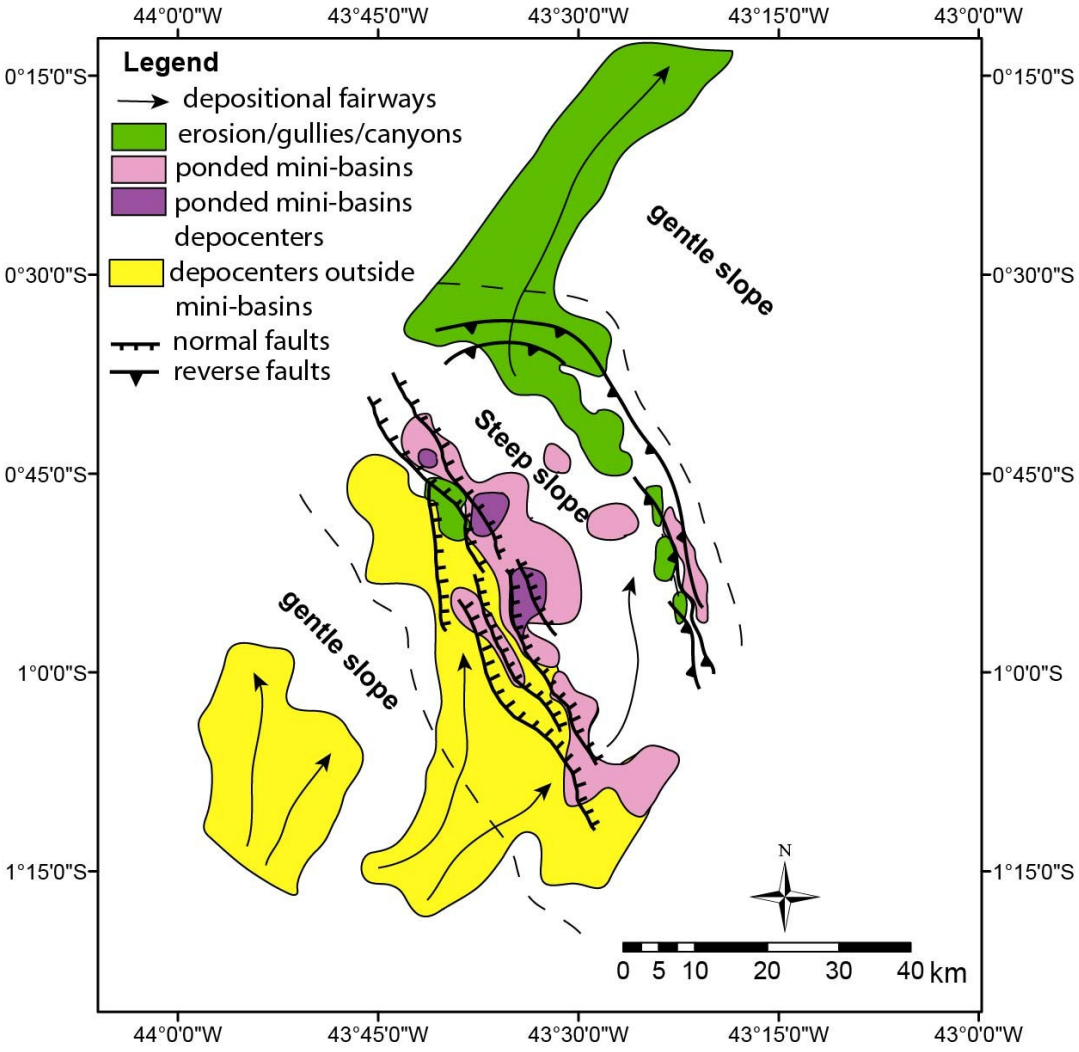

Figure 3-42. Depositional environments from ~27 to 10 Ma.

3.6.2.4 *Upper Miocene to Present (11.608 to 0 Ma)*

The Upper Miocene to present unit, highlighted in blue in figure 3-35, is a progradational sequence deposited above the mid-Miocene unconformity and is a time of increased sedimentation on the margin. The isochron map between the mid-Miocene unconformity and the sea-floor (Fig. 3-43) represents the sediment accumulation from the Mid-Miocene unconformity until present day. The Upper Miocene to present day is the thicker sequence deposited on the ponded mini-basins, causing all the mini-basins in the study area to coalesce into a large ponded mini-basin (Fig. 3-44). Depocenters are thicker in the hanging walls of the normal faults at the edge of the continental platform and in the hanging walls of the thrust faults at the toe of slope (Fig. 3-43). The fold at the toe of the slope has been eroded at Upper Miocene time and continues to be eroded until present day allowing sediments to be deposited in the abyssal plain (Fig. 3-44).

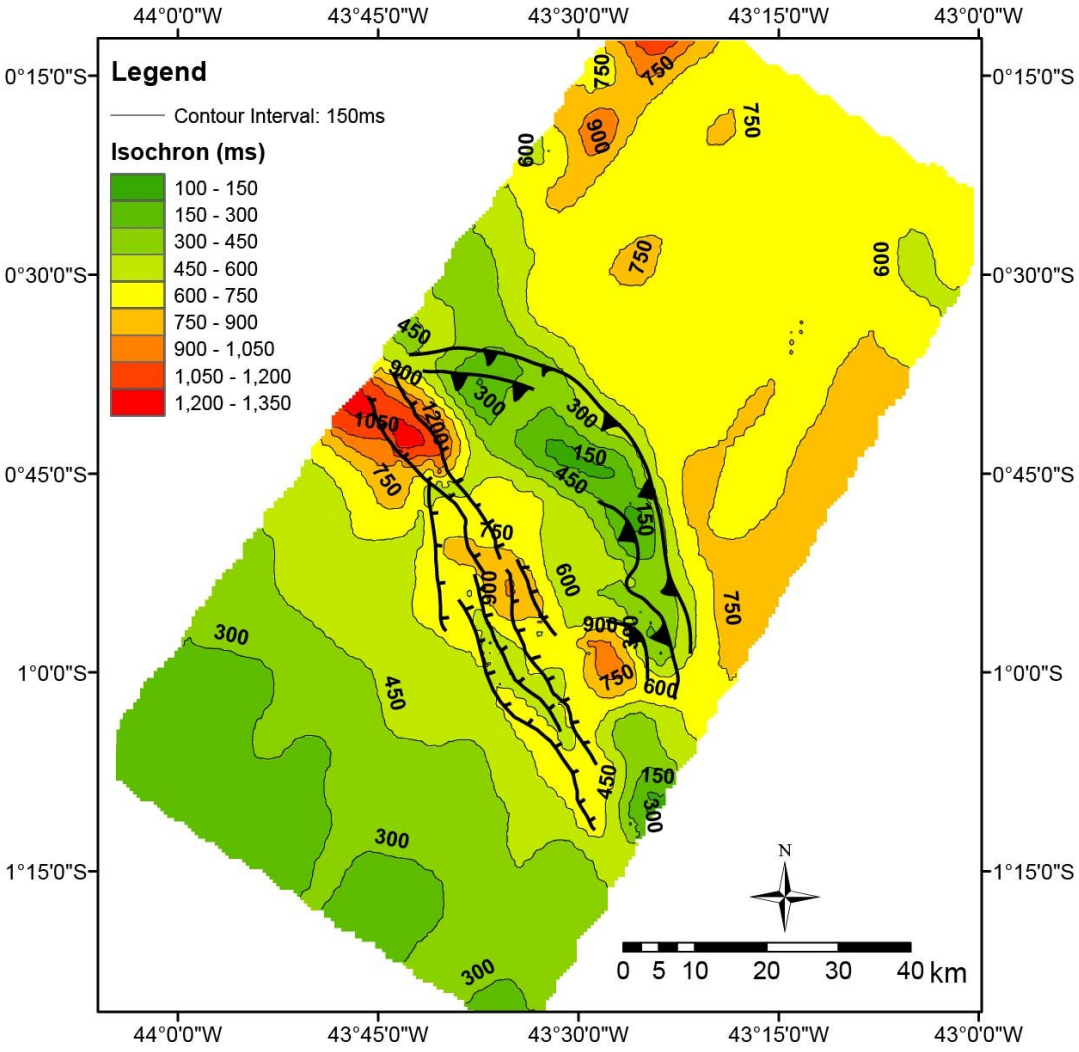

Figure 3-43. Isochron map between the Miocene age (~ 10 Ma) and the sea-floor.

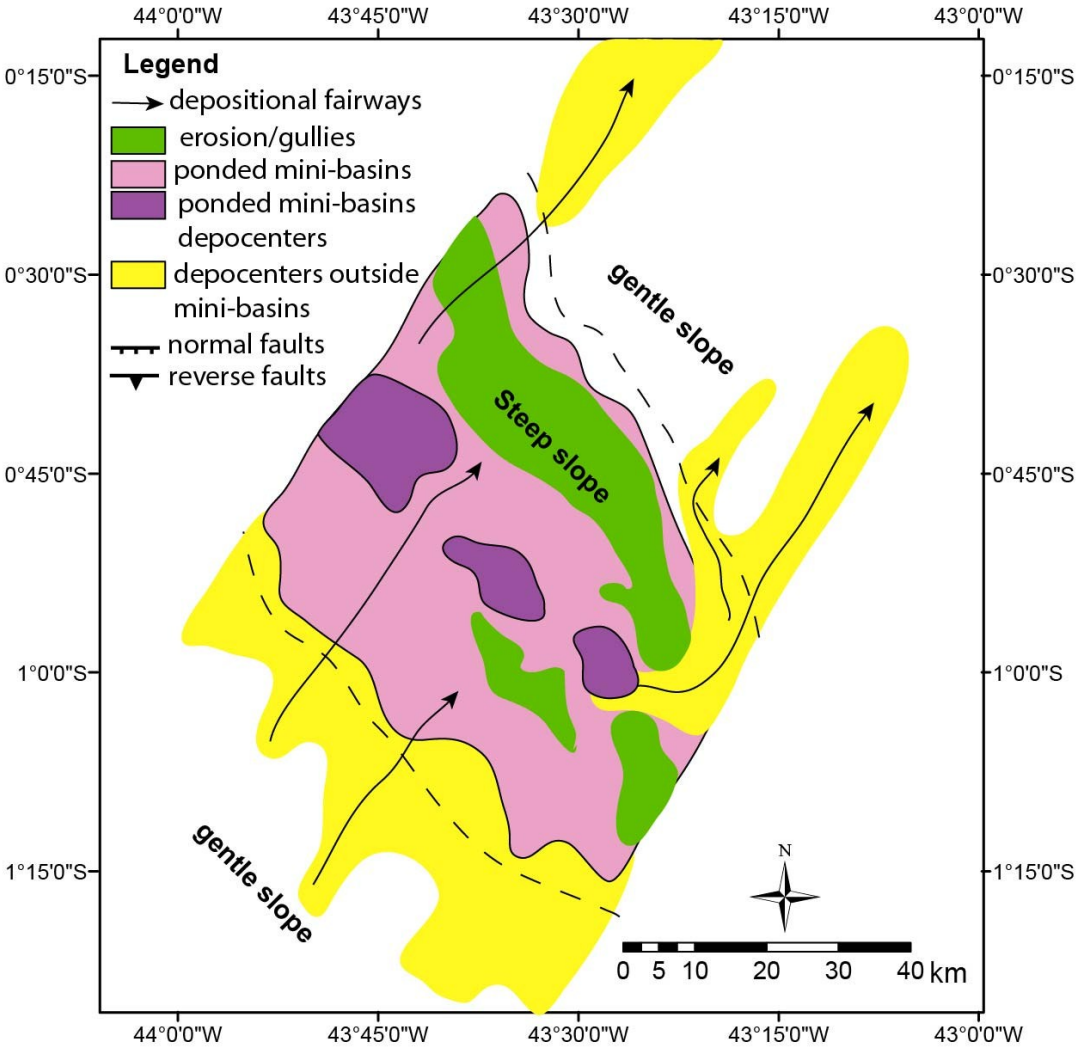

Figure 3-44. Depositional environment of the past 10 Ma.

3.7 STRUCTURAL ANALYSIS

The post-rift geology of this part of the Barreirinhas Basin can be viewed as consisting of a series of shale-detached collapse systems and all mapped faults in this study are listric detachment faults of those systems. In order to understand deformation rates on the faults, fault propagation and fault linkage between normal and thrust faults we have performed structural palinspastic restorations and kinematic analysis of the faults at different times.

3.7.1 Structural Palinspastic Restorations

The present-day deformed state section (Fig. 3-45) was restored to four earlier configurations in (1) Miocene (~10 Ma), (2) Oligocene (~27 Ma), (3) Eocene (~ 42 Ma), and (4) Santonian (~ 84 Ma) times. Restorations were constructed preserving bed-lengths and assuming flexural slip/flow kinematics. The sections are sub-perpendicular to the axial trends of folds, and the strike of thrust and normal faults.

Other fold structures comparable to those analyzed in this study are known in the Barreirinhas and Pará-Maranhão Basins, and each is a highly complex three-dimensional system. Variations in the exact timing of fault movement within the various basins seem likely. Our work focuses on one representative set of structures, and more work will be necessary to identify the timing of deformation in other systems within the Barreirinhas and Pará-Maranhão Basins.

3.7.1.1 *Present (0 Ma)*

At present day most of the deformation in the study area is distributed among four normal faults and two large thrust faults. There is also a smaller back-thrust fault associated with a minor fold collapse feature. The present day shortening measured on our representative cross-section is ~2170 meters and the present extension is ~1495 meters (Fig. 3-45).

3.7.1.2 *Miocene (10 Ma)*

Displacement on all four normal faults was restored to the paleogeometry of 10 million years ago and resulted in an extension of ~425 meters. Restoration of the thrust faults for the same interval resulted in a shortening of ~535 meters. This restoration time step resolved 75 % of the shortening and 72% of the extension on the cross-section (Fig. 3-45).

3.7.1.3 *Oligocene (27 Ma)*

Displacement on the four normal faults and the two thrust faults was restored to the paleogeometry of 27 million years ago and resulted in an extension of ~180 meters and a shortening of ~430 meters. After this second restoration time-step 80% of the shortening and 89% of the extension has being resolved.

3.7.1.4 *Eocene (42 Ma)*

Displacement on the four normal faults and the two thrust faults was restored to the paleogeometry of 42 million years ago and resulted in no change from the previous time-step at 27 Ma, an extension of ~180 meters and a shortening of ~430 meters (Fig. 3-45).

3.7.1.5 *Santonian (83.5 Ma)*

During the Coniacian-Santonian (Fig. 3-45) a prograding shelf and a high sedimentation rate in deep water (226 m/my) (Fig. 3-21) caused slope instability and triggered the formation of a series of normal listric faults at the shelf and thrust faults at the toe of slope. This wide linked extensional-compressional system developed very rapidly, all the deformation and the infilling of the deformed sea-floor took place during Santonian (85.8 to 83.5 Ma) within the sequences represented in blue and pink in Figure3-45. Because of limited stratigraphic resolution within this interval, and poor seismic imaging due to subsequent deformation by a younger fault system (Fig. 3-22) detailed interpretation and restoration of individual faults is not possible. Depiction is schematic for this event (Fig. 3-45).

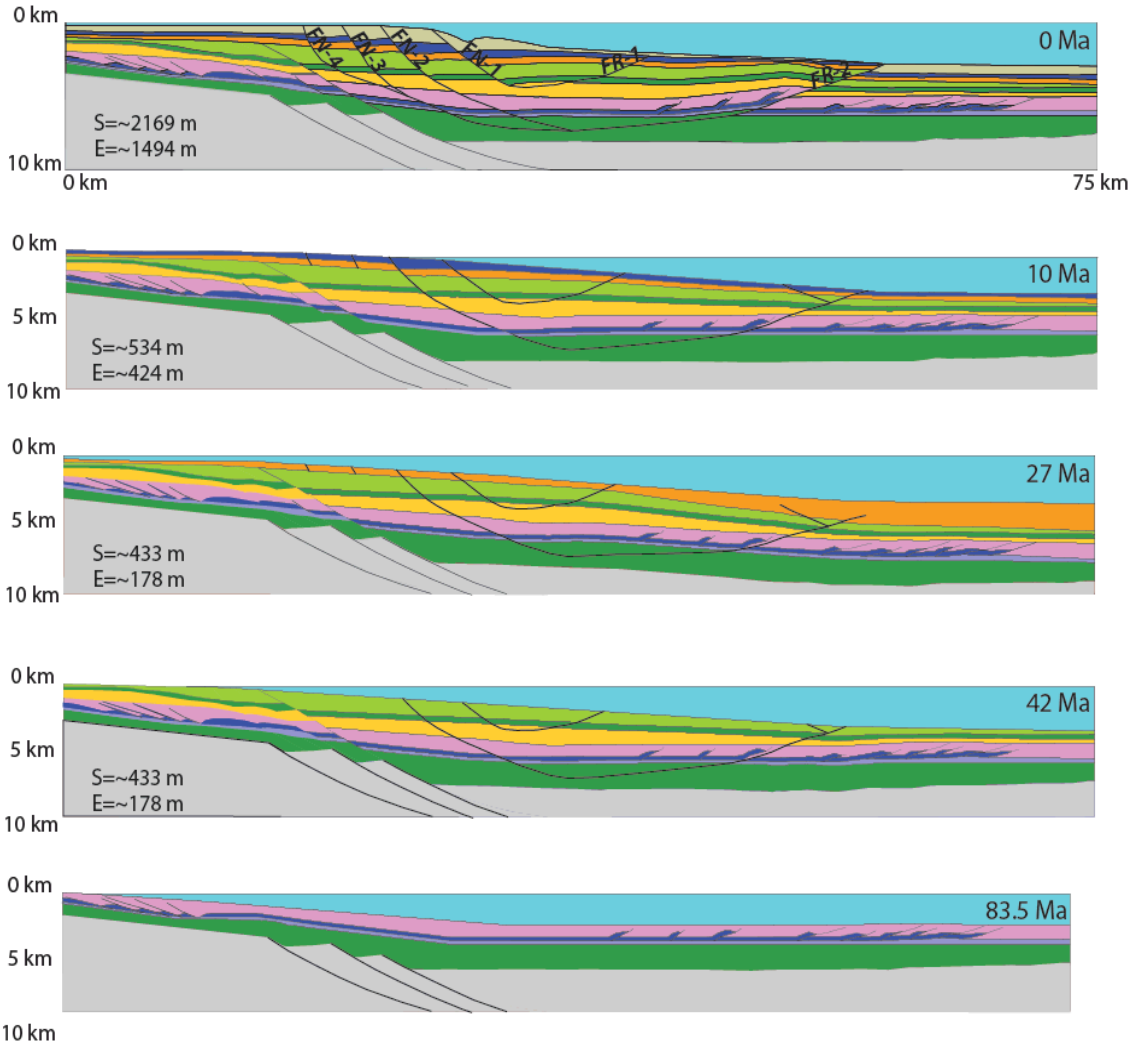

Figure 3-45. Palinspastic restorations. During the Santonian (83.5 Ma) a prograding shelf and a high sedimentation rate in deep water (226 m/my) caused slope instability and triggered the formation of a series of normal listric faults at the shelf and thrust faults at the toe of slope. During the Eocene (~42 Ma) a second deformation event started to develop as the shelf margin collapsed. Deformation continued during the Oligocene (27

Ma) with motion on both normal and thrust faults, but deformation rates were slow. During the Miocene after 10 Ma deformation rates increased significantly, with major normal growth faulting on the shelf margin, and uplift of folds at the toe of the slope at 0 Ma. Additional normal faults developed in the footwall of preexisting normal faults. Major canyon systems were subsequently incised into the shelf margin, cutting both normal faults and growth folds.

3.7.2 Cenozoic Deformation: Fault Analysis

Cenozoic deformation involved a thick (>4km) sedimentary sequence and it cross-cuts the pre-existing Cretaceous deformed sequence (Fig. 3-45). The Cenozoic fault and fold system is 30 km long and 40 km wide, bounded by a normal fault system along the shelf and a fold and thrust belt at the toe of the slope (Fig. 3-46). A detachment connecting the two systems is not clear on the seismic reflection profiles (Figs. 3-7, 3-8, 3-9, and 3-10). However, the normal and thrust fault systems project towards one another, at a similar stratigraphic level and delineate a bowl-shaped, through-going basal detachment (Fig. 3-35).

Interpretation of the seismic reflection data demonstrated the presence of two linked extensional and contractional fault systems of Cenozoic age. The Cenozoic system represented on the seismic line in figure 3-35A is color coded on figure 3-35B. The sequence in green was deposited prior to deformation and sequences highlighted in yellow and blue were deposited during deformation. Normal faults (FN-1, FN-2, FN-3, and FN-4) and thrust faults (FR-1 and FR-2) used for the quantitative analysis are labeled in figure 3-35.

To further assess the linkage of the normal and thrust fault systems and estimate the deformation rates involved we used the palinspastic restoration time-steps to measure fault-parallel displacement through time (Fig. 3-45). The fault linkage is analyzed in terms of deformation rate timing relationships.

Displacement, throw, and heave were measured for a representative pre-growth section, the top of Cretaceous (Fig. 3-46) on fault cut-offs for the following time-steps; 1) 0 Ma, 2) ~10 Ma, 3) ~27 Ma, and 4) ~42 Ma (Fig 3-45). Measured cumulative net displacement is plotted versus time for the present configuration (0 Ma), and for the restored time steps (~10 Ma, ~27 Ma, and ~42 Ma) (Figs. 3-47, 3-48, and 3-49).

The displacement versus time plot (Fig. 3-47) demonstrates the changing deformation rate through time. Deformation that began in the Eocene (~42 Ma) continued during the Oligocene with motion on both normal and thrust faults, but deformation rates were slow, (Fig. 3-47). Deformation rates increased significantly in the Miocene as indicated by expanded Miocene section on the downthrown side of shelf-margin normal faults (Fig. 3-35). In post-Miocene time deformation rates continued to increase (Fig. 3-47), with major normal growth faulting forming synclines on the shelf margin, and fold crests rising toward the sea bed at the toe of slope (Fig. 3-35). Additional normal faults (FN-3 and FN-4) developed in the footwall of pre-existing normal faults (FN-1 and FN-2) (Fig. 3-46).

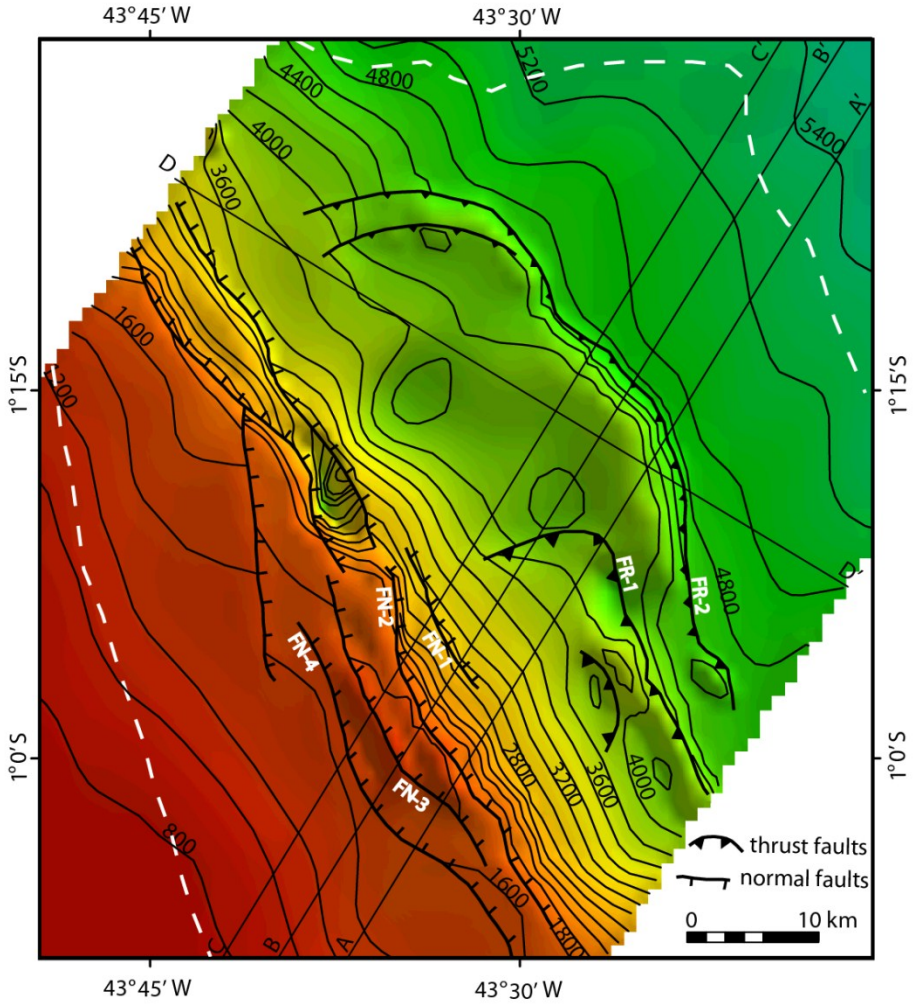

Figure 3-46. Detail on the Maastrichtian age (~66 Ma) Structural map. Structural map of the top of pre-growth section showing the location of seismic lines used in this study. White dashed line represents updip and downdip limits of the earlier Turonian-Santonian deformation system. The thrust faults (FR-1 and FR-2) and normal faults (FN-1, FN-2, FN-3, FN-4) used in our structural analysis are labeled on the map.

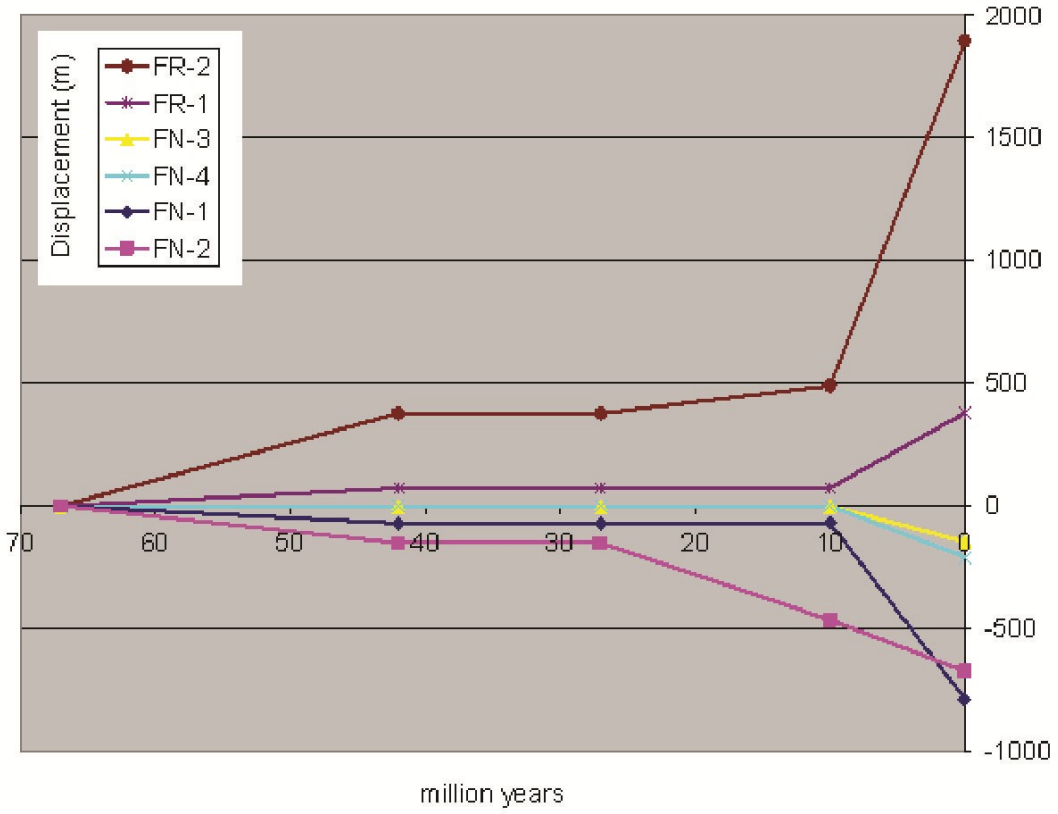

Figure 3-47. Displacement versus time plot. Displacement was measured and plotted for a representative pre-growth section, the top of Cretaceous (Fig. 16) on fault cut-offs for the following time-steps; 1) 0 Ma, 2) ~10 Ma, 3) ~27 Ma, 4) ~42 Ma (Fig. 3.45). The plot depicts the changing deformation rate through time. Deformation began in the Eocene (~42 Ma) continued during the Oligocene with motion on both normal and thrust faults, but deformation rates were slow. Deformation rates increased significantly in the Miocene as indicated by expanded Miocene section on the downthrown side of shelf-margin normal faults (Fig. 3-35). In post-Miocene time deformation rates continued to

increase, with major normal growth faulting forming synclines on the shelf margin, and fold crests rising toward the sea bed at the toe of slope (Fig. 3-35). Additional normal faults (FN-3 and FN-4) developed in the footwall of preexisting normal faults (FN-1 and FN-2) (Fig. 16). Total fault displacement plotted as a function of time for linked normal faults (negative values) and reverse faults (positive values) in the Barreirinhas Basin. Note how most faults initiate early in the process of deformation, while some normal faults are younger. All faults remain active until near present time. Note also the abrupt increase in displacement in the last ten million years.

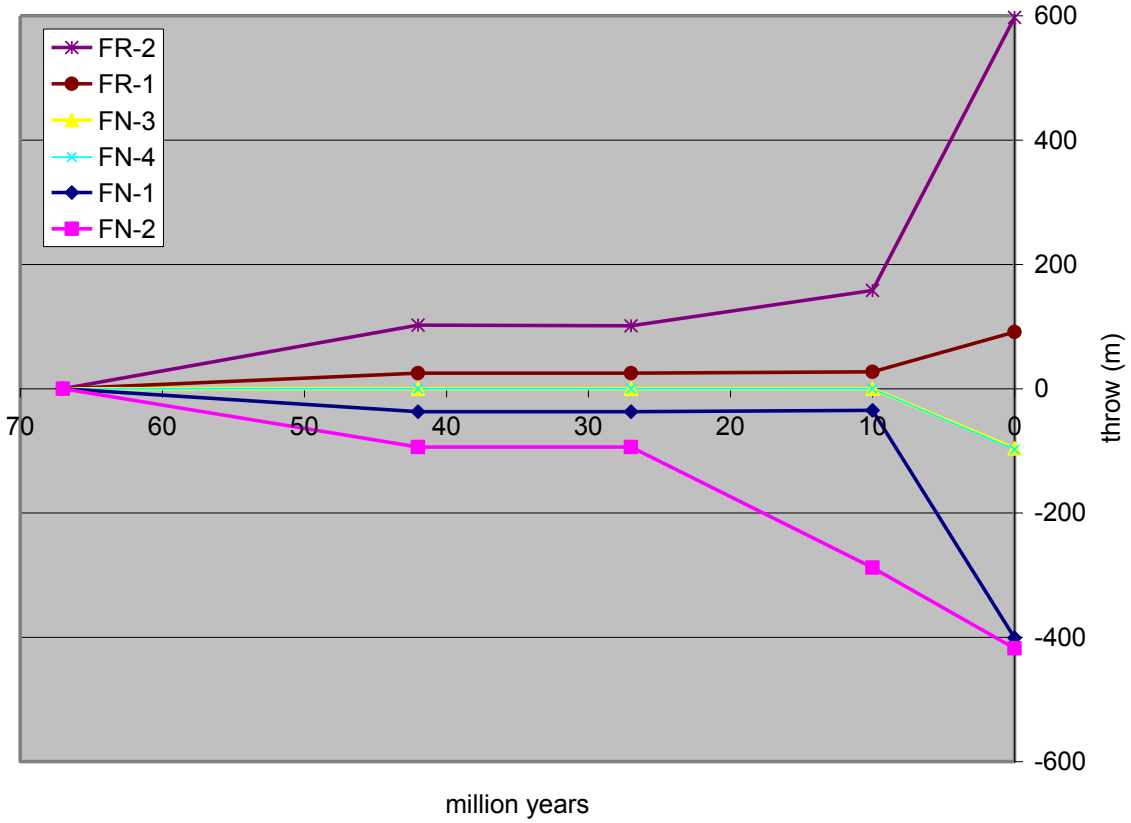

Figure 3-48. Total throw (vertical component of the displacement) plotted as a function of time for linked normal faults (negative values) and thrust faults (positive values) in the Barreirinhas Basin. The same observations made on figure 3-47 can be seen in this figure.

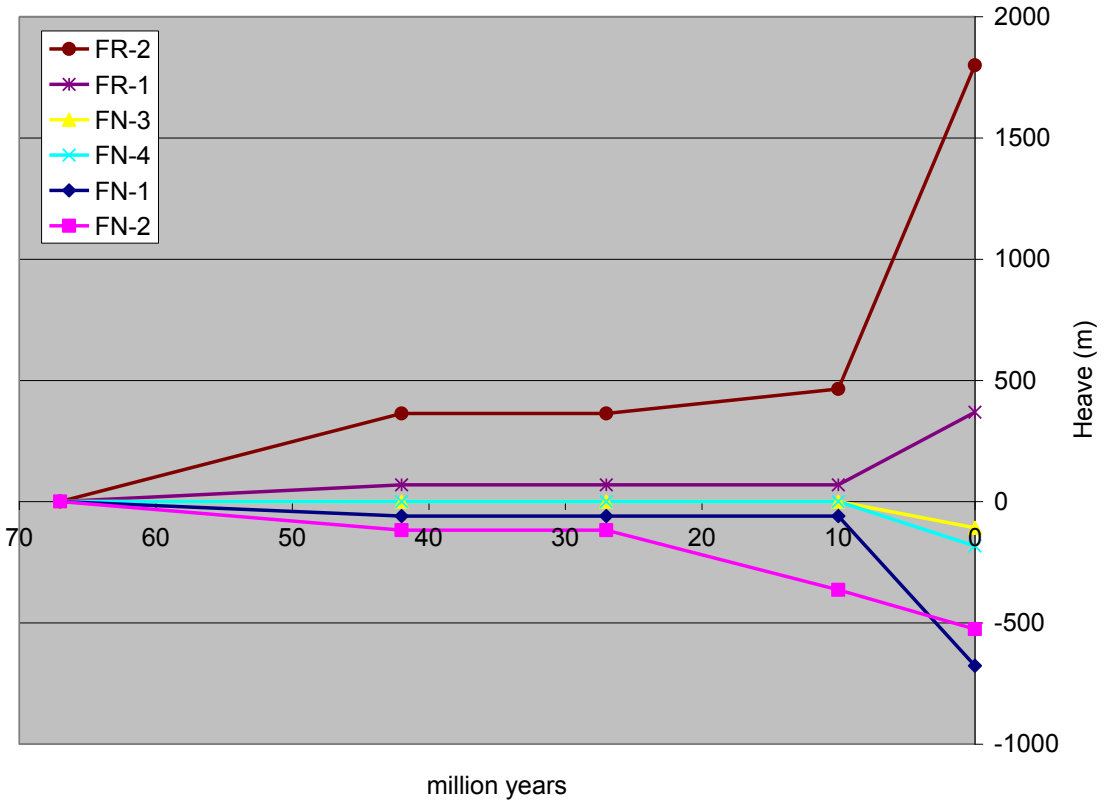

Figure 3-49. Heave (horizontal component of the displacement) plotted as a function of time for linked normal faults (negative values) and thrust faults (positive values) in the Barreirinhas Basin. The heave pattern suggests the same linkage between normal faults and thrust faults observed in figures 3-47 and 3-48. Comparison to figure 3-48 depicts relative dominance of downslope transport.

3.8 DISCUSSION

Shale-detached systems similar to the Barreirinhas Basin have been described from many basins worldwide, such as Niger Delta (Damuth, 1994; Rowan et al., 2004; Krueger and Gilbert, 2006 and 2009; Sultan et al., 2007), Pará-Maranhão (Zalan, 2005), and Namibia (Butler and Paton, 2010). In deep-water fold belts structural deformation is driven by sediment progradation that may be linked to sea-level drop or tectonic events. In the Barreirinhas a steep continental slope combined with sediment progradation generated a surface slope sufficient to create instability on the shelf edge/upper slope and caused collapse structures which lowered the sea-floor slope. In the Barreirinhas collapse structures kept sea-floor slope below 5 degrees. The evolution of the sedimentary wedge through time was measured on the seismic and on the structural restorations; 1) 5^{o} at 0 Ma-, 2) 3.8^{o} at Miocene (10 Ma), 3) 3.6^{o} at Oligocene (27 Ma), 4) 3.3^{o} at Eocene (~42 Ma), and 5) 4^{o} at Santonian (Fig. 3-45).

The compression on the toe of slope is caused by friction at the detachment level and cohesion of the sliding rocks. Zalan (1998) associated compression at the toe of slope to a slowdown in the gravity-driven movement of the sediments due to either (1) change in the gradient of the detachment layer or (2) the buttressing effect of a more rigid body (such as an igneous intrusion, an ancient volcano, or a protruding rift-phase domino-type fault block). In the absence of any of the latter features, we identify the change in the gradient as the causative factor. Where observed, buttressing effects are relatively

isolated, and have the localized effect of forming imbricate fans, and locally deflecting the trend of the fold belt (Fig. 3-10).

Compressional deformation by thrusting and folding in the Barreirinhas Basin occurs at the edge of the oceanic crust for all deformed sequences, due to a change in the gradient of the basal slope (Fig. 3-7). On the oceanic crust the basal slope of the sediment pile is close to zero, creating conditions appropriate for the formation of a critical taper angle sufficient to initiate thrusting (Davis and Kusznir, 2004; Dahlen, 1984).

Deformation created anticlines and synclines across the depositional fairways (Fig. 3-46), providing a template across which submarine flows were focused (Figs. 3-50, 3-51 and 3-52). Sediments deposited in ponded mini-basins (Figs. 3-50, 3-51 and 3-52), onlapping deformed sediments (Fig. 3-35), as described in Nigeria by Hooper et al. (2002). In the down-dip shortened domain it is not always possible to determine whether onlap geometry on the ponded mini-basins indicates deformation has stopped, or that the rate of deformation slowed as a result of: (1) deformation continuing on some faults, but not on all; and (2) because of erosion and extensive canyon reaping to the sea-floor outcropping faults do not necessarily indicate active movement.

3.8.1 Differences and Similarities between Cretaceous and Cenozoic Deformed sequences

Both Cretaceous and Cenozoic deformed sequences are characterized by a landward system of normal faults linked through a detachment fault to a basinward system of folds and thrust faults. The Cretaceous deformed sequence has a Coniacian to Santonian age (89.3 to 83.5 Ma) and is less than 1.5 km thick. The geometry of the Cretaceous deformed sequence involves a 30 km wide set of listric normal faults (extensional domain) on the outer continental shelf and top of slope that merge into a bed-parallel detachment surface, forming a 30 km wide translational domain, that is linked to a 30 km wide zone of imbricate thrust faults (compressional domain) on the continental slope. The Cenozoic deformed sequence has a different geometry involving 4km sedimentary sequence of Cretaceous and Cenozoic rocks (Turonian to present day age), and cross-cuts the pre-existing Cretaceous deformed sequence. Normal faults connect to the thrust faults at depth, forming two discrete bowl-shaped fault detachment layers, linked at depth at different stratigraphic levels.

3.8.2 Cretaceous Deformation

The Cretaceous deformed section is cut by Cenozoic faults (Fig. 3-45), and polyphase deformation creates a complex set of structures (Fig. 3-22). Once the section is restored to its Cretaceous configuration (Fig. 3-45) it becomes possible to identify a single bed-parallel detachment in Turonian marls and shales. All normal and thrust faults associated with this deformational event sole into the Turonian surface (Fig. 3-7). Cretaceous deformation has a similar geometry to deep-water deformed sequences observed in Nigeria (Damuth, 1994; Corredor et al., 2005; Sultan et al., 2007) and Namibia (Butler and Paton, 2010).

The Cretaceous allochthon is approximately one kilometer thick (Fig. 3-22) and elongate, approximately 70 km in down-dip extent (Fig. 3-46). The elongate geometry of the allochthon suggests sediments experienced enough friction to form imbricates, but low enough for it to spread over a large area. That was probably a combination of a low basal slope with very high pore pressures in the Turonian shales. Because the detachment is parallel to bedding (Fig. 3-9), bed confined overpressure within the Turonian shales is a likely explanation (Cobbold et al., 2004).

We estimate the age of deformation to be Coniacian/Santonian (~89 to 83.5Ma, duration ~5.5 Ma), a period of eustatic sea-level fall and associated high sedimentation rate (Trosdtorf et al., 2007 after Haq et al., 1987) (Fig. 3-4), but also Andean tectonism

(Wilson and Burke, 1972; Zalan, 1998; Figueiredo, 2009). Andean tectonism affects sedimentation rates locally in the continental margin due to drainage rearrangements.

The Barreirinhas Basin during the Coniacian/Santonian (~89 to 83.5Ma) was a mud dominated system. Sedimentation rates were very high (226 m/my) during the Santonian and (93 m/my) during the Coniacian (Table 1) (Fig. 3-21).Suggesting a depositional system with a very high sedimentation rate similar to that observed today, just north of Barreirinhas on the Amazon Delta (Nancy Engelhardt-Moore, personal communication) (Table 1) (Fig. 3-21).

As the prograding sedimentary pile became unstable, normal listric faults developed, linked to a bed-parallel gliding surface and to imbricates downslope (Fig. 3-8). The Coniacian/Santonian deformed sequence was later buried in the Upper Santonian and Campanian. Santonian sediments filled anticlines created by the deformation (Fig. 3-50). This post-deformational sequence formed ponded mini-basins (Fig. 3-50) similar to those described by Hooper et al. (2002) and Corredor et al. (2005) in the Niger Delta.

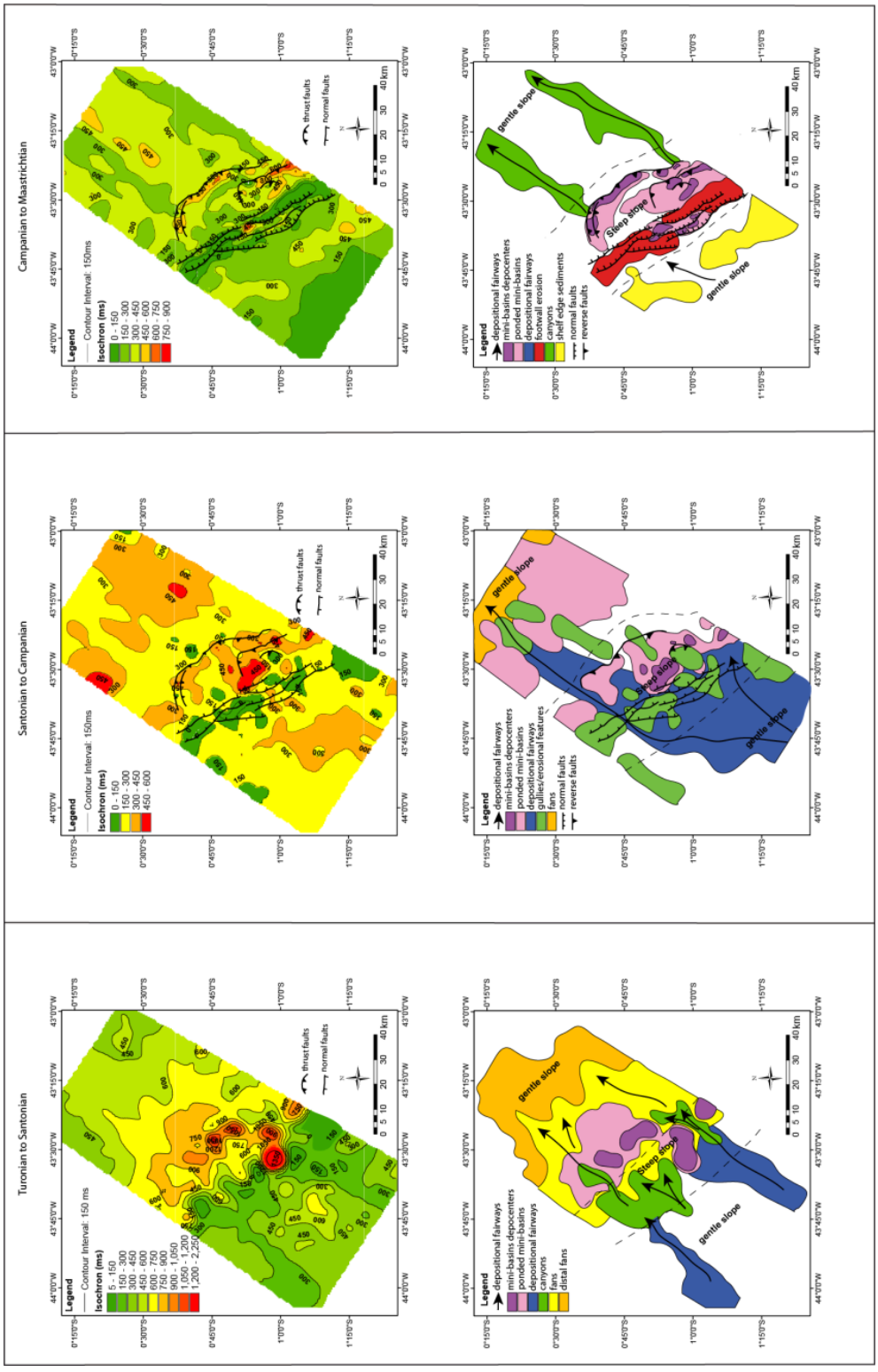
Turonian to Santonian
Santonian to Campanian
Campanian to Maastrichtian
Legend
Contour Interval: 150 ms
Isochron (ms)
5 - 150
150 - 300
300 - 450
450 - 600
600 - 750
750 - 900
900 - 1,050
1,050 - 1,200
1,200 - 2,250
thrust faults
normal faults
0 5 10 20 30 40 km
depositional fairways
mini-basins depocenters
ponded mini-basins
depositional fairways
gullies/erosional features
fans
normal faults
reverse faults
canyons
shelf edge sediments
distal fans
gentle slope
steep slope

Figure 3-50. Cretaceous isochrons representing fault growth in the drift units and related depositional systems. Three Cretaceous isochrons are represented in the figure; Turonian (89 Ma) to Santonian (84 Ma), Santonian (84 Ma) to Campanian (78 Ma), and Campanian (78 Ma) to Maastrichtian (65.5 Ma) lithounits. Thin isochrons areas are associated with canyons, gullies and other erosional features and thick areas isochrons are associated with depositional fairways, fans, ponded mini-basins, fault growth, and prograding wedges. The interpreted features are shown below each isochron map

3.8.3 Cenozoic Deformation

Gravity-driven systems are catastrophic in nature, but on and off deformation in the Cenozoic system has lasted for at least 40 my, from Eocene to present. The long period of syn-depositional deformation combined with less spreading has allowed for an accumulation of over 5 kms of deformed rocks (Fig. 3-35). The Cenozoic deformed area is less extensive (~ 30 km) both down-dip and along strike (Fig. 3-46), then the Cretaceous deformed area, so the allochthon is both thicker and less extensive than the Cretaceous (Fig. 3-22).

Two detachment faults associated with this system were mapped, both cross-cutting bedding and older Cretaceous structures (Fig. 3-35). The detachment faults form bowl-shaped fault systems at two different depths (Fig. 3-35). The geometry is different to the classic shale-detached DW-FTB as observed in Nigeria (Corredor et al., 2005) and described in this work on the Cretaceous system (Fig. 3-22).

3.8.4 Structural Restorations

3.8.4.1 *Eocene (42 Ma)*

During the Lower Eocene the shelf margin collapsed, developing two normal faults (FN-1 and FN-2) and one thrust fault (FR-2) (Fig. 3-45). The two normal faults linked to each other at depth and to the thrust fault (Fig. 3-10) forming a concave detachment fault with normal displacement downdip and reverse displacement updip (Fig. 3-45).

3.8.4.2 *Oligocene (27 Ma)*

Deformation continued during the Oligocene with motion on two normal faults (FN-1 and FN-2) and on one thrust fault (FR-2), but shortening was only 20% and extension only 12% of the present day deformation (Fig. 3-45).

3.8.4.3 *Miocene (10 Ma)*

Most of the deformation took place post 10 Ma with major normal growth faulting on the shelf margin, and uplift of folds at the toe of the slope (Fig. 3-45). Additional normal faults developed in the footwall of preexisting normal faults (Fig. 3-45) (FN-1 and FN-2). An additional thrust fault (FR-1) developed in the hanging wall of the pre-existing thrust fault. The two younger normal (FN-1 and FN-2) and thrust (FR-2) faults linked at depth to the pre-existing concave detachment (Fig. 3-35). During the

Miocene fault displacement increased significantly as indicated by expanded Miocene section on the downthrown side of shelf-margin normal faults (Fig. 3-45).

Major canyon systems were subsequently incised into the shelf margin, cutting both normal faults and growth folds (Figs. 3-51 and 3-52). The three-dimensional effects of the deformation can be seen on the Miocene (10 Ma) to present day isochron (Fig. 13), that shows development of a thick ponded mini-basin bounded by normal faults landward and thrust faults basinward.

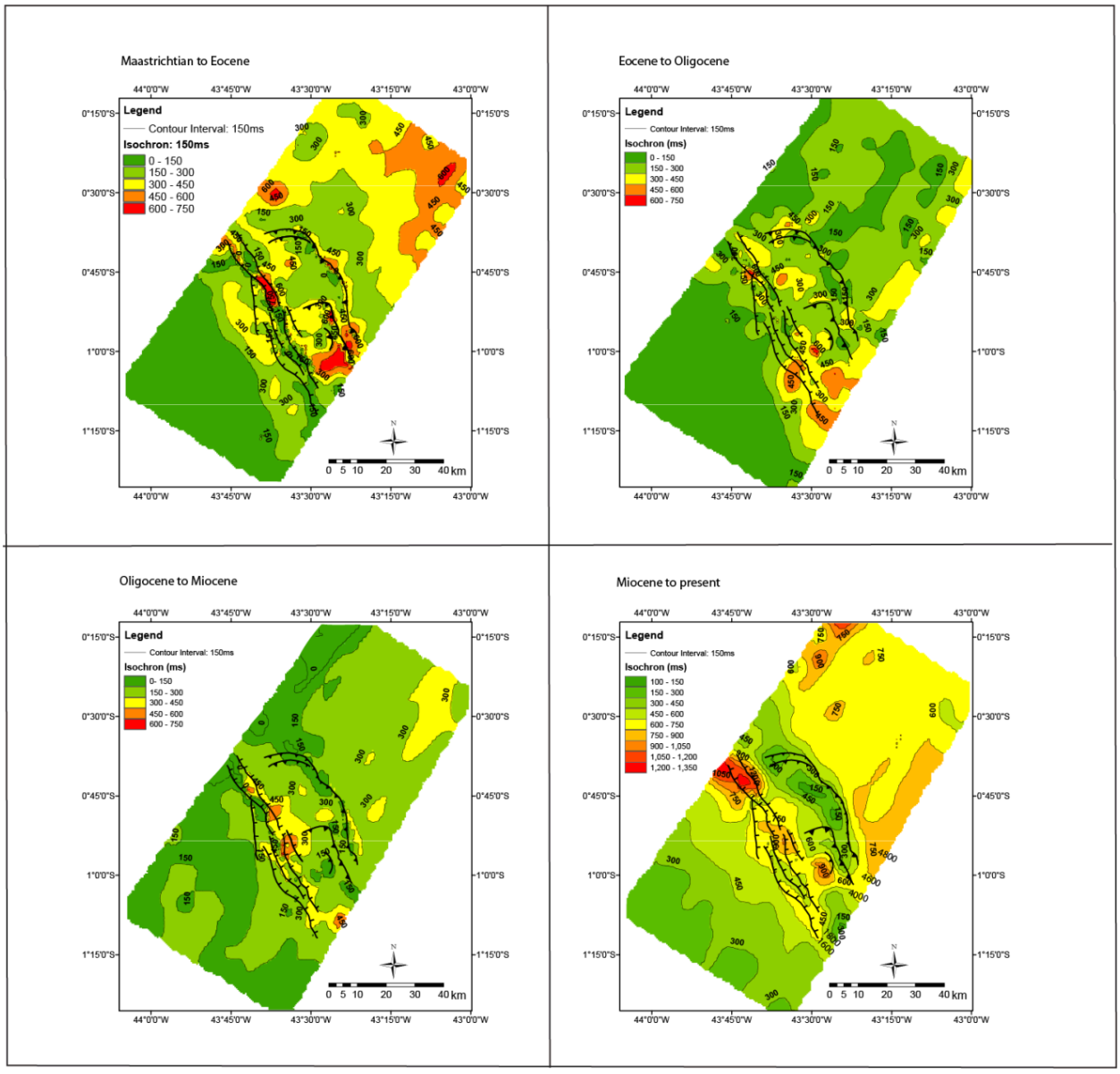

Figure 3-51. Cenozoic isochrons and interpreted sedimentary features for the Top of Maastrichtian (65.5 Ma) to Eocene (42 Ma), Eocene (42 Ma) to Oligocene (28 Ma), and Oligocene (28 Ma) to Miocene (10 Ma) lithounits. Isochron maps show thicks and thins that spatially correlate with the Cenozoic fault systems.

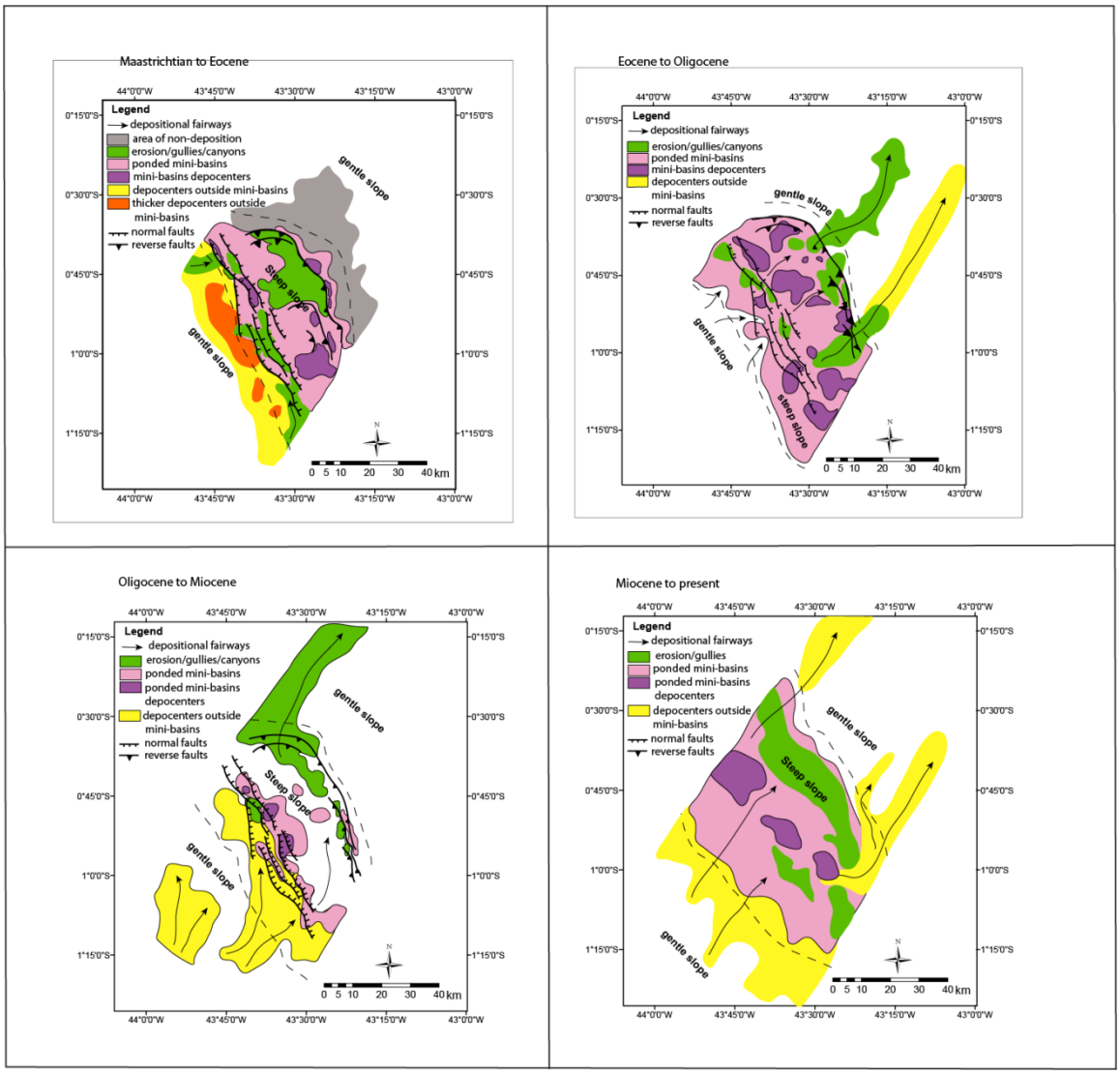

Figure 3-52. Cenozoic depositional systems Barreirinhas Basin, representing depositional fairways, and sediment ponded associated to fault growth.

3.8.4.4 *Results of the fault analysis*

1) Linked fault systems

Cumulative net displacement time plots (Fig. 3-47) depict changing deformation rate through time. The displacement versus time plot show that movement on both normal and thrust faults began at the same time on normal and thrust faults, and shortening and extension increased in the area at the same time intervals. The cumulative net displacement through time plot thus depict the expected linkage between normal and thrust faults, in terms of deformation rate, supporting the idea that the extensional deformation on the shelf is accommodated by shortening on the toe of slope.

2) Landward fault propagation

According to the fault deformation plots (Figs. 3-47, 3-48, and 3-49) normal faults 1 and 2 (Fig. 3-35) start to displace sometime in the Eocene prior to 42 Ma, but normal faults 3 and 4 (Fig. 3-35) did not form until Miocene (10 Ma).That implies the extensional province propagated landward through time (Fig. 3-46). The same is observed for thrust faults in the compressional province, thrust fault 2 (Fig. 3-35) displacement starts sometime in the Eocene prior to 42 Ma (Figs. 3-47, 3-48, and 3-49), but thrust fault 1 (Fig. 3-35) did not start moving until Miocene (10 Ma) (Figs. 3-47, 3-48, and 3-49). Therefore younger faults are located landward, and the deformation propagated landward on the shelf, changing the location of the shelf break and keeping the gradient of the slope below 5 degrees (Fig. 3-35).

3) Miocene deformation

The mid-Miocene unconformity is characterized by a transition from carbonate ramp to progradational clastic systems on the whole Brazilian Equatorial margin. This coincided with a major drainage reorganization described by Figueiredo et al. (2009) that diverted the Amazon River into the Atlantic Ocean introducing more clastics. The paleo-drainage rearrangement coincides with higher deformation rates on the faults in the study area, and to uplifts described in the Camamu Basin by Cobbold et al. (2010). Effects of this reorganization affected not only the Amazon River, but extended south, causing the sedimentation rates in the Barreirinhas Basin to increase during the late Miocene. Deformation has increased dramatically during the last ten million years, with movement in all earlier and some newly formed faults (Figs. 3-47, 3-48, and 3-49). Thrust fault 1 and normal faults 3 and 4 (Fig. 3-45) accommodate approximately 80% of the extensional and compressional deformation that took place in the last ten million years.

3.8.4.5 *Driving Mechanism*

The Tertiary event was likely triggered by increased sedimentation in the area, as shelf progradation increased the surface slope and caused shelf collapse events. Shelf collapse events decreased the surface slope to less than five degrees. Sediment progradation and shelf collapse created a feedback process that kept surface slopes close to equilibrium through time with multiple episodes of disequilibrium. Deformation rates in Eocene and Miocene times correspond to shelf instability at those times.

3.9 SUMMARY AND CONCLUSIONS

1) Cretaceous and Cenozoic faults and folds have different geometries

Two major deep-water fold and thrust belts linked landward to extensional fault systems are mapped in the Barreirinhas. Cretaceous and Cenozoic faults and folds have different geometries (Fig. 3-2). The Cretaceous deformed sequence is less than 1.5 km thick, involves a 30 km wide set of listric normal faults (extensional domain) on the outer continental shelf and top of slope that merge into a bed-parallel detachment surface, forming a 30 km wide translational domain linked to a 30 km wide zone of imbricate thrust faults (compressional domain) on the continental slope. The Cenozoic faults cut 4km of Cretaceous and Cenozoic sedimentary rocks (Turonian to present day age), and cross-cuts the pre-existing Cretaceous deformed sequence. Normal faults connect to the thrust faults at depth, forming a bowl-shaped fault detachment linked to large folds at the continental slope (Fig. 3-2).

2) Driving mechanism is increased sedimentation.

Gravity gliding is the driving mechanism for both Cretaceous and Cenozoic deformation. Loading and steepening of the shelf margin created by increased sedimentation rates caused extension on the shelf and compression at the slope. Sediment progradation and shelf collapse created a feedback process, in which sediment progradation increased the surface slope and shelf collapse decreased it, keeping surface slopes close to equilibrium through time.

3) Landward propagation of normal and thrust faults.

As more faults were introduced to the system younger faults were emplaced landward of the older faults. The deformed area in both extensional and compressional domains propagated landward on the shelf changing the location of the shelf break and keeping the gradient of the slope below 5 degrees (Fig. 3-45).

4) Deformation rates suggest linkage between extension and shortening.

The cumulative net displacement through time plot depict the expected linkage between normal and thrust faults, as extension and compression began at the same time and deformation rate increased at the same time intervals in both normal and thrust faults. This supports the theory that the extensional deformation on the shelf is accommodated by shortening on the toe of slope.

5) Increased deformation rates at 10 Ma, likely related to changes in the paleogeography at Late Miocene.

It is possible that the high deformation rates observed in the Barreirinhas Basin at Late Miocene are a consequence of large drainage reorganization in the whole Brazilian Equatorial margin. Drainage reorganization in northern South America was initiated between 11.8 and 11.3 Ma ago, and diverted the drainage west of the Purus arch into the present day Amazon Basin (Figueiredo et al., 2009). A consequence of this drainage reorganization is that localized deep-water fold and thrust structures are observed

continuously on the Brazilian Equatorial margin from the Amazon Cone (Araujo et al., 2009; Perovano et al., 2009) to the Barreirinhas Basin (Zalan, 1998; 2004; 2005).

REFERENCES CITED

Altamira-Areyan, A., 2009, The ribbon continent of northwestern South America [Ph.D. Dissertation], University of Houston, 215 p.

Almeida, M.E., Macambira, M.J.B., Oliveira, E.C., 2007, Geochemistry and zircon geochronology of the I-type high-K calc-alkaline and S-type granitoid rocks from southeaster Roraima, Brazil: Orosirian collisional magmatism evidence (1.97-1.96 Ga) *in* central portion of Guyana shield: Precambrian Research, v.155, p.69-97.

Amante C., and Eakins, B.W., 2009, ETOPO1 1 arc-minute relief model: procedures, data sources and analysis: http://www.ngdc.noaa.gov/mgg/global/relief/ETOPO1/ .

Amerman, R., Trudgill, B., Nelson, E.P., and Piles D.R., 2009, 4-D distribution of deepwater mass-transport deposit (Late Cretaceous Upper Gosau Subgroup, Muttekopf area, northern Calcareous Alps, Austria): Implications for syndepositional structural reconstruction: American Association of Petroleum Geologists Search and Discovery, article 30108.

Antobreh, A.A., Faleide, J.I., Tsikalas F., and Planke S., 2009, Rift-shear architecture and tectonic development of the Ghana margin deduced from multichannel seismic reflection and potential field data: Marine and Petroleum Geology, v. 26, p. 345-368.

Araripe, P.T., and Feijo, F.J., 1994, Bacia Potiguar: Boletim de Geociências da Petrobras, v. 8, no. 1, p. 127-141.

Araujo, E.F.S., Silva, C.G., Reis, A.T., Perovano, R., Gorini, C., Vendeville, B.C., and Albuquerque, N.C., 2009, Movimentos de massa multiescala na bacia da Foz do Amazonas - Margem Equatorial Brasileira: Revista Brasileira de Geofisica, v. 27, no. 3, p. 485-508.

Autin J., Bellahsen N., Husson L., Beslier M.O., Leroy S. & d'Acremont E. , 2010, Analog models of oblique rifting in a cold lithosphere. Tectonics, v.29, TC6016, doi:10.1029/2010TC002671

Becker, T.W., Conrad, C.P., Buffett, B., Müller, R.D., 2009, Past and present sea-floor age distributions and the temporal evolution of plate tectonic heat transport: Earth and Planetary Science Letters, v. 278, p. 233–242.

Bergerat, 1989, From pull-apart to rifting process: The formation of the Pannonian Basin. Tectonophysics, v.157, p.271-280.

Billotti, F., and Shaw, J.H., 2005, Deep-water Niger Delta fold and thrust belt modeled as a critical-taper wedge: The influence of elevated basal fluid pressure on structural styles: American Association of Petroleum Geologists Bulletin, v. 89, no. 11, p. 1475-1491.

Bird, D., 2001, Shear margins: Continent-ocean transform and fracture zone boundaries: The Leading Edge, February 2001, p.150-159.

Bird, D., Hall, S., Burke, K., Casey, J, and Sawyer, D., 2007, Central Atlantic Ocean seafloor spreading history: Geosphere, v. 3, p. 282–298, doi: 10.1130/GES00047.1

Bird, D.E. and Hall, S.A., 2010, South Atlantic kinematics and the evolution of Tristan da Cunha hotspot tracks. 72nd EAGE Conference & Exhibition incorporating SPE EUROPEC 2010 Barcelona, Spain, 14 - 17 June 2010

Brune, S., A. A. Popov, and Sobolev, S. V., 2012, Modeling suggests that oblique extension facilitates rifting and continental break-up, J. Geophys. Res., 117, B08402, doi:10.1029/2011JB008860

Buck, W. R., 2007, Dynamic processes in extensional and compressional settings - the dynamics of continental breakup and extension, in Treatise on Geophysics, v. 6, Crust and Lithosphere Dynamics, edited by A. B. Watts, pp. 335–376, Elsevier, New York.

Butler, R.W.H., and Paton, D.A., 2010, Evaluating lateral compaction in deepwater fold and thrust belts: How much are we missing form nature's sandbox?: GSA Today, v. 20, no. 3, p. 4-10.

Clifton, E.A., and Schlishe, R.W., 2001. Nucleation, growth, and linkage of faults in oblique rift zones: Results from experimental clay models and implications for maximum fault size: Geology, v. 29, no.5, p.455-458.

Cobbold, P.R., Mourgues, R., and Boyd, K., 2004, Mechanism of thin-skinned detachment in the Amazon Fan: assessing the importance of fluid overpressure and hydrocarbon generation: Marine and Petroleum Geology, v. 21, p. 1013–1025.

Cobbold, P.R., Gilchrist, G., Scotchman, I., Chiossi, D., Chaves, F.F., De Souza F.G., and Lilletveit, R., 2010, Large submarine slides on a steep continental margin (Camamu Basin, NE Brazil): Journal of the Geological Society [London], v. 167, p. 583-592.

Cochran, J.R., 1973. Gravity and magnetic investigations in the Guiana Basin, Western Equatorial Atlantic. Geological Society of America Bulletin, v.84, no. 10, p.3249-3268.

Cochran, J.R., 1983, A model for development of the Red Sea: American Association of Petroleum Geologists Bulletin, v. 67, p. 41–69

Corredor, F., Shaw, J.H., and Billotti, F., 2005, Structural styles in the deep-water fold and thrust belts of the Niger Delta: American Association of Petroleum Geologists Bulletin, v.89, no. 6, p. 753-780.

Cox, A., and Hart R. B., 1986, Plate Tectonics: How it Works: Blackwell Scientific Publications, 392 p.

d'Acremont, E., Leroy, S., Maia, M., Patriat, P., Beslier, M.-O., Bellahsen, N., Fournier, M., and Gente, P., 2006, Structure and evolution of the eastern Gulf of Aden:

Insights from magnetic and gravity data (Encens-Sheba MD117 cruise): Geophysical Journal International, v. 165, p. 786–803.

Dahlen, F.A., 1984, Noncohesive critical Coulomb wedges: and exact solution: Journal Geophysical Research, v.89, no.10, p.125-133.

Dahlen, F.A., 1990, Critical taper model of fold-and-thrust belts and accretionary wedges: Annual Review of Earth and Planetary Sciences, v. 18, p. 55-90.

Damuth, J.E., 1994, Neogene gravity tectonics and depositional processes on the deep Niger Delta Continental Margin: Marine and Petroleum Geology, v. 11, no. 3, p. 320-346.

Daoud, M. A., B. Le Gall, R. C. Maury, J. Rolet, P. Huchon, and H. Guillou, 2011, Young rift kinematics in the Tadjoura rift, western Gulf of Aden, Republic of Djibouti, Tectonics, 30, TC1002, doi:10.1029/2009TC002614.

Darros de Matos, R., 1999, History of the northeastern Brazilian rift system: kinematic implications for the break-up between Brazil and West Africa. Geological Society of London, Special Publications, v.153, p.55-73.

Davis D., Suppe, J., and Dahlen, F.A., 1983, Mechanics of fold and thrust belts and accretionary wedges: Journal of Geophysical Research, v.88, no.B2, p.1153-1172.

Davis, M., Kusznir, N.J., 2004, Depth-dependent lithospheric stretching at rifted continental margins, *in* Karner, G.D., Taylor, B., Driscoll, N.W., and Kohlstedt,

D.L., eds., Rheology and Deformation of the Lithosphere at Continental Margins: Columbia University Press, New York, p. 92-136.

Detrick, R.S., M.H. Cormier, R.A. Prince, D.W. Forsyth, and E.L. Ambos, 1982, Seismic constraints on the crustal structure within the Vema Fracture Zone, J. Geophys. Res., v.87, p.599-610.

Destro, N., Szatmari, P., Alkmim F. F., Magnavita L. P., 2003, Release faults, associated structures, and their control on petroleum trends in the Recôncavo rift, northeast Brazil, American Association of Petroleum Geologists Bulletin, July 2003, v. 87, p. 1123-1144.

Dick, H.J.B., Lin, J., and Schouten H., 2003, An ultraslow-spreading class of ocean ridge. Nature v.426, p.405-412.

Direen, N.G., Stagg, H.M.J., Symonds, P.A., and Norton, I.O., 2012, Variations in rift symmetry: cautionary examples from the Southern Rift System (Australia-Antarctica) *In*: Mohriak, W. U., Danforth, A., Post, P. J., Brown, D. E., Tari, G. C., Nemcˇok, M. and Sinha, S. T. (eds) 2012. Conjugate Divergent Margins. The Geological Society, London, Special Publications, 369, http://dx.doi.org/10.1144/SP369.4

Feijo, F.J., 1994, Bacia de Barreirinhas: Boletim de Geociências da Petrobras, v. 8, no. 1, p. 103-109.

Feijo, F.J., 1996, O início da livre circulação das águas do Oceano Atlântico: Boletim de Geociências da Petrobras, v. 9, no. 1/4, p. 157-164.

Figueiredo, J., Hoorn, C., Van der Ven, P., and Soares E., 2009, Late Miocene onset of the Amazon River and the Amazon deep-sea fan: Evidence from the Foz do Amazonas Basin: Geology, v. 37, p. 619-622.

Fournier, M., Huchon P. , K. Khanbari, and Leroy S., 2007, Segmentation and along-strike asymmetry of the passive margin in Socotra, eastern Gulf of Aden: Are they controlled by detachment faults?, G^3, v.8, Q03007, doi:10.1029/2006GC001526.

Fox, P.J. and Gallo, D.G., 1984, A tectonic model for ridge-transform-ridge plate boundaries: Implications for the structure of oceanic lithosphere, Tectonophysics, v.104, p.205-242.

Gradstein, F.M., Ogg, J.G., Smith, A.G., Bleeker, W., and Lourens, L.J., 2004, A new Geologic Time Scale, with special reference to Precambrian and Neogene: Episodes, v. 27, no. 2, p. 83-100.

Grant, C., 2004, The Upper Miocene deepwater fans of northwest Borneo: Indonesian Petroleum Association Proceedings, Deepwater and frontier symposium, p. 421-428.

Greenroyd, C.J., Peirce, C., Rodger, M., Watts, A.B., and Hobbs, R.W., 2008, Do fracture zones define continental margin segmentation? Evidence from the French Guiana margin: Earth and Planetary Science Letters, v. 272, p. 553-566.

Haq, B.U., Hardenbol, J., and Vail, P.R., 1987, Chronology of fluctuating sea levels since the Triassic (250 million years ago to present): Science, v. 235, p. 1156–1167.

Hayward, N.J. and Ebinger, C.J., 1996. Variations in the along axis segmentation of the Afar Rift system. Tectonics, v.15, 244–257

Hooper, R.J., Fitzsimmons, R.J., Grant, N., and Vendeville, B.C., 2002, The role of deformation in controlling depositional patterns in the south-central Niger Delta, West Africa: Journal of Structural Geology, v. 24, p. 847-859.

Krueger, A., and Gilbert, E., 2009, Deepwater fold-thrust belts: Not all the beasts are equal: American Association of Petroleum Geologists International conference and Exhibition, Cape Town, South Africa, article 30085.

Krueger, A.C.V.A., and Gilbert, E., 2006, Mechanics and kinematics of back thrusting in deep water fold-thrust belts – Observations From the Niger Delta: American Association of Petroleum Geologists Annual Meeting, Houston, Abstracts, v. 15, p. 58.

Kumar, N., 1979, Origin of "paired" aseismic rises: Ceará and Sierra Leone rises in the Equatorial, and the Rio Grande Rise and Walvis ridge in the South Atlantic: Marine Geology, v. 30, p. 175-191.

Lizarralde, D., Axen, G.J., Brown, H.E., Fletcher, J.M., González-Fernández, A., Harding, A.J., Holbrook, W.S., Kent, G.M., Paramo, P., Sutherland, F., and

Umhoefer, P.J., 2007, Variable styles of rifting in the Gulf of California: Nature, v. 448, p. 466–469.

Long, L.E., Sial, A.N., Nekvasil, H., and Borba, G.S., 1986, Origin of granite at Cabo de Santo Agostinho, Northeast Brazil: Contributions to Mineralogy and Petrology, v. 92, no. 3, p. 341-350.

Magnavita, L. P., 1992, Geometry and kinematics of the Recôncavo-Tucano-Jatobá rift, northeast Brazil: Ph.D. dissertation, University of Oxford, Oxford, United Kingdom, 493 p.

Manatschal, G., 2004, New models for evolution of magma-poor rifted margins based on a review of data and concepts from West Iberia and the Alps. International Journal of Earth Sciences, v. 93, 432–466.

Maus, S., U. Barckausen., H. Berkenbosch, N. Bournas, J. Brozena, V. Childers, F. Dostaler, J.D. Fairhead, C. Finn, R.R.B. Von Frese, C. Gaina, S. Golynsky, 2009, EMAG2: A 2-arc minute resolution Earth magnetic anomaly grid compiled from satellite, airborne, and marine magnetic measurements. G^3 , v.10, no.8.

McKenzie, D., 1978. Some remarks on the development of sedimentary basins, Earth Planetary Science Letters., v. 40, p. 25–42.

McClay, K.R., and Ellis, P.G., 1987, Geometries of extensional fault systems developed in model experiments: Geology, v.15, p.341-344.

McClay, K.R., and White, M.J., 1995, Analogue modeling of orthogonal and oblique rifting: Marine and Petroleum Geology, v.12, p.137-151.

Mizusaki, A.M.P., 1989, A Formação Macau na porção submersa da Bacia Potiguar: Boletim de Geociências da Petrobras, v. 3, no. 3, p. 191-200.

Morais Neto, J.M., Hegarty, K., and Karner, G.D., 2006, Abordagem preliminar sobre paleotemperatura e evolução do relevo da bacia do Araripe, nordeste do Brasil, a partir da análise de traços de fissão em apatita: Boletim de Geociências da Petrobras, v. 14, no. 1, p. 113-118.

Morais Neto, J.M., Hegarty, K.A., Karner, G.D., and Alkmim, F.F., 2009, Timing and mechanisms for the generation and modification of the anomalous topography of the Borborema Province, northeastern Brazil: Marine and Petroleum Geology, v. 26, p. 1070–1086.

Morley, C.K., King, R., Hillis R., Tingay M., and Backe G., 2011, Deepwater fold and thrust belt classification, tectonics, structure and hydrocarbon prospectivity: A review: Earth-Science Reviews, v. 104, p. 41-91.

Mourgues, R., Lecomte, E., Vendeville, and B., Raillard S., 2009, An experimental investigation of gravity-driven shale tectonics in progradational delta: Tectonophysics, v. 474, p. 643-656.

Müller, R.D. and Smith W.H.F., 1993. Deformation of the oceanic crust between the North American and South American plates. Journal of Geophysical research, v.98, no. B5, p.8275-8291.

Müller, R.D., Sdrolias, M., Gaina, C. and Roest, W.R.., 2008, Age, spreading rates and spreading asymmetry of the world's ocean crust, G^3, v.9, no 4, Q04006, doi1029/2007GC001743.

Peel, F.J., Travis, C.J., and Hossack, J.R., 1995, Genetic structural provinces and salt tectonics of the Cenozoic offshore U.S. Gulf of Mexico: a preliminary analysis, *in* Jackson, M.P.A., Roberts, D.G., and Snelson, S., eds., Salt Tectonics: a Global Perspective: American Association of Petroleum Geologists Memoir, v. 65, p. 153-175.

Perovano, R., Reis, A.T., Silva, C.G., Vendeville, B.C., Gorini, C., Oliveira V., Araujo, E.F.S., 2009, O processo de colapso gravitacional da secao marinha da bacia da foz do Amazonas-Margem Equatorial Brasileira: Revista Brasileira de Geofisica, v. 27, no. 3, p. 459-484.

Reston, T.J., 2007, The formation of non-volcanic rifted margins by the progressive extension of the lithosphere: the example of the West Iberian margin. Geological Society, London, Special Publications January 1, 2007, v. 282, p. 77-110, doi: 10.1144/SP282.5.

Rowan, M.G., Peel, F.J., and Vendeville, B.C., 2004, Gravity-driven foldbelts on passive margins, *in* McClay, K.R., ed., Thrust Tectonics and Hydrocarbon Systems: American Association of Petroleum Geologists Memoir, v. 82, p. 157-182.

Rowan, M.G.; Trudgill, B.D., and Fiduk, J.C., 2000, Deep water, salt-cored foldbelts: lessons from the Mississippi fan and the Perdido foldbelts, Northern Gulf of Mexico, *in* Mohriak, W., and Talwani, M., eds., Atlantic Rifts and Continental Margins: American Geophysical Union Geophysical Monograph, v. 115, p. 173-191.

Sandwell, D.T. and W.H.F. Smith, 2009, Global marine gravity from retracked Geosat and ERS-1 altimetry: Ridge segmentation versus spreading rate. Journal of Geophysical Research, v. 114, B01411, doi:10.1029/2008JB006008.

Schobbenhaus, C. and Bellizia, A., 2001, Geological Map of South America, CGMW-CPRM-DNPM-UNESCO: http://www.cprm.gov.br.

Sial, A.N., 1976, The post-Paleozoic volcanism of Northeast Brazil and its tectonic significance: Anais da Academia Brasileira de Ciências, v. 48 (Suplemento), p. 299–311.

Sibuet, J.C., Srivastava, S., and Manatschal, G., 2007, Exhumed mantle-forming transitional crust in the Newfoundland-Iberia rift and associated magnetic anomalies, Journal of Geophysical Research, v.112

Snow, J., J. Wilfried, E. Hellebrand., Muhe, R. and shipboad party, ARKXV/2, 2001, Magmatic and hydrothermal activity in Lena Trough Arctic Ocean. EOS, Transactions American Geophysical Union, v.82, N.17, p.193-198.

Sobolev, S.V., and Babeyko, A.Y., 2005, What drives orogeny in the Andes?: Geology, v. 33, no. 8, p. 617-620.

Sultan, N., Voisset, M., Marsset, B., Marsset, T., Cauquil, E., Colliat, J., 2007, The potential role of compressional structures in generating submarine slope failures in the Niger Delta: Marine Geology, v.237, p. 169-190.

Torsvik, T. H., S. Rousse, C. Labails, and M. A. Smethurst (2009), A new scheme for the opening of the South Atlantic Ocean and the dissection of an Aptian salt basin, Geophys. J. Int., v. 177, 1315–1333.

Trosdtorf, Zalan, P. V., Figueiredo, J. J. P. Soares, E. F., 2007. Bacia de Barreirinhas. B. Geoci. Petrobras, v.15, n.2, p.331-339.

Trudgill, B.D., Rowan, M.G., Fiduk, C., Weimer, P., Gale, P.E., Korn, B.E., Phair, R.L., Gafford, W.T., Robberts, R.G., and Dobbs, S.W., 1999, The Perdido Fold Belt, northwestern deep Gulf of Mexico, Part 1: Structural geometry, evolution and regional implications: American Association of Petroleum Geologists Bulletin, v. 83, p. 88-113.

Underwood, M.B., Moore, G.F., Taira, A., Klaus, A., Wilson, M.E.J., Fergusson, C.L., Hirano, S., Steurer, J., and the LEG 190 shipboard scientific party, 2003, Sedimentary and tectonic evolution of a trench-slope basin in the Nankai subduction zone of southwest Japan: Journal of Sedimentary Research, v. 73, no. 4, p. 589-602.

Umhoefer, P.J., Schiarizza, P., Robinson, M., 2002, Relay Mountain Group, Tyaughton-Methow basin, southwest British Columbia: a major Middle Jurassic to Early Cretaceous terrain overlap assemblage. Can. J. Earth Sci. v. 39, p. 1143-1167.

Umhoefer P.J., 2011, Why did the Southern Gulf of California rupture so rapidly? – Oblique divergence across hot, weak lithosphere along a tectonically active margin. GSA Today, v. 21, no. 11, doi: 10.1130/G133A.1

Vendeville, B.C., and Nilsen, K.T., 1995, Episodic growth of salt diapirs driven by horizontal shortening. *in*: Travis, C.J., Harrison, H., Hudec, M.R., Vendeville, B.C., Peel, F.J., Perkins, B.F., eds., Gulf Coast section SEPM Foundation Sixteenth Annual Research Conference: Program with papers, p. 285-295.

Vendeville, B.C., 2005, Salt tectonic driven by sediment progradation: Part II – Radial spreading of sedimentary lobes prograding above salt: American Association of Petroleum Geologists Bulletin, v. 89, p. 1081-1089.

Weimer, P., and R. Buffler, 1992, Structural Geology and evolution of the Mississippi Fan Fold Belt, deep Gulf of Mexico: American Association of Petroleum Geologists Bulletin, v.76, p.225-251.

Wernicke, B.P., 1985. Uniform-sense normal simple shear of the continental lithosphere, Can. J. Earth Sci., v. 22, 108–125.

Wilson, J. T., and Burke, K., 1972, Two types of mountain building: Nature, v. 239, p. 448-449.

Yang, W. and Escalona, A., 2011, Tectono-stratigraphic evolution of Guyana Basin: American Association of Petroleum Geologists Bulletin, v.95, p.1339-1368.

Zalan, P.V., 1998, Gravity-driven compressional structural closures in Brazilian deep-waters – a new frontier play: American Association of Petroleum Geologists Annual convention, Salt Lake City, Utah, article 90937.

Zalan, P.V., 2004, Evolução Fanerozóica das bacias sedimentares Brasileiras, *in* Mantesso-Neto, V., Bartorelli, A., Carneiro, C.D.R., and Neves, B.B.B., eds., Geologia do Continente Sul-Americano – Evolução da Obra de Fernando Flávio Marques de Almeida, Beca Produções Culturais Ltda.: São Paulo, p. 595-612.

Zalan, P.V., 2005, End member of gravitational fold and thrust belts (GTFBs) in the deep waters of Brazil, *in* Shaw, J.H., Connors, C., and Suppe, J., eds., Seismic Interpretation of Contractional Fault-related Folds: An American Association of Petroleum Geologists Seismic Atlas, Studies in Geology, no.53.

Ziegler, P. A., and S. Cloetingh (2004), Dynamic processes controlling evolution of rifted basins, Earth Sci. Rev, v. 64, p. 1–50.